How do we power decarbonization? Land and other resources in Canada's West

Kevin Gordon Palmer-Wilson
BEng, Bochum University of Applied Sciences, 2010
MSc, University of Freiburg, 2013

A Dissertation Submitted in Partial Fulfillment
of the Requirements for the Degree of

DOCTOR OF PHILOSOPHY

in the Department of Mechanical Engineering

How do we power decarbonization? Land and other resources in Canada's West

Kevin Gordon Palmer-Wilson
BEng, Bochum University of Applied Sciences, 2010
MSc, University of Freiburg, 2013

SUPERVISORY COMMITTEE

Dr. Andrew Rowe (Department of Mechanical Engineering)
Co-Supervisor

Dr. Bryson Robertson (Department of Mechanical Engineering)
Co-Supervisor

Dr. Peter Wild (Department of Mechanical Engineering)
Department Member

Dr. Tom Gleeson (Department of Civil Engineering)
Outside Member

Abstract

Mitigating climate change requires elimination of fossil fuel related greenhouse gas emissions. Transitioning electricity generation to low-carbon sources and substituting fossil fuels with electricity in non-electric sectors is considered to be a key strategy. This dissertation investigates resource options to and land area impacts of decarbonizing electricity generation and electrifying adjacent sectors. Three studies analyze transition options in the western Canadian provinces of Alberta and British Columbia.

The first study investigates technology transition pathways and land area impacts of reducing electricity generation related carbon emissions in fossil fuel-dominated Alberta. A final 70% share of wind, solar, and hydro power reduces emissions by 90% between 2015 and 2060. This scenario requires designating 5% additional land area to electricity generation annually. Land is largely designated to the required space between wind turbines, with smaller areas attributed to ground-mounted solar and hydro power. System planners can reduce the land area impacts by deploying more compact geothermal, rooftop solar and natural gas with carbon capture and sequestration (CCS) technologies. These technology compositions can hold land area impacts constant in time if depleted natural gas and CCS infrastructure is expediently reclaimed, but total net present system costs increase by 11% over the 45-year period. Without reclamation, fuel extraction and carbon sequestration increase land area impacts at least fourfold within this time period.

The second study investigates sedimentary basin geothermal resources in northeastern British Columbia. Geothermal energy is a potentially low-cost, low-carbon, dispatchable resource for electricity generation with a relatively small land area impact. A two-step method first geospatially overlays economic and geological criteria to highlight areas favourable to geothermal development. Next, the Volume Method applies petroleum exploration and production data in Monte Carlo probability simulations to estimate electricity generation potential at the four areas with highest favourability (Clarke Lake, Jedney, Horn River, and Prophet River). The total power generation potential of all four areas is determined to be 107 MW. Volume normalized reservoir potentials range from 1.8

to 4.1 MW/km^3. The required geothermal brine flow rate to produce 1 MW of electric power ranges from 27.5 to 60.4 kg/s.

The third study investigates electricity impacts of electrifying space heat and road transportation using a portfolio of renewable energy sources. The Metro Vancouver Regional District in British Columbia serves as a case study. The district's 2016 fossil fuel demand is converted to an equivalent electricity demand at hourly resolution. The annual electricity demand of 30 TWh increases by 48% to 81%, depending on space heating efficiency. A one-year capacity expansion and dispatch model quantifies a broad range of feasible electricity system compositions. Results reveal that between 70 and 2203 km^2 of additional land area need to be designated to electricity generation to supply the additional demand. Increasing the space heating coefficient of performance from 1.08 to 3.5 halves land area impact and electricity system costs. The maximum potential 8.8 GW of rooftop solar capacity can generate up to 23% of the district's annual electrified demand. Required electricity storage capacities range from 6 to 61 GWh.

Table of Contents

List of Tables

List of Figures

Acknowledgments

First and foremost, I want to express deep gratitude and love for my partner Alicia Urquidi Diaz. I admire her ability to find structure in chaos, see solutions where others see problems, and create perspective from within the most entangled of positions. Her support created the delicate balance in life and mind that was so vital to completing this PhD program.

I thank my supervisors, Andrew Rowe and Peter Wild, for building the respectful, welcoming, supportive, and collaborative research group that has so greatly inspired the work in this dissertation. Their support for exploration of new and fascinating ideas, paired with their keen eye focused on the goal of graduation, has made this PhD program so academically rewarding.

I thank my supervisor, Bryson Robertson, for his incredible dedication to his students' success. He goes above and beyond to teach the nuts and bolts of creating and communicating research in intricate detail. Thanks to Bryson, I can now read and write about science.

I thank Susan Walton and Pauline Shepherd for deeply caring for the IESVic community and the wellbeing of each individual student. Their personal and professional support paved the road to successfully completing this PhD program.

I thank my research colleagues, Ben Lyseng, Iman Moazzen, Victor Keller, Taco Niet, Jeff English, James Donald, McKenzie Fowler, Cameron Wade, Sven Scholtysik, and Jennifer Mauel for their inspirational ideas and their personal friendship. Much of their thought and work contributed to this dissertation.

I thank Warren Walsh and Jonathan Banks for lending me their in-depth knowledge and experience on geoscience. Their support and friendship were crucial to learning about geothermal energy and beyond.

I want to thank the Pacific Institute for Climate Solutions for their kind academic and financial support.

Dedication

I dedicate this dissertation to my parents, Richard and Dagmar Palmer-Wilson, and to my grandparents, Gerhard and Ilka Radke. The weight of this work calmly rests on their unending love, support, patience and wisdom.

„Wenn die Kinder jung sind, gib ihnen tiefe Wurzeln. Danach gib ihnen Flügel.“

1 Introduction

1.1 Motivation

The 2015 Paris Agreement committed Canada and 194 other countries to limit global warming to well below 2 °C, and to pursue efforts to limit warming to 1.5 °C in comparison to pre-industrial levels. Achieving the 2 °C or 1.5 °C target requires decreasing global GHG emissions to net zero by approximately 2070 or 2050, respectively (IPCC, 2019).

In 2017, Canada emitted 716 Mt of CO_2 equivalent (CO_2e) GHGs and combustion of fossil fuel energy sources were responsible for 74% of those emissions (Environment and Climate Change Canada, 2019a). Elimination of these combustion emissions over the next 30 to 50 years will require implementation of a range of strategies across economic sectors including: reducing energy demand through conservation and improved efficiency; balancing variable supply with demand via demand side management; developing low-carbon fuels; and expanding low-carbon electricity generation (Trottier Energy Futures Project, 2016). The lowest-cost solution strategy includes decarbonizing the electricity sector and replacing fossil fuels with low-carbon electricity in the non-electric sectors (Vaillancourt et al., 2017). Challenges to implementing this strategy differ across the country. Canada's provinces vary significantly in economic activity, energy demand, energy resource potential, and existing energy infrastructure, but each province must reduce emissions to meet Canada's overall commitment.

In the coming decades, renewable energy technologies are expected to provide increasing amounts of low-carbon electricity (International Energy Agency, 2018). Land area requirements of some renewable energy sources may exceed those of fossil fuels (McDonald et al., 2009; Fthenakis and Kim, 2009; Trainor et al., 2016). However, comparing land requirements between energy technologies is sensitive to selection of spatial and temporal boundaries. Thus, the scholarly debate around the land area impact of decarbonizing electricity via renewable energy deployment is ongoing. This dissertation is motivated by the need to better understand resource options and the land requirements of rapidly reducing energy related greenhouse gas emissions in western Canada.

1.2 Outline

This dissertation investigates three selected challenges to reducing fossil fuel combustion emissions in Canada's western provinces, Alberta and British Columbia. These investigations are separate but related to the strategy of decarbonizing electricity generation and electrifying adjacent sectors. Each investigation stands on its own with limited overlap between investigations. Chapter 2 contextualises the investigations in the relevant literature.

Chapter 3 investigates alternative technology pathways and associated land requirements that decarbonize electricity generation in Alberta. Some renewable energy technologies can increase land requirements in comparison to fossil fuel based electricity generation. A long-term generation capacity expansion and dispatch model is amended to determine cost-optimal low-carbon technology compositions that reduce emissions by 90% between 2015 and 2060. Land constrained scenarios determine alternative technology pathways and costs of impacting a smaller land area. Subsequent analyses investigate the sensitivity of these results to the selected spatial and temporal boundaries of technology-specific land area impacts.

Chapter 4 investigates the sedimentary basin geothermal energy potential to quantify the contribution this dispatchable technology can make to low-carbon electricity in British Columbia. A spatial multi-criteria decision analysis identifies the most favourable areas for geothermal electricity generation in the British Columbian section of the Western Canada Sedimentary Basin. Next, the Volume Method applies a large set of petroleum production data to evaluate hydrothermal reservoir characteristics and electric power generation potential.

Chapter 5 investigates demand and supply side impacts of electrification in British Columbia's Metro Vancouver Regional District. First, the additional electricity demand of electrifying the space heat and road transportation sectors is determined from fossil fuel consumption observed in 2016. A detailed input-output model creates hourly electricity demand scenarios assuming high or low-efficiency space heating, and evening-peaking or constant-rate electric vehicle demand. Next, capacity expansion and dispatch optimization determines feasible electricity system compositions able to supply electrified demands with 100% renewable energy from combinations of urban and rural sources. A broad range of land impact costs internalize the costs of rural land area impacts not normally borne by the electricity system. This approach reveals the potential share of urban energy production within Metro Vancouver, and the minimum feasible to maximum necessary rural land area required to supply the remaining share.

Chapter 6 summarizes this dissertation's contributions to understanding the available choices and impacts of reducing fossil fuel combustion emissions. Finally, recommendations for future work identify questions that warrant further investigation.

1.3 Contributions by colleagues

Much of the work described in chapters 3 to 5 has benefited from contributions by fellow graduate students, supervisors, and researchers. Table 1-1 applies the Contributor Role Taxonomy (Allen et al., 2019) to attribute contributions by the author of this dissertation and his colleagues for each of those chapters.

Table 1-1 Attribution of contributions to chapters 3 to 5

Contributor	**Contributions**
Ch. 3 Impact of Land Requirements on Electricity System Decarbonisation Pathways	
Palmer-Wilson, K.	Conceptualization, Methodology, Software, Formal analysis, Investigation, Data Curation, Writing - Original Draft, Writing - Review & Editing, Visualization
Donald, J.	Conceptualization, Methodology, Writing - Review & Editing
Robertson, B.	Conceptualization, Methodology, Resources, Data Curation, Writing - Review & Editing, Visualization, Supervision, Project administration, Funding acquisition
Lyseng, B.	Conceptualization, Methodology, Software, Data Curation
Keller, V.	Conceptualization, Methodology
Fowler, M.	Conceptualization, Methodology
Wade, C.	Conceptualization, Methodology
Scholtysik, S.	Conceptualization, Methodology
Wild, P.	Conceptualization, Methodology, Resources, Writing - Review & Editing, Supervision, Project administration, Funding acquisition
Rowe, A.	Conceptualization, Methodology, Resources, Writing - Review & Editing, Supervision, Project administration, Funding acquisition
Ch. 4 Sedimentary Basin Geothermal Favourability Mapping and Power Generation Assessments	
Palmer-Wilson, K.	Conceptualization, Methodology, Software, Validation, Formal analysis, Investigation, Data Curation, Writing - Original Draft, Writing - Review & Editing, Visualization, Project administration, Funding acquisition
Banks, J.	Conceptualization, Methodology, Software, Validation, Formal analysis, Investigation, Data Curation, Writing - Original Draft, Writing - Review & Editing, Visualization
Walsh, W.	Conceptualization, Methodology, Software, Validation, Formal analysis, Investigation, Resources, Data Curation, Writing - Review & Editing, Supervision, Funding acquisition
Robertson, B.	Conceptualization, Resources, Writing - Review & Editing, Supervision, Project administration, Funding acquisition
Ch. 5 Renewable energy related land requirements of an electrified city: a case study of Metro Vancouver, Canada	
Palmer-Wilson, K.	Conceptualization, Methodology, Software, Formal analysis, Investigation, Data Curation, Writing - Original Draft, Writing - Review & Editing, Visualization
Niet, T.	Conceptualization, Methodology, Software, Formal analysis, Investigation, Data Curation, Writing - Review & Editing
Wade, C.	Conceptualization, Methodology, Software, Formal analysis, Investigation, Data Curation
Keller, V.	Conceptualization, Methodology, Software, Formal analysis, Investigation, Data Curation
Scholtysik, S.	Conceptualization, Methodology, Software, Formal analysis, Investigation, Data Curation
Robertson, B.	Conceptualization, Methodology, Resources, Writing - Review & Editing, Supervision, Project administration, Funding acquisition
Wild, P.	Conceptualization, Methodology, Resources, Writing - Review & Editing, Supervision, Project administration, Funding acquisition
Rowe, A.	Conceptualization, Methodology, Resources, Writing - Review & Editing, Supervision, Project administration, Funding acquisition

2 Context

2.1 Land area impacts of decarbonizing electricity generation in Alberta

Alberta can significantly reduce GHG emissions by decarbonizing its fossil fuel dominated electricity supply. In 2017, the electricity sector emitted 44.3 Mt CO_2e GHGs, second only to the 137.1 Mt CO_2e emitted by the oil and gas sector (Environment and Climate Change Canada, 2019b). Natural gas and coal fuels generated 90% of the electricity making this province the highest emitter of electricity related GHGs across Canada (Canada Energy Regulator, 2019). Alberta's Climate Leadership Plan will shut down all coal fired power plants by 2030 and procure 30% of the annual electricity demand from renewable sources (Alberta Government, 2018). This plan will reduce electricity related emissions by ~ 50% but expand the share of natural gas (Lyseng et al., 2016). Significant additional low-carbon generation capacity will be required to decarbonize electricity in Alberta.

Renewable energy, fossil fuels with carbon capture and sequestration (CCS), and nuclear energy technologies can supply low-carbon electricity. Wind, solar and, to some extent, hydro power are the most abundant renewable energy sources. Their global installed capacity will likely continue to expand in the coming decades; global investments in each of these three technologies exceed investments in nuclear or CCS technologies (International Energy Agency, 2018).

In some circumstances, renewable energy technologies require more land area than fossil fuels to provide equivalent amounts of energy (Denholm et al., 2009; Fthenakis and Kim, 2009; Ong et al., 2013). These circumstances depend on the selected spatial and temporal boundaries that delineate land area impacts of specific energy technologies. Wind power exemplifies the challenge of selecting appropriate spatial boundaries. The footprint of wind turbines is relatively small and excludes any other use. The space required between the turbines of a wind farm is fragmented by those turbines and extends over a much larger land area, but this area permits other uses like agriculture or forestry. Wind farm noise and visual appearance affect an even larger land area. Natural gas fields exemplify another spatial boundary challenge associated with the fragmentation of wildlife habitat (Jordaan et al., 2009). The linear features of natural gas infrastructure, like pipelines and seismic lines, create long edges between human and natural land areas. The effect of the edges on flora and fauna extend perpendicularly into the natural land area and thus impact a much larger area than the directly altered land.

Selecting the appropriate temporal boundary presents another challenge. Renewable energy infrastructure can continuously produce electricity without requiring additional land area. Fossil fuels extraction must relocate when an area is depleted. Depleted land areas require reclamation. Without reclamation, the cumulative land impact of fossil fuel extraction can exceed land impact by renewable energy. Since reclamation can require decades to restore original ecosystems, renewables may require less land than fossil fuels in this perspective.

Reducing GHG emissions by substituting fossil fuels with wind, solar and hydro power requires designating additional land to renewable electricity generation, although this substitution avoids designating land to fossil fuel extraction. Using land for any form of energy production changes its prior state and infringes upon other uses (Devine-Wright, 2009; Trainor et al., 2016). Public opposition to these changes can pose a barrier to rapid, large-scale deployment of low-carbon energy projects (Cohen et al., 2014; Soini et al., 2011; Sovacool, 2008).

Possible technology pathways for decarbonising electricity generation and their land area implications are not yet well understood. Several studies quantify the land area required to implement selected low-carbon futures (Arent et al., 2014; Konadu et al., 2015; McDonald et al., 2009; Wu et al., 2015) However, these studies provide limited information on alternative decarbonization pathways, their land area impact and associated costs. Investigating land area impacts of alternative low-carbon technology pathways can inform energy policy, land-use planning, and help mitigate potential conflict over competition for land.

2.2 Decarbonizing non-electric sectors with low carbon electricity in British Columbia

In British Columbia, electricity related emissions are small in comparison to Alberta. The existing low-carbon electricity supply can potentially support efforts to decarbonize adjacent sectors. In 2017, the most emissions-intensive sectors were transportation with 23.0 Mt CO_2e, oil and gas with 13.4 Mt CO_2e, and buildings with 8.2 Mt CO_2e (Environment and Climate Change Canada, 2019b). The electricity sector emitted only 0.2 Mt CO_2e because renewable sources supplied 97% of the electricity. Hydropower generated the largest share (90%); smaller shares were generated by forest biomass (6%) and wind power (1%) (National Energy Board of Canada, 2019).

Electrifying the transportation and building sectors in British Columbia may require expanding low-carbon electricity sources. British Columbia has been a net electricity importer in 7 of the 11 years between 2005 and 2015 (Canada Energy Regulator, 2015). Electrifying the transportation sector would increase British Columbia's annual electricity demand by ~ 25 TWh in 2055 (Keller et al., 2019a). This additional demand is equivalent to ~50% of the annual demand observed in 2015 (BC Hydro, 2016). Most of that additional demand must be supplied by renewable energy. The 2010 Clean Energy Act prohibits nuclear power and mandates that renewable sources generate at least 93% of the electricity in British Columbia. Electrifying the non-electric sectors in British Columbia warrants, 1) forecasting the additional electricity demand and 2) identifying additional renewable energy supply options.

2.2.1 Geothermal energy potential in British Columbia

The utility BC Hydro has identified large potential of variable renewable energy sources to supply additional energy in British Columbia (BC Hydro, 2013a). Unfortunately, high penetration of variable renewable electricity generation requires significant system flexibility, such as electricity storage or demand side management (Jenkins et al., 2018; Kondziella and Bruckner, 2016). These flexibility requirements can increase system costs. Dispatchable generation technologies mitigate the need for these flexibility requirements.

Electricity generation from geothermal energy is a potentially low-cost, low-carbon dispatchable resource with a relatively small land area requirement (EIA, 2013; Kristmannsdottir and Armannsson, 2003; Trainor et al., 2016). Globally, most geothermal electricity is generated from convection dominated high-enthalpy plays (Moeck, 2014). Exploration of geothermal energy in British Columbia has focused on these types of geothermal systems and their potential is relatively well understood. Comprehensive provincial assessments have identified the most favourable locations for geothermal development and subsequently refined potential capacity estimates from between 150 to 1070 MW (BC Hydro, 2002), to 340 MW (Pletka and Finn, 2009), to the most recent estimate of 287 MW for convection dominated locations across British Columbia (Geoscience BC, 2015). This potential is relatively small in comparison to provincial demand. Identifying additional geothermal resources may provide further opportunity to mitigate flexibility requirements.

Conduction dominated geothermal systems have received less attention in British Columbia because their lower enthalpy makes commercial exploitation less economical. These systems are commonly found in sedimentary basins. The Western Canada Sedimentary Basin (WCSB) spans from northeastern British Columbia through Alberta into Saskatchewan. Several studies indicate availability of geothermal resources in the British Columbian section of the WCSB. Kimball geospatially overlays several geological and economic criteria to identify favourable locations in the WCSB (Kimball, 2010), Walsh finds 34 MW of potential capacity at Clarke Lake (Walsh, 2013), and Geoscience BC finds 37 and 25 MW at Clarke Lake and Jedney, respectively. However, a comprehensive geothermal resource assessment that first identifies favourable locations and then estimates the electricity generation potential across the British Columbian WCSB section is not available. Such a comprehensive assessment could inform energy system planners on the availability of additional dispatchable renewable energy sources and aid decarbonization efforts.

2.2.2 Electrifying space heat and road transportation in Metro Vancouver

The Metro Vancouver Regional District (Metro Vancouver) can contribute significant GHG emission reductions to British Columbia's efforts. Metro Vancouver houses 53% of British Columbia's population and has committed to reducing emissions by 80% between 2007 and 2050 (Metro Vancouver, 2018). The City of Vancouver, the largest city in the district, plans to use 100% renewable energy by 2050 (City of Vancouver, 2015). This plan is ambitious in spite of the existing renewable electricity supply. In 2014, 69% of energy used for building heating and road transportation in the City of Vancouver were derived from fossil fuels. To achieve 100% renewable energy, the city plans to double its electricity consumption to eliminate natural gas and gasoline in the heating and transportation sectors (City of Vancouver, 2017). Use of additional renewable energy sources will be needed to achieve the district's emission reduction targets and substitute fossil fuels with electricity.

Public opposition can be a barrier to deploying new energy infrastructure in rural areas. The land and landscape impacts of renewable energy technologies can negatively affect local residents by infringing on cultural values, place attachment, and economic well-being (Botelho et al., 2016; Cohen et al., 2014; Devine-Wright, 2009; Jefferson, 2018; Jones and Pejchar, 2013; Pasqualetti, 2011; Rand and Hoen, 2017). Rural land area impacts can be reduced by deploying city-integrated urban renewable energy options. Urban options include rooftop solar, small-scale wind, biomass and waste-to-energy (Kammen and Sunter, 2016). However, comparison of renewable energy supply and demand per unit area (power density) shows that densely populated cities cannot satisfy their energy demand from urban renewable sources alone (Smil, 2019). Transitioning the building and transportation sectors to renewable energy sources will require Metro Vancouver to deploy some additional energy infrastructure in rural areas.

Several studies investigate urban renewable energy options and land area requirements to supply urban energy demands. Bagheri et al. (2018) find that a solar-wind-biomass-battery system using 22 km^2 of land area could supply the electricity demand of the City of Vancouver, but this finding might be low because monthly average wind and solar profiles supply the hourly demand. Arcos-Vargas et al. (2019) find that a solar-battery system could provide the electricity demand of Seville, Spain using 11.2 or 3.5 km² of land area, depending on battery capacity. Munu and Banadda (2016) find that ground-mounted solar using 7.6 km² of land area could supply the annual electricity demand in Kampala, Uganda. Saha and Eckelman (2015) find that biomass production on 26.6 km² of marginal land available in Boston, Massachusetts could supply 0.6% of the city's primary energy demand.

The available studies provide limited information on the potential electricity system compositions and related land area requirements able to supply electrified heating and transportation demands in Metro Vancouver. First, no study includes land required for electricity storage. Pumped storage is presently the lowest-cost long-term electricity storage technology (Schmidt et al., 2019), but its reservoirs impact a large area (Knight Piésold Ltd., 2010). Second, these studies quantify the land requirements of prescribed systems. Alternative systems that impact a smaller or larger land area may be available to system planners. Assessing the full range of feasible electricity system compositions, their land area requirements, and their costs allows system planners to make an informed choice on the composition of renewable energy technologies they deploy, and the land area this deployment will impact.

The following chapters address the gaps identified in the literature. Chapter 3 investigates land area impacts associated with alternative transition pathways that decarbonize electricity generation in Alberta. Chapter 4 shifts focus to British Columbia and quantifies geothermal electricity generation potential in the Western Canada Sedimentary Basin. Chapter 5 quantifies the electricity demand of electrifying space heat and road transportation, and renewable energy related land area impacts of alternative system compositions able to supply the electrified demand. Chapter 6 summarizes the contributions and recommendations made in this dissertation.

3 Impact of Land Requirements on Electricity System Decarbonisation Pathways[1]

3.1 Introduction

Limiting global warming to <2 °C by 2100 requires drastic reduction of carbon emissions from electricity generation by mid-century (IPCC, 2014 Figure 7.9). Globally, wind, solar and hydro power are expected to provide a significant share of carbon-free electricity for future demand. Depending on the selected boundaries, some renewable energy flows are spatially less energy-dense than concentrated fossil fuel stocks (Fthenakis and Kim, 2009; Denholm et al., 2009; Ong et al., 2013). The amount of land surface area impacted to produce equivalent amounts of electricity from renewable and non-renewable sources is an important and, often overlooked characteristic, of future energy system pathways. Given that the overall area impacted by power generation varies significantly by technology mix (Berrill et al., 2016), an increasing *land area impact* (LAI) dedicated to energy production may pose an obstacle to emission reduction pathways.

Land is always subject to some form of use, e.g. agriculture, recreation, tourism or conservation. To use land for electricity production requires changing, or at least infringing upon its prior use. This change has implications for both nature, as it can pose a threat to maintaining biodiversity, and the integrity of wildlife habitat (McDonald et al., 2009; Fargione et al., 2012; Jones and Pejchar, 2013) and people, by undermining the aesthetic and cultural value of an area (Pasqualetti, 2011; Devine-Wright, 2009). This study introduces and defines LAI as the physical footprint of the infrastructure (e.g. buildings, flooded area of a hydropower reservoir), the area between structures (e.g. area between wind turbines of a wind farm and spacing between the solar arrays), and the land area

[1] An earlier version of this chapter was published in: Palmer-Wilson, K., Donald, J., Robertson, B., Lyseng, B., Keller, V., Fowler, M., Wade, C., Scholtysik, S., Wild, P., Rowe, A., 2019. Impact of land requirements on electricity system decarbonisation pathways. Energy Policy 129, 193–205. https://doi.org/10.1016/j.enpol.2019.01.071

impacted by fuel resource mining (e.g. open pit coal mines, natural gas well pads), but excludes area for electricity transmission.

A number of studies suggest the extent of land area impacts contributes to public resistance to low carbon energy projects (Sovacool, 2008; Soini et al., 2011). This resistance can delay, or prevent, low-carbon energy projects and inhibit efforts to address climate change (Cohen et al., 2014). To overcome these barriers, energy policy and system planning must take land-use into consideration (Jaccard et al., 2011).

This study investigates emission reduction pathways for the electricity supply system while viewing land area as a constraining resource. *Pathway* refers to the technological transition of the system. The analysis identifies pathway alternatives, and the trade-off between LAI and system costs. Section 3.2 contextualizes land and energy production historically, discusses different approaches to quantifying energy related land area requirements, and reviews existing energy planning literature that consider land. Section 3.3 describes the electricity system model and the representation of land area applied in this study. Section 3.4 describes the case study of Alberta (Canada), its modelling parameters and scenario assumptions. Results in section 3.4.2 quantitatively compare the technological evolution of the system and its LAI under unconstrained and constrained conditions, and identifies the trade-offs between LAI and system costs. Section 3.5 discusses trends in energy-related land impact, in the context of recent historic developments, and compares the forecast magnitude of change to similar energy planning studies. Section 3.6 concludes with policy implications for plans that aim to reduce carbon emissions.

3.2 Land use in the context of energy production

There exists a knowledge gap in the land area impact of electricity supply system decarbonisation, and feasibility of technological alternatives that reduce the expansion of land designated for energy production. First, this section will explain the historic and future relevance of land and energy production. Second, the challenging task of defining relevant land area impacts for different types of electricity generation technologies is explored, and the use of *footprint + spacing* in this work justified. Finally, a brief review will summarize previous approaches to analysing LAI in energy planning studies.

Historically, industrializing societies shifted from using spatially dispersed fuels (e.g. wood and other biomass) to spatially concentrated energy dense subterranean fossil fuel stocks (e.g. coal and oil). This shift reduced the LAI per unit energy production and permitted enormous expansion of energy use (Huber and McCarthy, 2017). More recently, transitions to more spatially dispersed, lower energy density wind and, to some extent, solar energy flows reverse this trend, leading to a larger LAI to meet electricity demands (McDonald et al., 2009; Wu et al., 2015; Trainor et al., 2016; Berrill et al., 2016).

Expanding transmission to connect distributed renewable electricity generation compounds the land area impacts effect, because renewable sources are more decentralized and location dependent than thermal generation (Sovacool, 2008). Electrifying the transportation and heating sectors will add to the land area challenge (Williams et al., 2012; Wei et al., 2013). In conclusion, rapid and extensive deployment of low-carbon electricity production may require the use of an unprecedented amount of land area in the coming decades (Smil, 2010; Huber and McCarthy, 2017).

Different power plant types, and their different impact on land, make comparison of land area impact challenging. A consistent method to selecting spatial and temporal boundaries around specific energy technologies has not yet emerged in the literature, but this work identifies three common approaches to quantify land impacted by energy production: *footprint*, *footprint + spacing*, and *life-cycle* land requirement. The latter is subdivided into *land occupation*, a metric for land that is continuously occupied, and *land transformation*, which describes land area transformed from a reference state.

The *footprint* approach includes land area covered by power plant infrastructure, such as buildings, roadways, flooded area of a hydroelectric reservoir or the base of a wind turbine, and area used for fuel extraction, e.g. coal mines or natural gas production facilities. This methodology has been sufficient for fossil fuels based systems, its application to future variable renewable energy systems can be problematic. For example, the footprint approach does not capture the significant amount of land infringed upon by the spacing between turbines of a wind farm, where minimum distances between turbines are required to avoid efficiency losses and mechanical fatigue.

The *footprint + spacing* approach includes land required for spacing the turbines of a wind farm, or spacing between panels in solar farms. Such spacing land may still be available for agriculture, but excludes residential or recreational use and can disturb and fragment wildlife habitat. Several works have applied both the footprint and the footprint + spacing method to account for land, e.g. (McDonald et al., 2009; Jacobson, 2009; Ong et al., 2012; Ong et al., 2013; Wu et al., 2015; Trainor et al., 2016). In the work reported here, the magnitude of Land Area Impact (LAI) is defined by the *footprint + spacing* approach. Electricity transmission related LAI is not included in this study.

The *life-cycle* approach includes the footprint, and up- and downstream value chain land impacts of converting energy resources to usable forms of energy. The value chain includes the manufacturing, construction and decommissioning processes executed before and after the operational life of a power plant. These processes and their impacted land areas may include mineral mining land, temporary construction areas, and decommissioning sites. This life-cycle approach is applied by (Hertwich et al., 2014; Berrill et al., 2016). Although this work includes some elements of the life-cycle approach (i.e. fuel extraction) this approach is not adopted consistently in this study for two reasons. First, life-cycle assessments typically exclude the spacing land, and in doing so may underestimate the effect on the aesthetic and cultural value of an area. Second, up- and downstream value chain impacts may occur outside of the energy system's jurisdiction, e.g. mineral mining. Although fuel imports from outside the jurisdiction would also qualify for exclusion under this reasoning, in this study all fuels are assumed to be produced within the study region and are therefore included in the footprint + spacing approach to LAI.

Two methods accounting for available land in energy planning studies exist. The first method post-processes land area impacts exogenously. The second method endogenously limits land area impacts within the model.

The *exogenous* method indicates that land area impacts of decarbonized energy systems vary significantly by technology mix and may exceed available land area (McDonald et al., 2009; Hertwich et al., 2014; Wu et al., 2015; Konadu et al., 2015; Berrill et al., 2016; Waite, 2017). McDonald et al. (2009) examine four US energy and greenhouse gas policy scenarios and conclude that, between 2006 and 2030, up to 290,000 km² of new land area may be impacted by energy developments. Hertwich et al. (2014) compare environmental impacts and construction material requirements of two European energy system scenarios, and conclude that life-cycle land occupation differs by 150% or ~220,000km² in 2050 between these scenarios. Arent et al. (2014) quantify land-use implications of reducing U.S. electricity emissions by 80% and estimate the additional land-use to be between 44,000 to 88,000 km². Wu et al. (2015) spatially map land requirements of five California energy system scenarios and conclude that insufficient land is available outside of environmentally sensitive areas to implement its 2050 'high renewable energy' wind capacity. Konadu et al. (2015) investigate land impact of the U.K.'s Carbon Plan and show that decarbonisation pathways significantly increase competition for land from bioenergy crop production. Berrill et al. (2016) show 44 European electricity scenarios to vary in annual land occupation from 40,000 to 600,000 km². Waite (2017) suggests that degraded land, e.g. contaminated or disposal sites, may host a large share of wind and solar installation demanded by US renewable portfolio standards. All the mentioned studies post process land requirements of decarbonisation pathways, so these studies provide limited information on feasible decarbonisation pathways when competition for land exists.

The *endogenous* method that limits land area impacts within the model has been applied exclusively within the context of bioenergy crop production. Welsch et al. (2014) and Hermann et al. (2012) determine energy system mixes, irrigation requirements and optimal domestic bioenergy crop production for Mauritius and Burkina Faso, respectively. Both studies highlight the benefit of linking energy, land use and water, such that a disparate assessment can overestimate the benefits of bioenergy crops. However, land requirements for other energy technologies are not included in these studies, so the knowledge gap of feasible decarbonisation pathways where competition for land exists remains.

3.3 Methodology

This study investigates long-term pathways to decarbonize electric power systems while recognizing that land is a constrained resource, and competition for land arises from expanding land use for energy production. The investigation is performed by optimizing power plant capacity expansion and dispatch while forcing annual system emissions to decline ~ 90% by 2060 (IPCC, 2014 Figure 7.9). The bottom-up, linear programming model OSeMOSYS (Howells et al., 2011) is amended by *land area impact factors* and optional land area constraints to: 1) quantify land area impacts associated with electricity production, and 2) to investigate alternate technology mixes and the cost trade-off in land-constrained scenarios.

The OSeMOSYS model is well suited for this analysis and has been applied in similar studies, e.g. on the effects of carbon taxes (Lyseng et al., 2016), electricity trade (Taliotis et al., 2016; English et al., 2017; Pinto de Moura et al., 2017), and emissions uncertainty (Niet et al., 2017).

3.3.1 Electricity system model

The OSeMOSYS model must meet an exogenously defined electricity and capacity demand within every point in time of the chosen modelling period. The model can install generators and dispatch them to meet the electricity demand. The capacity demand is met when dispatchable (i.e. non-variable) generator capacity matches annual peak electricity demand plus a chosen reserve margin. The optimization minimizes total net present system cost over the entire modelling period at an annual 6% discount rate. Costs include newly installed capacity (capital cost), generator dispatch (operating costs) and resulting greenhouse gas emissions (carbon tax). Long-term carbon emission reduction goals (i.e. exogenous annual carbon emission constraints) drive the model to decarbonise the electricity mix.

The model can choose to install and dispatch any of thirteen conventional, low-carbon or renewable technologies, as shown in Figure 3-1. Conventional technologies are Coal, Combined Cycle Gas Turbines (CCGT), Open Cycle Gas Turbines (OCGT), Co-Generation (COGEN), and Reciprocating Internal Combustion Engines (RICE). Conventional technologies emit carbon dioxide. Emissions depend on dispatched electricity production and the exogenously defined efficiency of converting coal and natural gas resources to electricity. Low-carbon technologies apply carbon capture and sequestration (CCS) to conventional generators. Coal-CCS and CCGT-CCS reduce emissions by 90% and 80%, respectively. Renewable technologies include Biomass, Hydro, Geothermal, Wind, and rooftop or ground-mounted Solar; all of which are assumed to emit zero carbon dioxide. Electricity storage is explicitly not included in this model to avoid introducing additional uncertainty related to future costs and performance of that technology.

Performance characteristics of thermal generator technologies, i.e. heat rates, remain constant throughout the modelling period, in line with the Annual Energy Outlook published by the Energy Information Administration (2017a). Improvements in wind and solar technologies are captured via declining capital costs based on forecasted learning rates (National Renewable Energy Laboratory 2017).

The capacity demand can be met by installing any generator technology, except solar, because this technology does not supply electricity when demand peaks in evening hours. Wind contributes 15% of its capacity to the capacity demand, based on spatial diversity and a conservative interpretation of Voorspools and D'haeseleer (2006). Wind and solar are not dispatched by the model, but generate electricity based on exogenously defined profiles.

The model formulation allows for the representation of different wind and solar "regions" and corresponding generation profiles to capture the benefits of spatial distribution. Electricity transmission constraints within the model jurisdiction and trade with other jurisdictions is disregarded. Hence, all electricity demand and generation occurs at a single, isolated node.

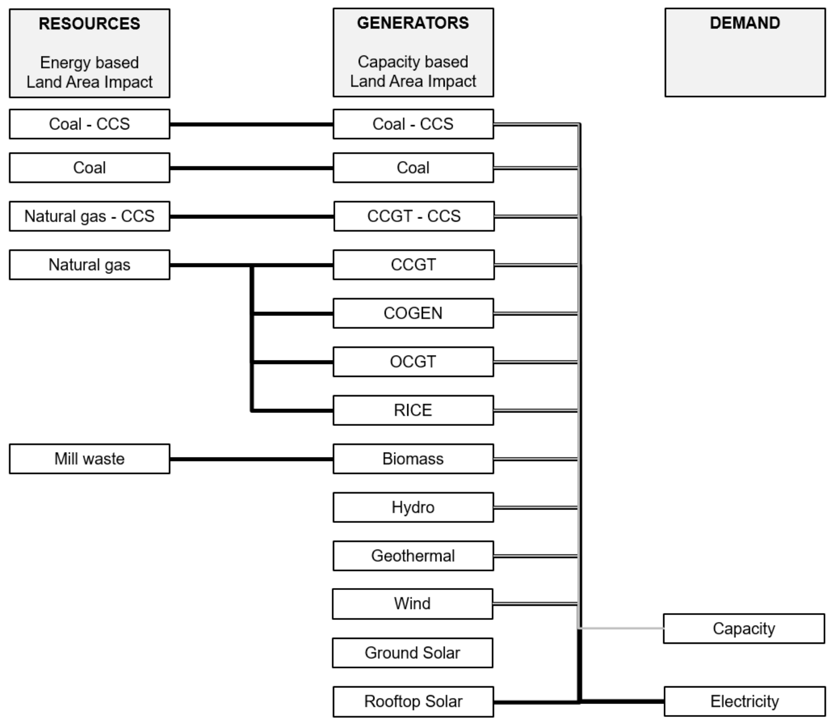

Figure 3-1. Representation of the electricity supply system model. Dispatching installed generators uses fuel resources to fulfill the electricity demand. Installing dispatchable generators can fulfill the capacity demand. Solar power is not dispatchable, and wind contributes only 15% of its installed capacity to the capacity demand. Installed capacity and generator dispatch are decision variables. Use of resources impacts land area dependent on energy production. Installation of generators impacts land area based on installed capacity. CCS versions of coal and natural gas fuels are modelled separately to include the additional land required for carbon sequestration.

The model's temporal representation is simplified to reduce computational complexity. Rather than modelling every hour for the chosen modelling period, each model year consists of six representative days. Each representative day consists of eight time slices selected by *k-means clustering*, as described in Supplementary Information section 3.7.2. Representative days are scaled to match total annual electricity demand and generation from renewable sources. This approach reduces complexity significantly while preserving variability of demand and generation.

3.3.2 Land area constraint implementation

This study defines land area impact (LAI) as the amount of land area directly impacted by power plant infrastructure and fuel extraction. The definition includes spacing between infrastructures, as discussed in the paragraph on *footprint + spacing* in section 3.2. LAI of electricity transmission is not included. Power plants impact land area based on both installed capacity (km^2/GW) and fuel resource consumption (m^2/GWh).

The *total land area impact* ($LAI_{tot,y}$) in any given year is determined by:

$$LAI_{tot,y} = \sum_{G} \left(LAI_{C,G} \times C_{G,y} + LAI_{E,R} \times E_{G,y} \right) \quad \forall G \tag{3.1}$$

where $LAI_{C,G}$ is the *capacity land area impact factor* of generator *G*, and $C_{G,y}$ is the installed capacity of generator *G* in model year *y*. $LAI_{E,R}$ is the *energy land area impact factor* of fuel resource *R*, and $E_{G,y}$ is the electricity produced by generator *G* in model year *y* using fuel resource, *R*.

A constraint can be placed on the total annual land area impact. This constraint simulates the effect of limiting the spatial expansion of land designated for electricity production. Maximum LAI values are exogenously defined for every model year. The total LAI in the first model year $LAI_{tot,y=1}$ determines the base value. Constraint values for subsequent model years $LAI_{max,y}$ are a function of compounded increase of this base value such that

$$LAI_{max,y} = LAI_{tot,y=1} \times (1+i)^{y} \qquad with\ y > 1 \tag{3.2}$$

where i is the permitted annual LAI increase. Note that $LAI_{max,y}$ values are only based on LAI observed in the first model year, but do not account for observed LAI in subsequent model years. This implementation method preserves the linear formulation of the objective function and reduces computational complexity.

3.3.3 Land Area Impact factors caused by installed generators and fuel mining

Land area is impacted by the footprint + spacing requirements of the electricity supply infrastructure. Table 3-1 lists capacity ($LAI_{C,G}$ in km²/GW) and energy LAI factors ($LAI_{E,R}$ in m²/GWh) applied to generator technologies and fuel resources. The factors can vary between power plants of the same technology type due to different possible configurations. For example, a thermal plant with a once-through cooling system may require less land area than evaporative cooling, or the spacing between turbines of a wind farm may vary by geographic setting. The range of 25th percentile, median and 75th percentile values captures that variability.

Capacity LAI factors vary by two orders of magnitude between renewable generator technologies (except biomass) and the fossil fuel / low-carbon generators. This variation results from spacing requirements and the natural low energy density of renewable energy flows. Comparison of scenarios with exclusive application of 25th, median, or 75th percentile values revealed that LAI of low-carbon, biomass power plants and fuel resources is negligible in comparison to LAI of the remaining renewable generators. Hence, this study does not apply 25th, median or 75th percentile values consistently across technologies, but selects 75th percentile LAI factors for conventional, low-carbon, biomass power plants and fuel resources. This approach leads to a comparison of renewables to a 'worst case' fossil fuel land impact, where LAI of renewables still vastly exceeds that of fossil fuels.

Underlined LAI factors are used to generate the results shown in section 3.4.2. Values not underlined do not inform those results, but are listed to provide a sense of the variation magnitude. LAI factors are chosen based on an exhaustive study of relevant literature (Robeck et al., 1980; Pimentel et al., 1994; Gagnon et al., 2002; Idaho National Laboratory, 2006; Denholm et al., 2009; McDonald et al., 2009; Fthenakis and Kim, 2009; Ong et al., 2012; Ong et al., 2013; Trainor et al., 2016; Cheng and Hammond, 2017; Jordaan et al., 2017; International Renewable Energy Agency, 2017). Literature is deemed relevant when LAI factors are quantified using a footprint + spacing method. LAI factors are selected from those studies using two qualitative criteria. First, the method to producing the LAI factors must be well documented and reproducible. Second, the infrastructure components included in the LAI factors must be comparable between technologies.

Capacity LAI factors of renewable generators are based on Trainor et al. (2016), who surveyed literature to compile a comprehensive dataset of technology specific LAI factors. The source data includes 32 solar farms with a rated capacity greater than 20 MW and 161 wind farms (Ong et al., 2013), 70 geothermal plants (Ong et al., 2012) and 47 hydropower reservoirs (United States Geological Survey, 2014). Energy and capacity LAI factors of coal are based on Fthenakis and Kim (2009) and Robeck et al. (1980), who compile data from several studies by the United States Department of Energy, and coal mine permitting and reclamation data. These energy LAI factors of coal are based exclusively on surface mining averages of several U.S. states. The coal seam thickness significantly varies the impacted land area per coal energy mined. Natural gas energy and capacity LAI is based on Jordaan et al. (2017), who interpret satellite images of the Barnett shale infrastructure in Texas, United States. Note that spacing between natural gas infrastructure and the relatively large area impacted by edge effects (Jordaan et al., 2009) are excluded from LAI in this study. Capacity LAI of carbon capture and sequestration assumes a 25% reduction in net capacity, due to parasitic load of carbon dioxide removal (Rochelle, 2009). Energy LAI of carbon capture and sequestration is added to the LAI of fuel production. CCS energy LAI factors assume subterranean reinjection of gaseous carbon dioxide and therefore an infrastructure with LAI equivalent to that of natural gas production. For all technologies, the temporary land area impact during construction, and land impacts from mineral mining and decommissioning of power plants, is excluded.

Table 3-1. The selected LAI factors applied to generator technologies and fuel resources are underlined. 25th percentile, median and 75th percentile values capture the variability of land area impacts between power plants of the same technology type. Supplementary Information section 3.7.1 contains a full description of infrastructure components included in LAI factors of each technology.

Generator Technology	Capacity $LAI_{C,G}$ (km^2/GW)			Source
Percentile	**25th**	**Median**	**75th**	
Wind	202.3	368.3	465.4	(Trainor et al., 2016)
Ground Solar	28.2	34.4	38.9	(Trainor et al., 2016)
Rooftop Solar	0	0	0	No additional land needed
Hydro	23.9	84.6	321.9	(Trainor et al., 2016)
Geothermal	16.2	38.8	82.9	(Trainor et al., 2016)
Biomass	1.3	2.0	4	Coal (no sources)
Coal	1.3	2.0	4.0	(Robeck et al., 1980)
Coal-CCS	1.7	2.5	5.0	(Rochelle, 2009)
RICE	0.2	0.3	1.8	CCGT (no sources)
CCGT	0.2	0.3	1.8	(Jordaan et al., 2017)
CCGT-CCS	0.3	0.4	2.2	(Rochelle, 2009)
SCGT	0.2	0.3	1.8	CCGT (no sources)
CoGen	0.2	0.3	1.8	CCGT (no sources)
Fuel Resource	**Energy $LAI_{E,R}$ (m^2/GWh)**			
Percentile	**25th**	**Median**	**75th**	
Coal	63.9	124.2	270.3	(Fthenakis and Kim, 2009)
Coal-CCS	128.7	268.3	536.8	Coal + N. Gas infrastruct.
Natural Gas	64.8	144	266.4	(Jordaan et al., 2017)
Natural Gas-CCS	129.6	288	532.8	double N. Gas infrastruct.
Mill Waste	0	0	0	waste stream

3.4 Case Study: Alberta electricity system

The fossil-fuel dominated Canadian province of Alberta lends itself to an investigation of the effects of decarbonising an electricity system. In 2017, 87% of electricity production was fossil fuel based. The province is planning an extensive energy transition in the coming years. Key policy instruments driving the plan are an increase in carbon taxes to 50 $/tCO_2$ by 2022, mandated decommissioning of all coal-fired power plants by 2030 (Alberta Government, 2018), and an increasing penetration of renewables.

To investigate the electricity system transition, this study models future scenarios for the period from 2016 to 2060. The investigation builds upon the OSeMOSYS model used by Lyseng et al. (2016). Updates include the 2015 capacity of the power plant fleet, technology and fuel costs of natural gas and coal (Energy Information Administration, 2017b), resource limits and capacity factors of wind, hydro, biomass, and geothermal. Additions include land area impacts and constraints, and a carbon cap that limits annual system emissions. Aforementioned policy instruments are reflected within the model formulation.

The existing 2015 capacities, future maximum capacity and fuel resource limits are described in Table 3-2. Existing capacities decline in accordance with an exogenously determined retirement schedule. This schedule is based on power plant specific commissioning years and expected lifetimes. Maximum capacities for each technology vary throughout the modelling period, and reflect the unique policy or resource availability in Alberta (e.g. coal, biomass, CoGen, geothermal), and development lead times (e.g. hydro). The maximum annual capacity expansion per technology is limited to 5% of the annual average load to reflect the economy’s ability to gradually, rather than instantaneously, deploy large quantities of generation capacity.

Generator technologies have associated capital, fixed and variable costs available from the U.S. Energy Information Administration Energy Information Administration (2017a). Generator specific emissions intensities result in additional operational costs to cover carbon taxes.

Table 3-2. Existing generator capacities in 2015, and justification of capacity limits provided to the power system model. Data is publicly available from the Alberta Electric System Operator (2018). Details regarding lifetimes and expected decommissioning are available in Lyseng et al. (2016).

Technology	2015 Capacity (MW)	Notes on Capacity Limits
Wind	1463	-
Hydro	894	2.3 GW max in 2034, stepped to 3.3 GW in 2050
Biomass	404	Fuel limit based on forestry industry
Coal	6290	Capacity declines with expected/mandated retirements
CCGT	1716	-
SCGT	996	-
CoGen	4502	CoGen capacity is limited by the heat demanded by bitumen extraction and processing
Geothermal	None	Geothermal capacity is limited to medium temperature (80 – 150 °C) resource estimates of 1.1 GW (Banks and Harris, 2018)

Four separate ‘wind regions’ are defined to reflect the spatial variability of wind power generation within Alberta. Wind regions are delineated by comparing historic correlations of wind farm power output, and to reflect different geographic terrains (Alberta Electric System Operator, 2007). Generation profiles, capacity factors and the implied levelized cost of wind energy differ between regions. Generation profiles are based on historical data of four selected wind farms with capacity factors between 33 and 35%. Solar power generation is based on a single region, because hourly solar power output varies little with spatial diversity in Alberta. Solar power generation profiles are temporally identical, but scaled to a capacity factor of 29 and 18% for ground based (single-axis tracking) and rooftop (fixed tilt) solar generators, respectively. Wind capital costs decline by 15% and 20% by 2030 and 2050, in comparison to 2015 values; rooftop and ground-mounted solar capital costs decline 2.5% annually (National Renewable Energy Laboratory, 2017).

The annual electricity demand is based on values forecasted by the Alberta Electric System Operator (2017) until 2037, and an annual 1% demand growth thereafter. The capacity demand requires an 18% reserve margin above annual peak load, in line with historical requirements.

3.4.1 Scenarios

The study investigates impacted land area associated with different decarbonisation pathways; a pathway represents a temporally coherent evolution of technologies. First, the reference scenario determines the cost optimal pathway when LAI is unconstrained. Then, six LAI-constrained scenarios limit the annual compounded LAI increase (i in eq. 3.2) to 5%, 4%, 3%, 2%, 1% and 0%. LAI constraints are exogenously defined as discrete annual values, where the LAI value of the first model year is equal to that of the reference scenario.

All scenarios apply an exogenously defined carbon cap to equally reduce carbon dioxide emissions by ~90%. The cap limits annual emissions to 50 Mt CO_2 between 2015 and 2020, with subsequent linear decline to 5 Mt CO_2 by 2060. This carbon cap approximates the trend of global projected electricity generation emissions in the IPCC's RCP 4.5 climate stabilization scenario (IPCC, 2014 Figure 7.9). In Alberta, observed emissions in 2015 to 2017 were slightly below 50 Mt. The non-constraining value of 50 Mt is chosen to represent current conditions where carbon emissions are effectively unconstrained, but future emissions must decrease to meet climate change mitigation goals.

3.4.2 Results

The following sections explore changes in the electricity supply system and associated land area impacts. First, the reference scenario establishes the baseline decarbonisation pathway where no LAI constraining policies exist. Then, LAI constrained scenarios are described in terms of installed capacities and energy sources, and how these metrics deviate from the reference scenario. A snapshot of the energy system in 2060 highlights the different scenario outcomes and compares total system costs. The annual variation of carbon emissions are compared between all scenarios. Finally, a sensitivity analysis investigates observed changes when applying 1) alternative methods to quantifying LAI factors and 2) to accounting for energy LAI cumulatively.

3.4.2.1 Land area impacts of the land-unconstrained reference scenario

The reference scenario establishes the least-cost technological pathway of decarbonizing the electricity supply system when no constraint on LAI exists. Figure 3-2 shows the evolution of LAI, driven by technology-specific installed capacities and associated electricity production, from 2015 to 2060. Figure (A) shows total capacity and energy LAI where the top of the stacked area is the total land area impact. Figure (B) shows installed capacities of each generator, while (C) shows electricity production by generator. These figures reveal three important findings.

First, the characteristics of the electricity supply system can be divided into three 'eras'; a *coal era*, a *gas era* and a *cap era*. Each era is characterized by common technology trends and driving forces. During the *coal era*, Alberta policy retires coal fired electricity along the exogenous decommissioning schedule from 44% in 2015 until extinction in 2031. The *gas era* lasts until ~2044 where the majority of electricity is produced by the least-cost natural gas generators, CCGT and CoGen. The *cap era* is preceded by CCGT capacity and energy production declines, due to the need for early installation of ground-mounted solar to meet the future clean energy demands. This early installation is caused by the exogenous constraint that limits annual capacity expansion of any technology to 5% of mean electric load. Solar capacity expansion is limited by this constraint in almost all years of the gas era. Additional, but significantly smaller, expansion of wind and hydro power are caused by declining wind installation costs and relaxing the exogenous constraint on hydro capacity. During the *cap era*, the carbon cap starts limiting carbon emissions drastically (see section 3.4.2.4) and forces rapid expansion of renewable and low-carbon generators. Wind and ground-mounted solar capacity reach their exogenous expansion limits and their variable output cannot provide electricity in all time slices, so additional expansion of CCGT-CCS supplements the need for low-carbon electricity. OCGT is required to meet the capacity demand (peak load plus reserve margin as earlier defined), but does not contribute significant electricity production due to its low efficiency and higher operational costs.

Second, land area impacts increase almost tenfold, from 700 to 6750 km² between 2015 and 2060. This spatial expansion is driven by capacity expansion of wind, and to a lesser degree by solar and hydro. Wind is the main driver of LAI increases. Wind LAI factors are tenfold the solar LAI factors which are approximately tenfold the LAI factor of all other generators (except hydro). In the coal era, the impacted land area remains almost unchanged, because CCGT expansion of comparable spatial density substitutes coal fired electricity and satisfies the demand increase. LAI increases by ~ 60% within the gas era, with approximately equal contributions by ground-mounted solar, hydro and wind expansion. The expansion of hydro and its associated LAI increase is exogenously limited due to Alberta's geography and its lack of development opportunities. In the cap era, forced emission reductions cause rapid expansion of renewable and low-carbon generators, and decrease the share of natural gas fired electricity. First, lower efficiency CCGT and later higher efficiency CoGen electricity is replaced by continued expansion of solar, increasingly rapid expansion of wind and, starting mid-cap era, rapid expansion of CCGT-CCS. Wind capacity expansion causes the majority of that LAI increase, despite ground-mounted solar expansion being significantly larger in the gas era. Ground-mounted solar causes smaller but significant shares of total LAI. The vast difference in observed LAI as opposed to installed capacities is an effect of the large variability of LAI factors between generators.

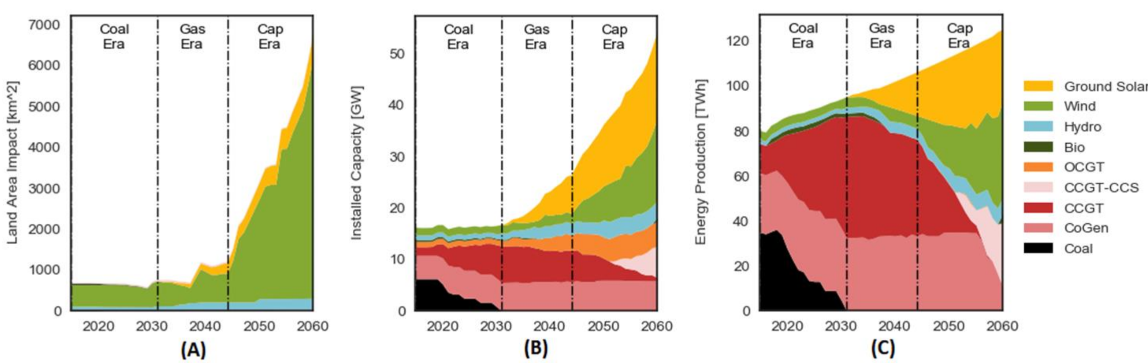

Figure 3-2. Reference scenario decarbonisation pathway from 2015 to 2060. Land area impacts (A) are dependent on installed capacity of individual generators (B) and the fuel consumed for electricity production (C). All capacity and energy based LAI are displayed on the charts, but capacity based LAI of low-carbon and fossil fuel generators and energy based LAI of fuels are so small that they do not appear visible. Note that energy LAI is accounted for only in the year where the energy is produced. This representation assumes immediate reclamation of land depleted by fossil fuel extraction. The top of the stacked energy production chart represents the electricity demand.

3.4.2.2 Decarbonisation technology changes with limited Land Area Impacts

LAI-constrained scenarios investigate electricity supply system pathways that are necessary to meet LAI and decarbonisation constraints. Figure 3-3 shows the pathways where LAI constraints become increasingly restrictive from left to right. Each vertical column in Figure 3-3 are LAI, installed capacity, and electricity production respectively. The comparison of LAI-constrained and unconstrained scenarios reveals three major trends.

First, all scenarios differ significantly from the reference scenario in the cap era, with smaller differences in the gas era. No significant differences occur during the coal era. The LAI constraints becomes binding at different times of the modelling period. LAI constraints take effect in the cap era in every scenario, because the carbon cap forces rapid expansion of renewables. In the 1% and 0% scenarios, the LAI constraint takes effect within some periods of the coal era, because rising electricity demand requires overall capacity expansion. The gas era remains unaffected by LAI constraints in all scenarios. In the 0% scenario, LAI decreases in the gas era, because the rate limit on rooftop solar expansion requires substituting wind power with zero-LAI rooftop solar relatively early in the model period.

Second, stricter LAI constraints lead to earlier expansion of spatially denser technologies. First, wind is replaced with ground-mounted solar, then ground-mounted solar is replaced with rooftop solar. This change is driven by the tenfold difference in LAI between wind and ground-mounted solar, and the absence of rooftop solar LAI. Expansion of base load CCGT-CCS mitigates the variable output and the exogenous expansion-limit of solar. Stricter LAI and carbon emission constraints make small shares of higher cost renewables (e.g. geothermal) cost-competitive.

Third, stricter LAI constraints decrease the share of renewable energy (RE) and increase low-carbon energy. The total wind and solar electricity production decreases with stricter LAI constraints. This reduced RE share results from the difference in capacity factors between these technologies. Equivalent capacity of rooftop solar produces less energy than ground-mounted solar, which produces less energy than wind. To substitute the decline in electricity production, stricter LAI constraints increase CCGT-CCS capacities and begin deployment in an earlier model year. For example, in the 0% scenario CCGT-CCS expansion begins 9 years before expansion begins in the reference scenario. In 2060, CCGT-CCS produces ~21% of total electricity in the reference scenario, but ~55% of total electricity in the 0% scenario. A small share of rooftop solar power substitutes ground-mounted solar power in the 1% scenario. In the 0% scenario, rooftop solar power substitutes a larger ~70% share of ground-mounted solar power starting at the earlier mid-gas era. These substitution effects result from the higher rooftop solar cost traded off against the LAI of ground-mounted solar technology. Less strict LAI constrained scenarios (i.e. > 1%) feature no rooftop solar power.

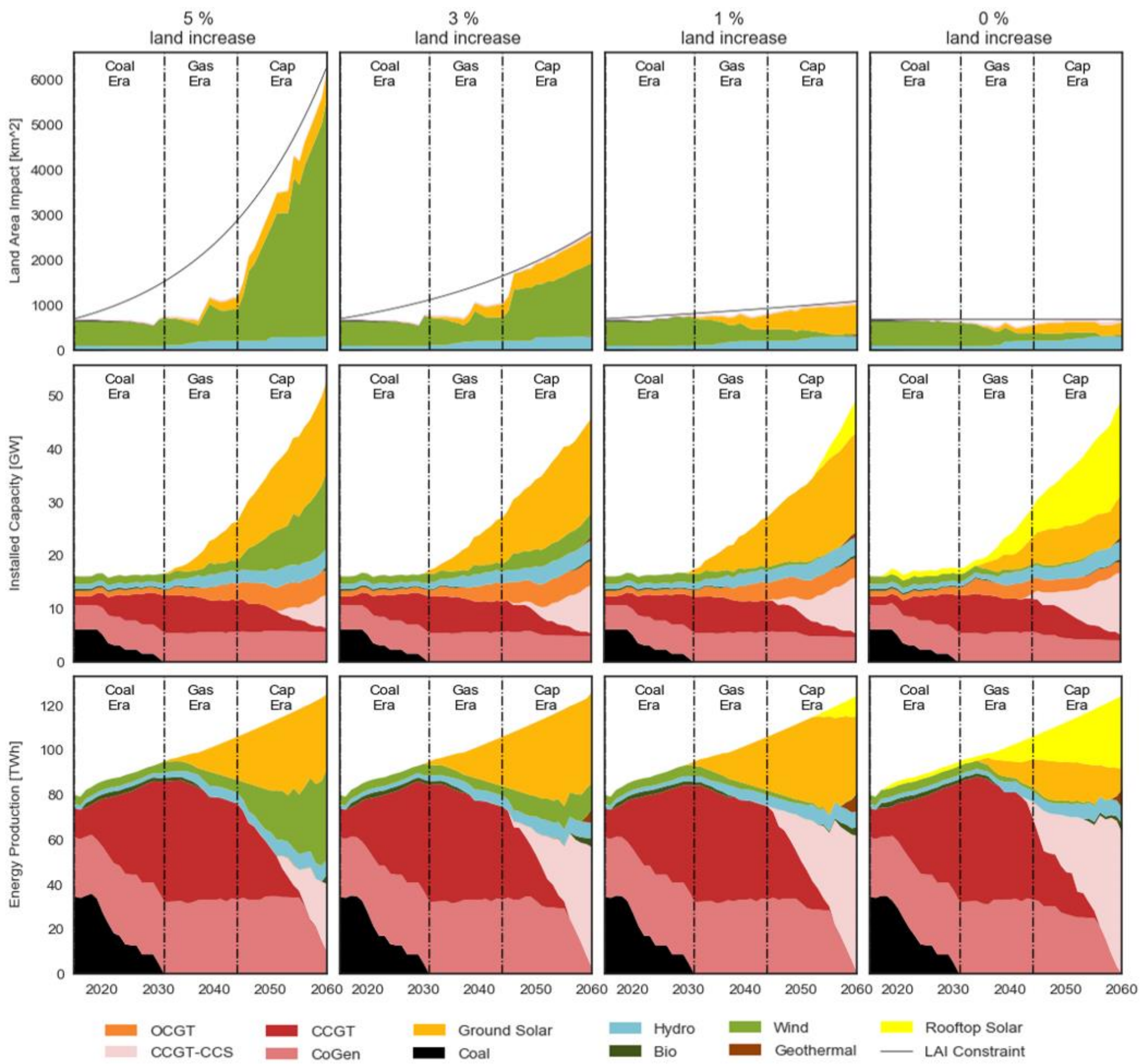

Figure 3-3. Charts within each column show decarbonisation pathways of the 5%, 3%, 1% and 0% LAI constrained scenarios. LAI increase is least constrained in the left column (5% annual increase) and most constrained in the right column (0% annual increase). Rows show observed LAI and LAI constraints (top row), installed capacities (center row) and electricity production by source (bottom row) between 2015 and 2060 within each scenario.

3.4.2.3 Comparison of final-year electricity supply systems and costs

This section compares the electricity supply systems in 2060 to highlight the different technologies deployed and the resulting total system costs. Figure 3-4 highlights the installed capacities and electricity mix trends as LAI constraints become stricter. Figure (A) shows stacked installed capacity by technology in 2060. The solid black line shows the total undiscounted system costs (capital plus operation and maintenance plus emissions costs minus salvage value) from 2015 to 2060. Figure (B) shows stacked electricity generation by technology in 2060. In (A) and (B), the left side depicts the reference scenario. LAI constraints become increasingly strict towards the right sides. This figure highlight three findings.

First, stricter LAI drives the need for spatially dense CCS. LAI constraints reduce the share of wind and increase the share of solar, especially rooftop solar. Even higher-cost geothermal energy becomes cost-competitive. LAI constraints first decrease, then increase the total installed capacity from 55 GW to 43 GW to 49 GW in the unconstrained, 2% and 0% scenarios, respectively. The decrease results from substituting lower capacity factor wind power with higher capacity factor CCGT-CCS. The increase results from substituting higher capacity ground-mounted solar with lower capacity factor rooftop solar. Note that rooftop solar capacity reaches 17.9 MW, which would be equivalent to installing 19 kW on every detached home in Alberta today; an unrealistically high value but illustrative reality check.

Second, total undiscounted system costs increase with stricter LAI constraints. The cost curve delineates the trade-off between greater LAI versus greater system costs. The increase results from deploying higher cost technologies to meet the LAI constraints. This trade-off is most notable between the 1% and 0% scenario, where a large fraction of the cost increase attributes to the higher cost and lower capacity factor of rooftop solar, which substitutes high LAI ground-mounted solar.

Third, stricter LAI constraints may lead to stranded assets, because the carbon cap forces a rapid change in technologies, leading to shorter lifetimes. This effect can be observed where CoGen and CCGT capacities remain approximately constant across all scenarios, but CCGT electricity production is nil and CoGen electricity declines with stricter LAI. CoGen is replaced with CCGT-CCS electricity due to the carbon constraint and the need to supplement the lower capacity factor of solar. Thus, the carbon cap and increasing LAI forces dispatch of the more carbon-efficient CCGT-CCS capacities.

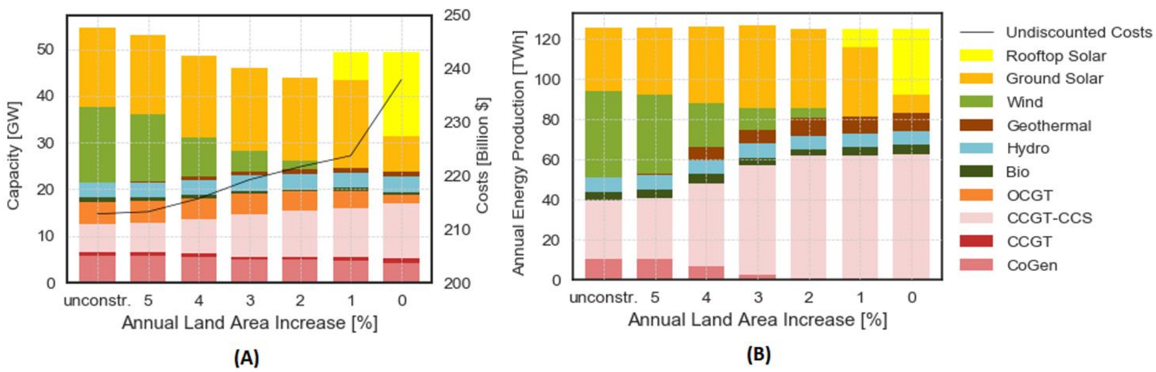

Figure 3-4. Comparison of the resulting 2060 electricity supply system between the unconstrained reference and LAI constrained scenarios. (A) shows installed capacity and total undiscounted system costs. (B) shows electricity production by source.

3.4.2.4 Pathway emissions

This section compares observed emissions between scenarios to analyze whether annual emissions differ between LAI-constrained and the reference scenario. Observed annual carbon emissions and the exogenous carbon cap are shown in Figure 3-5. This chart reveals that annual emissions follow similar decreasing trends, with little variation between scenarios.

Overall, the carbon cap forces all scenarios to reduce carbon emission by ~90% between 2015 and 2060. Emissions peak at ~48 Mt in 2018 and then rapidly decline to ~26 Mt at the end of the coal era. CCGTs replace decommissioned coal plant capacity and increase their capacity factor to meet the growing electricity demand. The lower emission factor of CCGTs (335 kg-CO2/kWh$_e$) over coal plants (1100 kg-CO2/kWh$_e$) drives emission reductions within the coal era.

In the gas era, emissions decline to ~22 Mt at a slower, steadier rate. The decline in CCGT energy production is exclusively responsible for the decline of emissions within the gas era. These emission reductions occur at a slower pace than the decline of the carbon cap, so that emissions become carbon constrained at the end of the gas era in all but the 0% scenario. The cap limits the 0% scenario as late as 2051 because the technology expansion constraint requires early expansion of CCGT-CCS to meet carbon and LAI constraints.

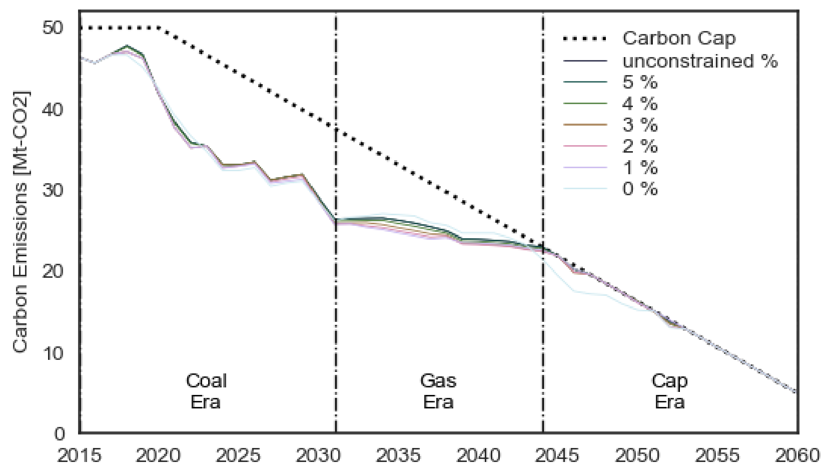

Figure 3-5. Observed carbon emissions and carbon cap between 2015 and 2060 in all LAI constrained and the unconstrained reference scenario.

3.4.3 Land Area Impact factor and accounting method sensitivity

3.4.3.1 Footprint + spacing and footprint-only LAI factors

This section repeats the analysis of previous sections, but applies LAI factors that account only for the *footprint*, instead of *footprint + spacing*. The purpose of this alternate analysis is to recognize the fact that land area impacts of different technologies manifest differently. For example, the space between wind turbines of a wind farm excludes residential uses and infringes upon ecology (e.g. bird migration or bat feeding grounds), but forestry or agriculture may still be possible here.

In this scenario, wind LAI now comprises only the surface area covered by the turbine base (3.8 km²/GW), while geothermal comprises only the well pad and the power plant (7.4 km²/GW). Prior to detailing the results presented in Figure 3-6, it is important to note that

LAI in the first model year of this scenario is ~200 km^2, significantly smaller than the same value in the footprint + spacing scenarios presented in all prior sections.

Figure 3-6 shows technology specific LAI in the reference, and the 5%, 3% and 1% LAI constrained scenarios. The bottom row shows the 2060 undiscounted total system costs and installed capacity (A) and electricity production (B). In comparison the *footprint + spacing analysis* this figure reveals differences in deployed technologies, but the overall pathway trends are similar.

In terms of technologies, solar and hydro dominate in the footprint-only LAI, while wind is negligible. Therefore, stricter LAI constraints reduce the share of wind and hydro electricity production, as opposed to reducing the share of wind in the footprint + spacing analysis. This difference is caused by the change in merit order, where solar and hydro LAI now exceed wind LAI. In terms of similar trends, LAI increases significantly between 2015 and 2060 in the reference scenario, albeit that increase is fivefold in the footprint analysis as opposed to tenfold in the footprint + spacing analysis. Costs increase by ~ 8% between the reference and the 0% scenario, and renewable energy is replaced with a higher share of low-carbon electricity.

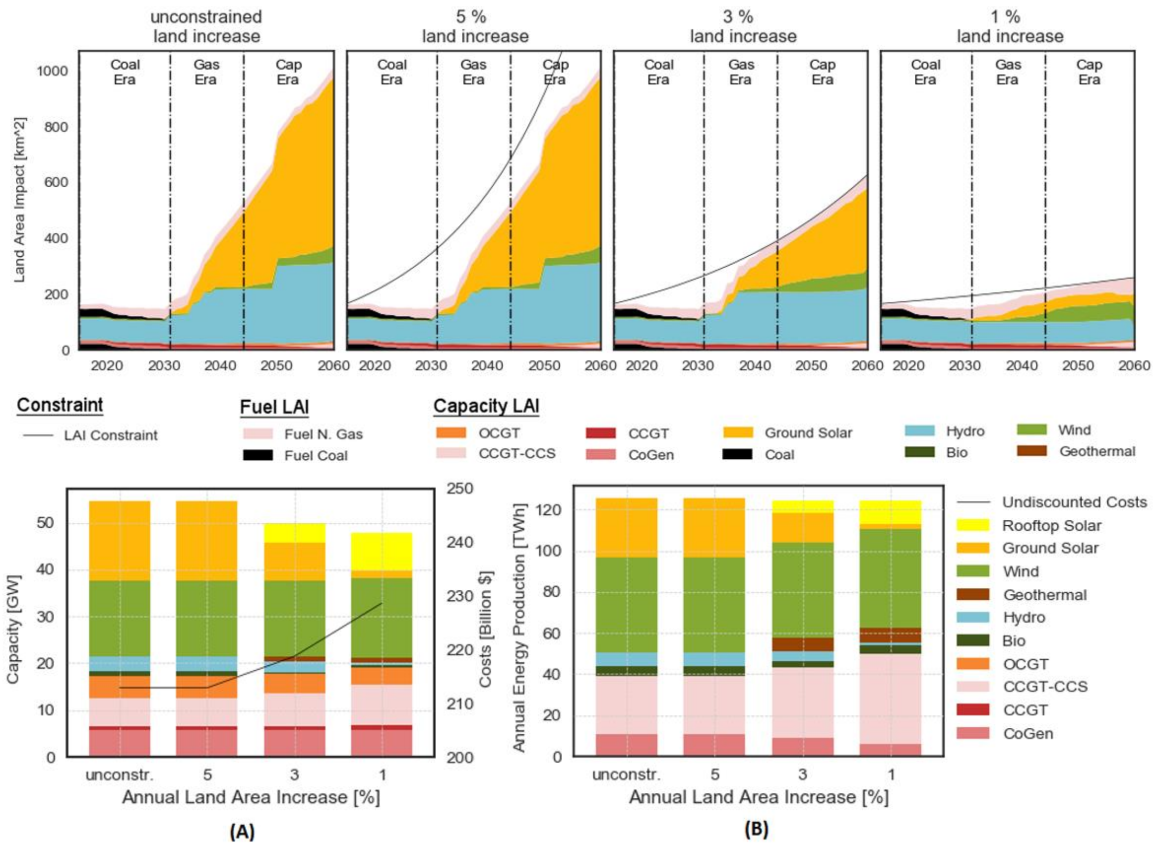

Figure 3-6. Observed LAI (top row), total undiscounted system costs and installed capacities in 2060 (A) and electricity production by source in 2060 (B) when computing results using footprint-only LAI factors.

3.4.3.2 Instantaneous and permanent energy LAI

This section reiterates results from scenarios described in section 3.4.1, but quantifies energy LAI cumulatively over the entire modelling period. This cumulative approach reflects that energy LAI may be permanent on a human timescale. Energy LAI results from mining fuel for fossil fuel generators and from sequestering carbon dioxide captured by CCS generators. Land may remain impacted long after its extracted fuel resource has been consumed or the carbon sequestered. All previous sections of this paper showed energy LAI exclusively within the year that the energy production occurs, which implies the land is available for use in the next year.

Figure 3-7 shows stacked capacity and energy LAI of the 5% and the 0% LAI-constrained scenarios where energy LAI is permanent. This figure reveals that assumed permanence drastically changes the significance of energy LAI. In the previous scenarios energy LAI was negligible. In contrast, permanent energy LAI from natural gas generators exceeds all other LAI in the 0%, and is significant even in the 5% scenario. Nevertheless, the total observed LAI from renewable sources in the 5% scenario exceeds the LAI from fossil fuels in the 0% scenario. Note that permanent energy LAI exceeds the constraint, because results presented here are the same results presented in previous sections with the additional step of cumulating energy LAI over the modelling period.

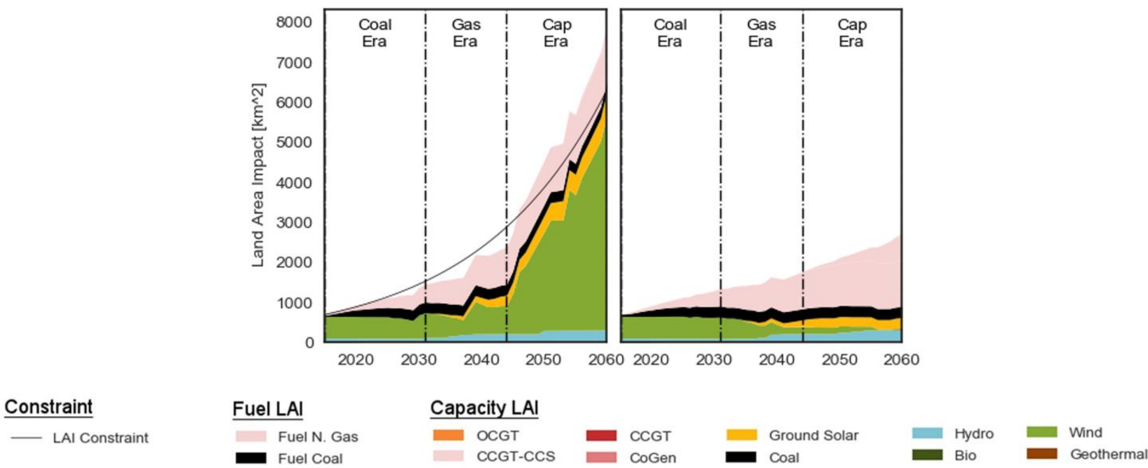

Figure 3-7. Land area impacts of 5% and 0% LAI increase scenarios are shown in the left and right column, respectively. These results differ from Figure 3-2 and Figure 3-3 by their representation of energy LAI. Here, energy LAI is cumulatively quantified throughout the modelling period, whereas all previous results show energy LAI only within the year where the respective electricity is generated.

3.5 Discussion

This study investigates associated land area impacts (LAI) of decarbonisation an electricity supply system. First, a reference scenario establishes the technological pathway under land-unconstrained conditions. Then, higher-cost alternate pathways with smaller land area impacts but similar carbon emissions are identified. Finally, the sensitivity analyses vary the selected spatial and temporal boundaries that define energy technology-specific land area impacts.

In comparison to current systems, a significantly larger land area will be impacted by a decarbonizing electricity generation using a large share of wind and solar. The reference scenario shows a tenfold increase in LAI by 2060, or ~0.92% of Alberta's total land area in 2060. These results are in line with Jacobson and Delucchi (2011), who suggest that all of earth's 2030 energy requirements using mostly solar and wind power would impact 1.9% of global land area. Although transmission related land area impacts have been excluded in this study, it is important to note the increased transmission requirement that results from geographically dispersed wind and solar generation will undoubtedly greatly increase the amount of land utilized for the greater energy system. Residents perceive transmission infrastructure negatively (Soini et al., 2011), and transmission expansion has been shown to decrease residential property values (Sims and Dent, 2005). While technically possible, utilizing vast swathes of land area may therefore increase the public resistance to the low-carbon energy transition (Breukers and Wolsink, 2007).

For a global perspective, Germany's recent power system transformation confirms the massive expansion of land impacted by renewable energy expansion. Between 2002 and 2017, installed capacities of on-shore wind increased from 12 to 51 GW and ground-mounted solar increased from 0.01 to 11 GW, but electricity demand has remained relatively flat. The electricity supply system's LAI in Germany has increased from 1.5% (5255 km^2) to 5.6% (19976 km^2) of Germany's land area (when applying the same capacity and energy based LAI factors used in this study). That represents a compounded annual LAI increase of 9.3%, higher than any scenario modeled in this study. Note that this simplified analysis has several limitation. First, European LAI factors may differ from the North American LAI factors applied here. Second, Germany's electricity transition has been accompanied by a shift from imported coal to domestic surface mined coal, a decline in nuclear power and increased use of imported natural gas, so the complexity of the transition is not reflected in this simplified analysis. Third, this analysis does not account for the vast LAI caused by historical coal mining. Nevertheless, the trend of increased LAI in Germany is significant, because in spite of the rapid expansion of LAI, a renewable energy transition has been achieved in Germany so far. Factors that may have positively influenced public acceptance are development of smaller wind farms with fewer turbines, close involvement of communities, and opportunities for local residents to invest or receive community benefits from these projects. Policy makers may need to implement similarly positive factors to make the expansion of LAI publicly acceptable and enable the energy transition.

Alternatively, the LAI can be reduced at a higher total system cost. The substitution of higher cost technologies increases undiscounted total system costs from \$213 to \$238 billion dollars, or 10.5%. That equates to a cost of 4.1 M\$/km² of land area not impacted by energy production. The magnitude of this trade-off highlights the need to recognize land area impacts as a differentiating factor between decarbonisation alternatives. Energy policy should consider the trade-off between impacting a lesser land area and imposing a higher cost to consumers, because "Some residents may be willing to pay to minimize the perceived negative visual impacts of proposed wind facilities" (Rand and Hoen, 2017). Note that costs are uncertain, because scenarios with reduced LAI assume availability of CCS. That technology is not yet mature, and the cost of identifying safe carbon sinks is not included in this study. Other spatially dense technologies, e.g. nuclear power, may mitigate technological and cost uncertainty. However, public opposition remains strong, especially in the context of long-term nuclear waste storage.

The carbon cap chosen in this study approximates global electricity system emissions in line with the IPCC's RCP 4.5 climate stabilization scenario. In this scenario the atmospheric CO_2 equivalent concentrations reach 530 – 580 ppm (IPCC, 2014 Figure 7.9), which lead to a projected median global air temperature in 2100 of 2.0 – 2.3 °C above preindustrial levels (IPCC, 2014 Table SPM.1). That warming exceeds the <2°C warming goal of the Paris Agreement (European Commission, n.d.). Lower (i.e. zero) CO2 emission goals might be desirable, but the electricity system model and technologies used in this study make lower emissions pathways infeasible. This infeasibility results from the selected technological options' inability to meet demand in all time slices; primarily caused by the heavy reliance on variable wind and solar power. Grid scale storage technologies may alleviate the infeasibility. Due to this study's focus on land area impacts of electricity generation, however, the additional uncertainty from modelling the characteristics of immature grid-scale storage technology has been excluded. This is an area warranting further study.

The demonstrated method of implementing land area requirements within a long-term energy system planning model is an improvement over previous approaches. Earlier work either post-processed land requirements after the energy planning process (McDonald et al., 2009; Hertwich et al., 2014; Wu et al., 2015; Konadu et al., 2015; Berrill et al., 2016; Waite, 2017), or limited the endogenous assessment of land requirements to bioenergy crop production (Hermann et al. 2012; Welsch et al. 2014). Nevertheless, the method used for accounting for land impacts has three caveats. First, energy LAI is accounted for only in the year in which a fuel resource is used, which implies immediate reclamation of the mining site. The sensitivity study in section 3.4.3.2 shows that accounting for energy LAI cumulatively, which implies no reclamation, significantly increases the total LAI of fuels, especially natural gas. In that sensitivity scenario, technological priorities change from solar to wind and the natural gas with CCS-dominated electricity system increases LAI fourfold over the 45-year modelling period. Extending the modelling period would lead the natural gas with CCS-dominated system to exceed land area impacts of a renewable-dominated system. Second, the definition of land area impacts used in this study is punitive to wind power, because wind farms require vast spaces between turbines. Including spacing between turbines increases wind LAI factors by 2 orders of magnitude. This perspective is debatable, because spacing may infringe on some land-uses (e.g. housing, recreation) but permits others (e.g. agriculture). Third, the energy LAI specific to natural gas does not account for the associated fragmentation of wildlife habitat and vast edge effects caused by the linear characteristics of natural gas infrastructure (Jordaan et al., 2009). Comparison of these edge effects between energy technologies warrants further study. Equating footprint and spacing for all technologies is a notable limitation of this study, because it fails to differentiate between the different types of land impact. The flooded reservoir of a hydroelectric dam may create new recreation space, where an open pit coal mine excludes any other use for humans and wildlife alike.

This study's definition of LAI differs from *land occupation* typically applied by life-cycle studies. Mineral mining, temporary construction, disposal impacts and secondary effects like wildlife habitat fragmentation and degradation are excluded in LAI factors. In contrast, LAI factors include land area required for spacing wind turbines and solar arrays. Spacing land area is typically excluded in life-cycle studies. Nevertheless, Berrill et al. (2016) find life-cycle *land occupation* to vary by a factor of 4.7 between renewable and natural gas based European electricity system scenarios – a difference of similar magnitude found in the work presented here.

3.6 Conclusion and Policy Implications

Limiting global warming to <2 °C by 2100 requires drastic reduction of carbon emissions from electricity generation by mid-century (IPCC, 2014 Figure 7.9). Globally, wind and solar power are expected to provide a significant share of carbon-free electricity for future demand. Designating sufficient land area to harnessing these dispersed renewable energy flows may present a barrier to the public acceptance of this transition.

This study amends a capacity expansion and dispatch model to enable investigating trade-offs between decarbonisation pathways and land area impacts under carbon emission constrained futures. A case study of the Canadian province of Alberta provides a reference to global decarbonisation efforts. With an 87% fossil fuel share in 2015, their electricity generation will undergo a significant transition in the coming decades. As outlined in the government's Climate Leadership Plan (Alberta Government, 2018), the electricity sector will include carbon taxes of 50 $/tCO_2$ by 2022, and all coal-fired power plants must be decommissioned by 2030.

Three main conclusions can be drawn from the results of this study. First, decarbonising a fossil fuel based power system via wind and solar energy can lead to a tenfold expansion of the land area impacted by electricity generation within the next 45 years. This expansion occurs because wind and solar impact a land area up to two orders of magnitude larger than fossil fuel generators. Thus, implementing wind and solar based emission reductions requires designating land for energy production at a compounded annual average rate of increase of ~5%. This estimate represents a lower bound, because dispersed wind and solar farms will require more transmission infrastructure than centralized thermal generators (Sovacool, 2008), and transmission related land area impacts have been excluded in this study. However, the tenfold expansion is highly sensitive to the selected boundaries that define energy technology-specific land area impacts. Determining definitions across different technologies that equitably represent their dissimilar impacts warrants further study. Second, this type of electricity supply system still requires substantial dispatchable capacity (if no grid-scale storage is available). In the land-unconstrained reference scenario, wind and solar provide ~60% of electricity. Nevertheless, 23% of electricity must come from fossil fuel generators with CCS, or similar low-carbon technologies, and 17% from dispatchable renewables. Third, an alternate electricity supply system that achieves similar carbon emission reductions but impacts a smaller land area is feasible, but comes at higher costs. A decarbonized system with present-day land area impacts will cost ~11% more than the least-cost wind and ground-mounted solar pathway. This low LAI system relies on low-carbon (CCS or similar) technologies for 50% of the electricity demand, includes no wind energy, produces ~35% of electricity from mostly rooftop solar, and fully utilizes the higher-cost resource potential of geothermal and biomass.

Rapidly expanding land use for energy production may increase competition for land near to resources and transmission infrastructure. This competition may result in social conflict in regard to prioritising types of land use, global versus local environmental protection, or preserving landscape character. Such conflicts pose a significant barrier to the acceptance and pace of the renewable energy transition, and thus hinder efforts to mitigate climate change. To overcome this barrier, regional or national energy policy may opt to limit the spatial impact of electricity generation by utilizing more energy dense low or zero carbon technologies like fossil fuels with CCS, or nuclear power. This option needs to be accompanied be expedient reclamation. In summary, policy support for developing more compact electricity generation or increasing land availability for electricity production, are likely necessary to significantly reduce carbon emissions and meet IPPC projections.

3.7 Supplementary Information

3.7.1 Infrastructure components included in generator technology and fuel resource LAI factors

Wind: Included factors are the footprint of the turbine base and the spacing in between turbines of a wind farm. Spacing differs between farms, based on available land and placement of turbines. For example, turbines placed in a single line, perpendicular to main wind direction require less spacing that turbines place in parallel to the main wind direction. Values in the table are 161 wind farms in the United States. (Trainor et al., 2016)

Solar: Included factors are the footprint and spacing between arrays of single axis tracking photovoltaic solar farms. Values in table are 25th / median / 75th percentile capacity weighted area values of 32 projects with an alternate current rating greater than 20 MW in the United States.

Hydro: Included factor is the flooded area by the hydroelectric dam. Run-of-river technology is not considered. 25th and 75th percentile values are sampled from 47 randomly selected dams in the United States (Trainor et al., 2016). The 'median' value here is the based on the Site-C hydroelectric dam, currently under construction in British Columbia, Canada.

Geothermal: Included factors are the entire well field, where hot fluid from several wells is piped to a central power plant location. Values in table are based on 25th / median / 75th percentile area values from 70 power plants in the United States, weighted by energy generation (Trainor et al., 2016).

Biomass: Biomass fired generators employ boiler technology that is similar to coal fired power plants. Their LAI factors are assumed equivalent to coal generators.

Coal (generator technology): Included components are powerhouse, fuel-handling system, air- and water-pollution control systems, cooling systems, stacks, and administration and laboratory buildings (Robeck et al., 1980). LAI factors are based on several power plants across the United States and were cross-checked with satellite images of the Genesee Generating Station in Alberta.

Coal-CCS (generator technology): Included components are equivalent to the coal generator. Required land area for carbon dioxide scrubbing was not available in literature. This study assumes a 25% reduction in net capacity, due to parasitic load of carbon dioxide removal (Rochelle, 2009).

RICE: Values are based on CCGT, due to lack of values in literature.

CCGT: Included components are the power plant site, access roads, and cooling water lake. Values are based on seven gas fired power plants in the Barnett shale, Texas, United States (Jordaan et al., 2017)**.**

CCGT-CCS: Included components are equivalent to the CCGT generator. Required land area for carbon dioxide scrubbing was not available in literature. This study assumes a 25% reduction in net capacity, due to parasitic load of carbon dioxide removal (Rochelle, 2009).

SCGT: Values are based on CCGT, due to lack of values in literature.

COGEN: Values are based on CCGT, due to lack of values in literature.

Coal (fuel resource): Coal fuel LAI factors include excavation area of open pit mines in Wyoming, Kansas and the Appalachia region in the United States (Fthenakis and Kim, 2009). Coal mining land area varies with coal heating value, seam thickness density and mining method. Values assume a heating value of 30000 kJ/kg. Values include 25% mass loss during preparation. Ash and sludge waste disposal area is included.

Coal-CCS (fuel resource): Included components are equivalent to the coal fuel resource. Additional land area impacted by CCS is accounted for by assuming that carbon sequestration infrastructure is similar to that of natural gas production.

Natural Gas: Included components are production sites, gathering pipelines, gathering sites, processing sites, transmission sites, and waste-water disposal sites. Data is based on satellite images of several hundred samples in the Barnett shale, Texas, United States (Jordaan et al., 2017).

Natural Gas-CCS: Included components are equivalent to the natural gas fuel resource. Additional land area impacted by CCS is accounted for by assuming that carbon sequestration infrastructure is similar to that of natural gas production.

Mill Waste: Biomass used for electricity production in Alberta is limited to lumber mill waste. Due to its waste stream nature, its LAI is disregarded.

3.7.2 Selection of representative days and time slices for reducing computational complexity

A set of representative days is produced for each model year, with these days being selected from a collection of historical days. Historical days consist of normalized hourly electrical load, wind generation and solar generation data. Each day is a single data point in a vector space that spans (N_L + N_W + N_S)*(24 hours) dimensions, where N_L, N_W, and N_S are the number of modelled load, wind and solar regions, respectively. Each historical day is assigned to one of six clusters by a k-means clustering algorithm (Lloyd, 1982). One day is selected from each cluster as representative, where the probability of selection is inverse to that day's distance from the cluster center.

Selected days are reduced from twenty-four to eight time slices. All possible combinations of time slice sets within a day are produced. Each time slice is assigned the average value of its constitutive hours. The set of eight time slices that best represent the historical day are selected by minimizing the root-mean-square error between the historical day and the resulting representative day. Time slice length can vary. For example, a representative day can consist of eight time slices of three hours each. It can also consist of seven time slices of one hour, and one time slice of 17 hours – which ever combination minimizes the error.

Each representative day is assigned to a fraction of the model year. That fraction is proportional to the cluster size from which the representative day was selected. Then, time slices are scaled such that total annual electricity demand, normalized wind generation and normalized solar generation matches historical and/or forecasted values.

4 Sedimentary Basin Geothermal Favourability Mapping and Power Generation Assessments[2]

4.1 Introduction

Geothermal energy is a baseload, renewable power source that provides ~13 gigawatts of electrical power and ~70 gigawatts of thermal power for global human consumption (Bertani 2015; Lund & Boyd 2015). The majority of this power is generated from convection-dominated geothermal systems, where point heat sources in the shallow subsurface elevate the geothermal gradient above the global mean and create circulation cells of hot, easily accessible ground water (Moeck, 2014). Convection-dominated geothermal systems are located predominantly in, or near, tectonically and volcanically active regions, and offer limited opportunities for long-term industry expansion. Recent trends in geothermal energy development have focused on conduction-dominated and low-enthalpy systems. Such geothermal systems are most commonly found in sedimentary basins and continental interiors, and are often more proximal to potential geothermal power end-users than convection-dominated systems (Moeck 2014).

A major challenge in developing new geothermal fields is the high up-front cost of exploration and resource characterization (Salmon et al. 2011). These risks are compounded in conduction-dominated and low enthalpy geothermal systems, which typically have no surface expression and host only low to mid-grade resources. Realizing the potential of these types of geothermal resources requires the development of inexpensive and expedient methods for identifying and evaluating unmeasured geothermal reservoirs.

This paper presents a two-step method for locating and quantifying the power generation potential of conduction-dominated geothermal systems hosted in sedimentary basins. First,

[2] This chapter was published in: Palmer-Wilson, K., Banks, J., Walsh, W., Robertson, B., 2018. Sedimentary basin geothermal favourability mapping and power generation assessments. Renewable Energy 127, 1087–1100. https://doi.org/10.1016/j.renene.2018.04.078

a favourability map is produced by considering the influence of several geological and economic criteria on the feasibility of constructing a geothermal power plant in a given locality. Second, the Volume Method (Williams et al., 2008) quantifies the power generation potential of areas deemed most favourable. The results reveal both the total gross power available to local end users, as well as power generation potential per unit reservoir volume.

The British Columbian portion of the Western Canadian Sedimentary Basin (WCSB) serves as a proxy for sedimentary basins with similar geothermal regimes and as a case study for this work. A nation-wide evaluation of Canada's geothermal resources identified the WCSB as an area of moderate commercial potential (Grasby et al., 2012). Localized research in the WCSB has included qualitative evaluations of specific Cambrian and Devonian formations (e.g. Weides, Moeck, Majorowicz, et al. 2013; Weides, Moeck, Majorowicz, et al. 2014; Weides, Moeck, Schmitt, et al. 2014) and power potential assessments in the Alberta foothills (Banks and Harris, unpublished results). The British Columbian portion of the WCSB has received less attention, but several areas of high geothermal potential were identified here by Fairbank et al. (1992) and Kimball (2010). Fairbank et al. (1992) applied a geothermal gradient > 45 °C to identify areas of high potential, while Kimball applied several geological and economic factors to map geothermal favourability. These studies offer relatively coarse resolution due to their Provincial scale, but warrant regionally focused research.

Two previous studies have quantified geothermal power generation potential in the British Columbian section of the WCSB by applying the Volume Method (Williams et al., 2008). Walsh (2013) investigated the Clarke Lake gas field, near the town of Fort Nelson. Geoscience BC evaluated 18 different regions throughout British Columbia (Geoscience BC 2015). That study included two sites in the WCSB, namely Clarke Lake and Jedney. Neither of these studies chose their locations based on systematic criteria; they were simply hypothesized to be potential resources. Through the two-step process of favourability mapping and quantitative resource assessment, this study is the first to provide a focused examination of the geothermal resource potential of the entire British Columbian portion of the WCSB. Similar two-step analyses of the more densely populated island of Sicily, Italy, are not applicable in the WCSB, because they do not consider proximity to energy consumers or transmission infrastructure (Trumpy et al. 2015; Trumpy et al. 2016).

The paper outlines the geological background of geothermal energy in the WCSB in Section 4.2. Methods for producing a favourability map, and input data derived from the case study area are described in Sections 4.3.1 to 4.3.3. Power generation potential estimates, methods and data are described in Sections 4.3.4 to 4.3.6. Results are described in Section 4.4 and followed by a discussion in Section 4.5. Conclusions from this work are drawn in Section 4.6.

4.2 Geologic Background of the Western Canada Sedimentary Basin[3]

The WCSB is a 600 – 1200 km wide NW – SE trending wedge of Proterozoic to modern sediment that spans over 3000 km from the Northwest Territories to Montana. The WCSB is bordered to the east by the Canadian Shield and to the west by the front ranges of the North American Cordillera, where it is greater than 5500 m deep adjacent to the mountain belt. Figure 4-1 shows the geographic location of the WCSB and surrounding geologic terranes. The study area is delimited to the west and south by the Cordilleran deformation front, to the north by the Yukon Territory border (60 °N latitude) and to the east by the Alberta border (120 °W longitude).

[3] This section 4.2 was written by Jonathan Banks, the second author of the published article.

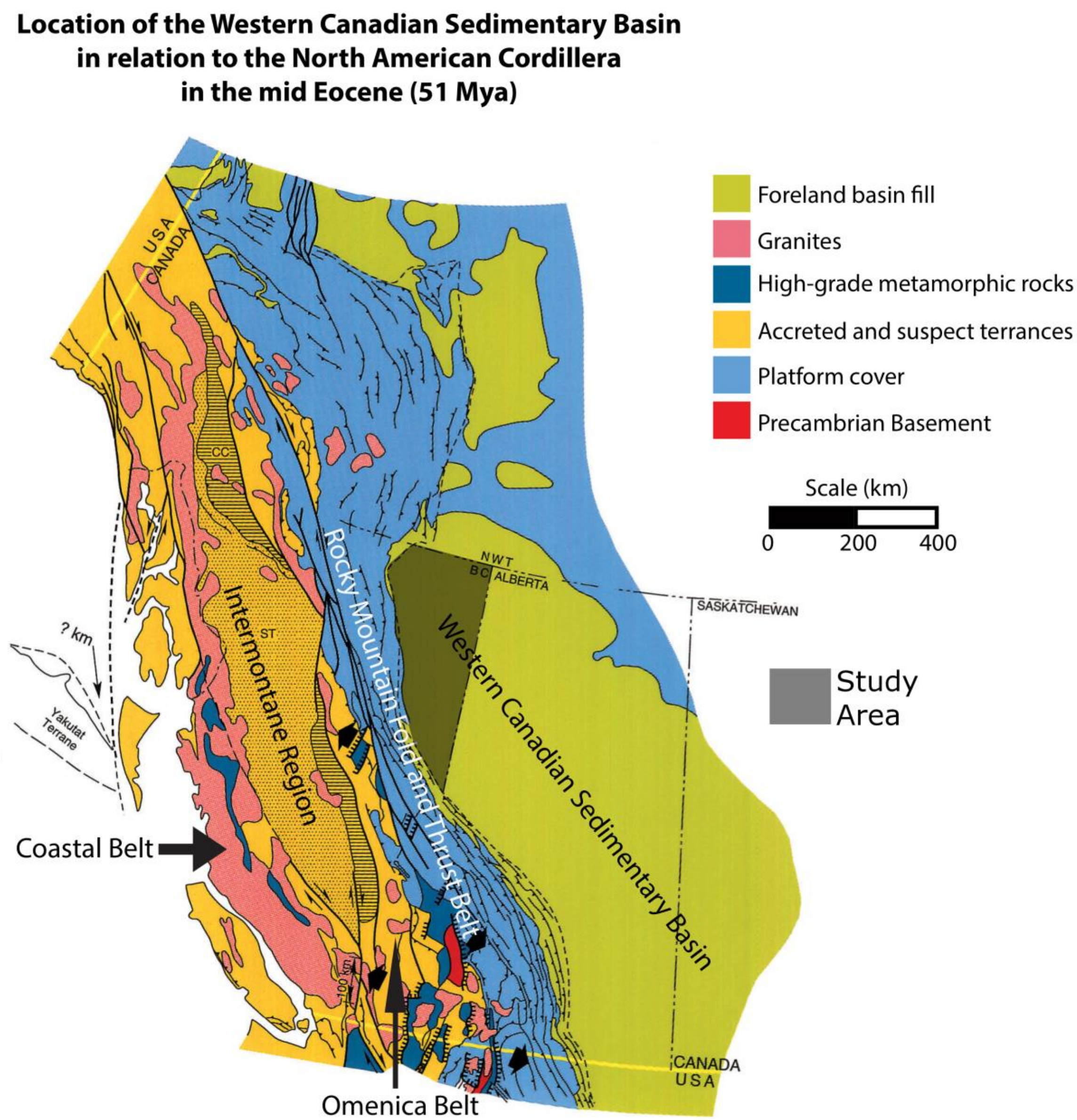

Figure 4-1. Modern tectonic and geographic setting of the Western Canadian Sedimentary Basin (adapted from Mossop & Shetsen 1994; Banks & Harris, unpublished results).

A collage of Precambrian crustal blocks and suture zones that formed the passive continental margin of North America's ancestral west coast underlies the WCSB. Sediments deposited upon this Precambrian basement preserve a long and relatively undisturbed history of transgressive and regressive marine sequences (Mossop and Shetsen, 1994, chap. 3). Prominent among these sequences are thick deposits of Devonian carbonate reefs and platforms; shales and fluvial and beach margin sandstones (Mossop and Shetsen, 1994, chaps. 10–13). The Devonian reefs and sandstones in the deeper parts of WCSB are hypothesized to contain reservoirs of hot brine, depending on local porosity (Walsh 2013; Weides & Majorowicz 2014; Banks & Harris, unpublished results). Formations of primary interest in this study are the Slave Point, Keg River and Chinchaga. Other potential water-bearing formations include the Sulphur Point, Wokkpash and Stone. All of these formations are major constituents of the Upper Givetian to Lower Frasnian Beaverhill Lake Group, as it is found north of the Peace River Arch (Mossop and Shetsen, 1994, chap. 11). The local thicknesses of these strata play an important role in the volumetric calculations of power generation potential, described in Section 4.3.5.

Extensive hydrocarbon development throughout the WCSB has created a robust set of thermo- and hydrodynamic data to evaluate the basin's geothermal setting. Heat flow within and beneath the WCSB has been studied for over half a century (e.g. Garland & Lennox 1962; Majorowicz & Jessop 1981; Lam et al. 1985; Jones et al. 1985; Majorowicz et al. 2012). Figure 4-2 (Weides & Majorowicz 2014) shows the geothermal gradients throughout the WCSB. Gradients range from 20 – 25 °C/km in the southern and southwestern-most portions, to > 50 °C/km in the far north of the basin. Within the study area, the basin deepens from about 2000 m in the upper northeast corner to about 5500 m in the west-central section, adjacent to the deformation front. Temperatures at the bottom of the basin (top of the Precambrian surface) range from ~100 °C in the shallower sections of the basin, where the gradient is high, to > 160 °C in the deepest parts of the area, where the gradient is lower (Weides and Majorowicz, 2014).

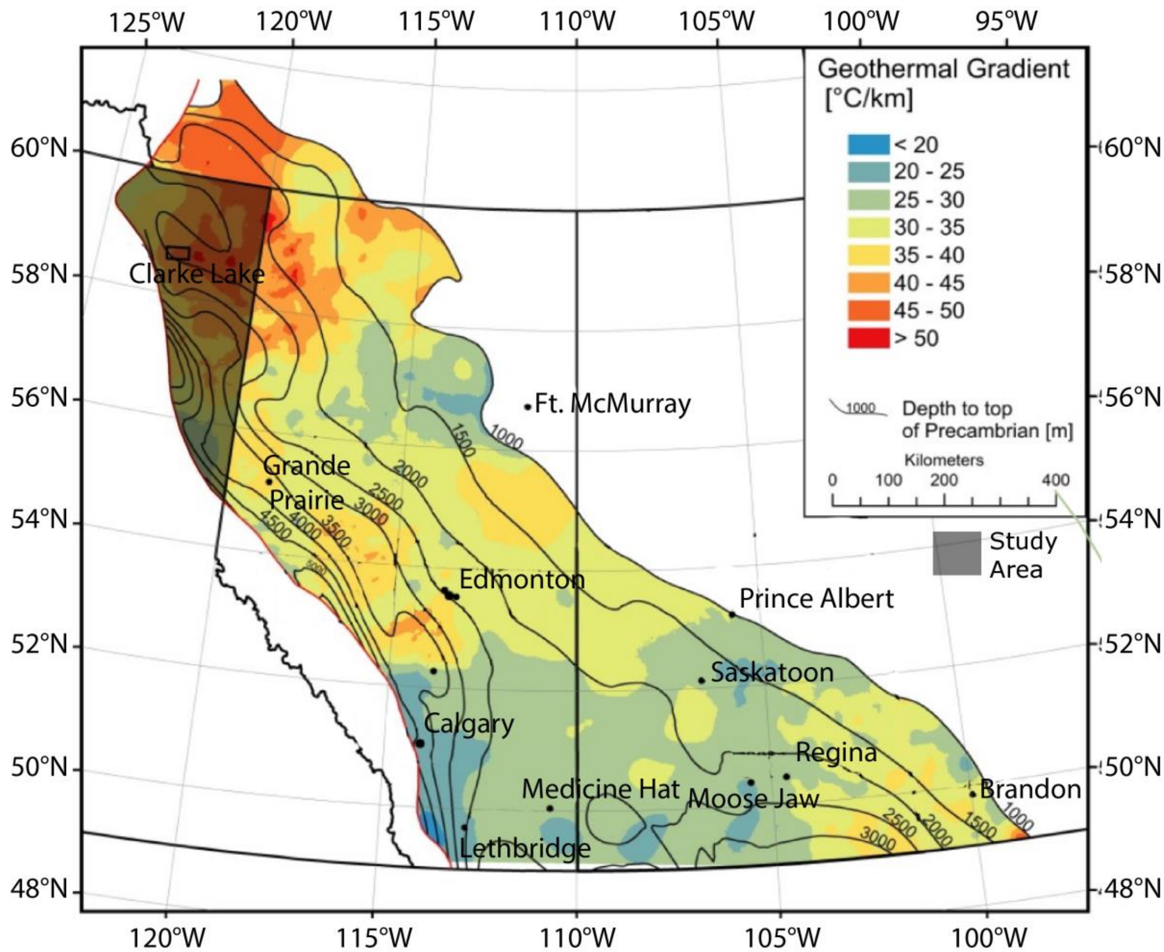

Figure 4-2. Geothermal gradient in the Western Canada Sedimentary Basin. The study area is located in the Canadian province of British Columbia. The center province is Alberta, adjacent to Saskatchewan to the east. The southern border (49 °N latitude) delimits the United States of America (adapted from: Weides & Majorowicz 2014).

4.3 Methods and Materials

This study employs a two-step method to locate favourable sites and quantify their potential for geothermal power generation in a sedimentary basin. First, a geothermal favourability map is produced by geospatially overlapping data that relate the technical and economic potential of a geothermal power project. Second, the electricity generation potential from areas of highest favourability is assessed via the Volume Method (Williams et al., 2008). As a case study, the method is applied in the British Columbian portion of the WCSB.

4.3.1 Favourability Mapping Procedure

Selecting favourable sites for geothermal power development is a geospatial multi-criteria decision problem (Greene et al., 2011). This study evaluates favourability based on geologic and economic criteria. Geologic criteria include reservoir temperature and hydraulic conductivity. Economic criteria include access to electrical transmission grids, potential for behind-the-fence electrification of the upstream petroleum sector, and proximity to population centers.

A geographic information system (i.e. ArcGIS) overlays sets of geospatial data pertaining to the aforementioned criteria into a ‘geothermal favourability map’. The map visualizes the ‘favourability score’ at any given location. The favourability score is the weighted sum of individual criteria scores, which measure the degree to which criteria are satisfied by input data. Identifying areas with high favourability scores narrows the regional scope for a detailed estimate of power generation potential.

As shown in Figure 4-3, the favourability score is generated by a two-stage weighted linear combination (Malczewski 2000; Malczewski & Rinner 2015). The left side of the flow diagram shows the two geological and four economic input layers; these contain the criteria scores. In the Weighted Summation Process section input layers are combined to form geological and economic summary layers. Aggregating the summary layers forms the final favourability map. The scores in each input and summary layer are multiplied by the given weights in each summation step.

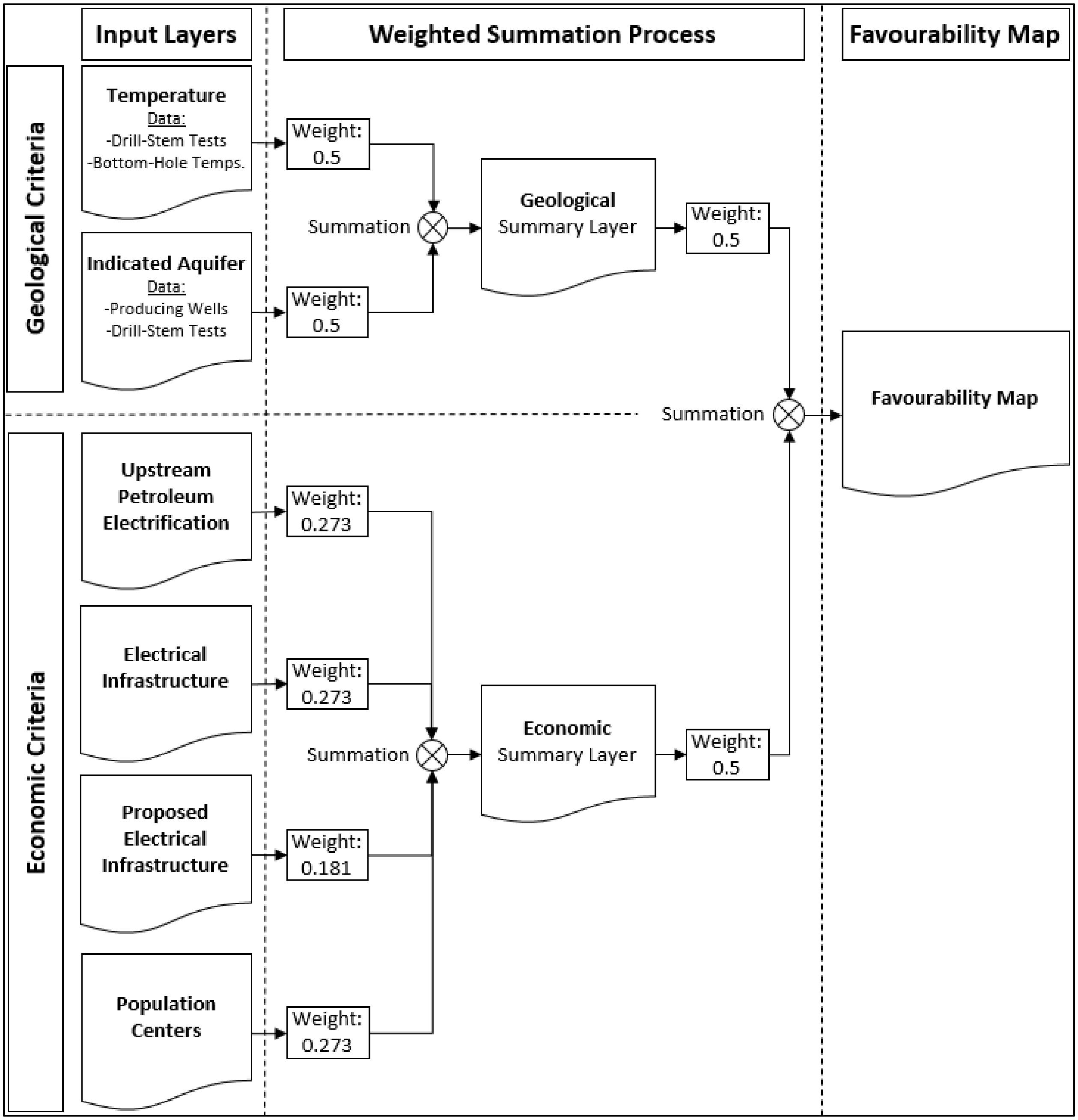

Figure 4-3. Flowchart of mapping geothermal favourability. Geological and economic criteria are represented by input layers which can consist of several data sets. Input layer weighting and summation produces summary layers. Summary layer weighting and summation produces the favourability map. Weights shown are used for the northeastern British Columbia case study.

Input data cannot be summed directly because data units and measurement scales differ. To enable weighted summation, the input data is normalized to a common unit-less scale, or ‘criteria score’ (Voogd 1983, Chapter 5; Massam 1988; Nyerges & Jankowski 2010, Chapter 7.1). Criteria scores range from 0 to 1 and identify the degree to which a specific criteria is satisfied at a given location. Datasets used to produce input layers are described in Section 4.3.2.

Input layers consist of georeferenced 100 m x 100 m cells containing individual criteria scores. The score S_{ij} is contained in the jth cell of the ith layer. Each weighted summation stage receives inputs from N input layers that consist of J cells. The jth cell of every input layer is geospatially congruent. Scores of congruent cells are multiplied by the weight w_i of the ith layer and summed as follows:

$$\bar{S}_j = \sum_{i=1}^{N} S_{ij} w_i \qquad \forall \in \{1, 2, \dots, J\} \tag{4.1}$$

As shown in Figure 4-3, first-stage summations produce summary layer scores and the second-stage summation produces favourability scores. Depending on the summation stage, $\bar{S}_j$ is the summary score or favourability score of the jth cell. Weights reflect a criteria’s importance to geothermal development. The sum of all weights w_i in each stage equals 1.

The favourability scores are plotted on a map using a colour scale. This favourability map highlights locations where geothermal power development is most favourable. Areas with a high score are selected for assessment of potential power generation.

4.3.2 Favourability Mapping Input Data

4.3.2.1 Geologic Criteria

Geological data is derived from drill-stem tests (DST), bottom-hole temperature measurements (BHT), and natural gas and oil producing well records (NGOW) taken from IHS Energy (2016). All three datasets are filtered for lower middle-Devonian and Beaverhill Lake Group strata (Mossop & Shetsen 1994, Chapter 11). Figure 4-4 shows locations where data was recorded. Red crosses mark temperature and blue dots mark indicated aquifer data records.

The Temperature Input Layer uses DST and BHT data. BHTs are Harrison-corrected (Harrison et al., 1983) to account for the cooling effect of drilling mud. Spatial interpolation and averaging of temperature data produces the underlying temperature map. Areas below 80 °C are excluded because this temperature is the minimum value for geothermal resources under the British Columbian Geothermal Resources Act (1996).

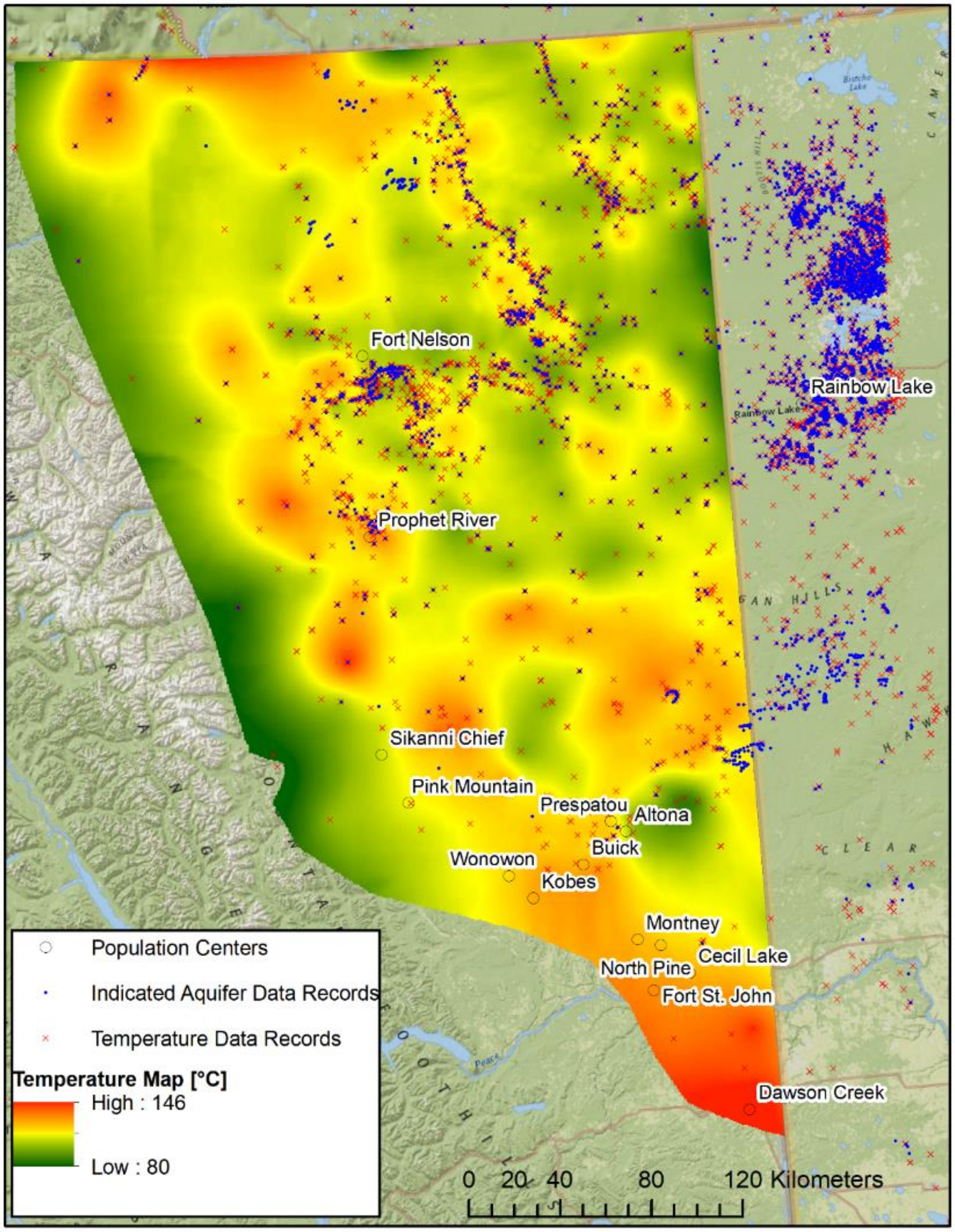

Figure 4-4. The two geological input layers are based on temperature (red crosses – BHT and DST) and indicated aquifer (blue dots – DST and NGOW) data records. Spatial interpolation and averaging produces the temperature map. Temperature data records vary in depths from approximately 1400 m in the northeast to 4000 m around Sikanni Chief in the southwest of the study area. Locations of data records extend into British Columbia's neighbouring provinces to avoid edge effects along provincial borders. The map shows the northeastern section of British Columbia and adjacent to sections of Alberta to the east, the Northwest Territories to the northeast and Yukon to the northwest.

The Indicated Aquifer Input layer qualitatively infers hydraulically conductive strata by including DST and NGOW that have recovered water. NGOW data are filtered for water production greater 0 m^3/day, a minimum production duration of 1 hour, a cumulative water production greater than 10 m^3, and production zones outside of shale formations. DST data is filtered by 'blow test' results. This test analyzes the fluid exiting the drill pipe during the pressure-release phase of the drill-stem test. The three fluid characteristics listed in the left column of Table 4-1 can infer aquifers. When a DST record contains a noted qualifying description for at least 2 characteristics, an aquifer is inferred.

Table 4-1. Results from 'blow tests' are used to infer aquifers. The blow test analyzes the fluid exiting the drill pipe during the pressure-release phase of the drill-stem test. When at least two of the three blow test characteristics (left column) include keywords from the qualifying description (right column), then a DST record indicates a potentially hydraulically conductive aquifer. Qualifying descriptions are based on author experience.

Characteristic	Qualifying Description
Surface Blow	Strong
	Good
Recovery	Water
	Salt
	Sulphur
Permeability	Average
	Good
	Excellent
	High

4.3.2.2 Economic Criteria

Economic input layer data identify potential locations for commercial power sales. These include regions with upstream petroleum production, electrical infrastructure and population centers. Areas with upstream petroleum production, and associated electrification opportunities, are identified from historical natural gas rights sales. These areas include the Northern Montney and Heritage Field, Horn River Pools A and D of the Muskwa Otter Park Formation, and the Cordova Embayment (Ministry of Natural Gas Development, 2016). Electrical Infrastructure data identifies locations with > 60 kV transmission lines and substations (BC Hydro, 2012a). A proposed transmission line between the Bennet Dam and Pink Mountain (ATCO Power, 2015) is included as Proposed Electrical Infrastructure. Population centers identify the approximate geographical centers of towns and communities that may provide economic opportunity for geothermal resources.

Figure 4-5 provides a map of economic input data locations. Areas with upstream electrification potential are traced in green. Transmission lines are depicted in orange. The purple proposed transmission line connects Pink Mountain to the Bennet Dam (not shown) in north-south direction. Existing substations along the transmission lines are shown as yellow dots. Population centers cluster in the south of the study area.

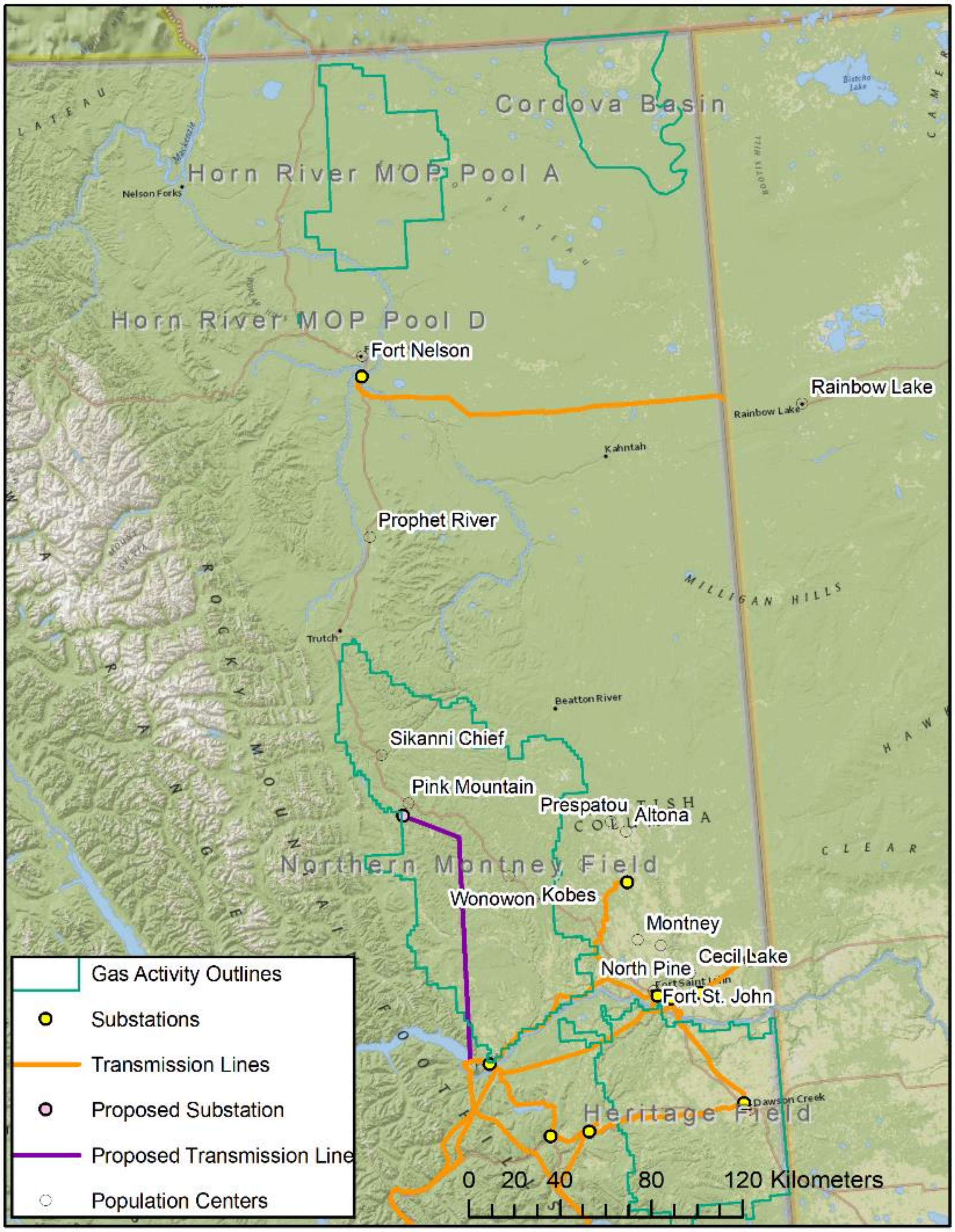

Figure 4-5. Economic input layers contain these data to represent potential for local electrification, proposed and existing electrical infrastructure that permits electricity sales to the grid, and population centers that have potential heat demand. Transmission infrastructure outside of the study area is excluded.

4.3.3 Criteria Scoring

Table 4-2 shows the conversion of data to criteria scores. Criteria scores can be: input value dependant (e.g. temperature), distance dependant (e.g. electrical infrastructure, aquifers, population centers), or location dependent (e.g. upstream petroleum electrification).

The maximum temperature (146 °C) is assigned a score of 1, and the minimum temperature (80°C) is assigned a score of 0. Intermediate temperature scores are linearly interpolated between these two points. Distance dependant scores are 1 at the location of a data point and linearly decline to 0 at or beyond a maximum distance. Maximum distances are 20 km for indicated aquifers, substations, and population centers. 10 km is used for transmission lines. The Upstream Petroleum Electrification Input Layer is binary and has a score of 1 within electrification areas and 0 outside of electrification areas. Rationale for the scoring methods are listed in the right column of Table 4-2.

Table 4-2. Input data is converted to input layers by assigning criteria scores to each location. The center column lists the type of score decay (linear or binary), the score determining parameter (temperature, distance or location) and examples that determine a score of 1 and a score of 0. The right column provides the rationale for the scoring method.

Input Layer	Criteria Scoring	Rationale
Temperature	<u>Linear decay based on temperature:</u> 1 at 146 °C 0 at 80 °C	Temperature map based on interpolated and spatially averaged DST and BHT records (Figure 4-4).
Indicated Aquifer	<u>Linear decay based on distance:</u> 1 at indicated aquifer 0 at 20 km distance from indicated aquifer	Probability to recover water decreases with distance from an indicated aquifer.
Upstream Petroleum Electrification	<u>Binary decay based on location:</u> 1 inside gas activity area 0 outside of gas activity area	Electrification opportunities may exist in petroleum production areas.
(Proposed) Electrical Infrastructure	<u>Linear decay based on distance:</u> 1 at transmission line or substation 0 at 20 km distance from substation 10 km distance from transmission line (Choose greater score value where overlap occurs.)	Transmission line scores decay faster with distance due to higher connection cost (BC Hydro, 2012b).
Population Centers	<u>Linear decay based on distance:</u> 1 at town center 0 at 20 km distance from town center	Economical heat transport distance in district heating system (Danfoss, 2014; International District Heating Association, 1983; Ulloa, 2007).

With the exception of Proposed Electrical Infrastructure, all criteria are equally weighted. The exception reflects the uncertain completion of proposed infrastructure. Input layer combination is performed by calculating Equation 4.1 in the ArcGIS 'raster calculator'. Favourability scores are plotted using a colour scale to produce the favourability map.

4.3.4 Estimating Power Generation Potential

The power generation potential of geothermal reservoirs are evaluated in regions of highest favourability using the Volume Method (Williams et al., 2008). The reservoir's gross thermal energy Q_R is derived from the reservoir's volume, temperature and heat capacity as follows:

$$Q_R = [(1 - \phi)(\rho_R C_R) + \phi(\rho_F C_F)]A_R D_R (T_R - T_0) \tag{4.2}$$

where ϕ is the reservoir porosity, ρ_R is the reservoir rock density, C_R is the reservoir rock specific heat capacity, ρ_F is the geothermal brine density, C_F is the geothermal brine specific heat capacity, A_R is the reservoir area, D_R is the reservoir thickness, T_R is the reservoir temperature and T_0 is the rejection temperature.

Equation 4.2 is modified from Williams et al. (2008) in two ways: 1) the porous fraction of the reservoir is assigned a specific heat capacity of geothermal brine, and 2) the reservoir volume term V_R is separated into the factors area A_R and thickness D_R, so that:

$$V_R = A_R D_R \tag{4.3}$$

Converting thermal energy to exergy accounts for entropy generation, which thermodynamically constrains the amount of useful work available from a temperature difference. Utilization efficiencies account for additional losses in a power plant. The total available electric energy is divided by project lifetime to estimate the gross power capacity. Gross power capacity (P) is calculated as follows:

$$P = \frac{\eta_u}{l}\left[Q_R r_g - \frac{Q_R r_g T_0 (s_R - s_0)}{h_R - h_0}\right] \tag{4.4}$$

where η_u is the power plant utilization efficiency, l is the power plant lifetime, r_g is the recovery factor, T_0 is the rejection temperature, s_R is the specific entropy of the geothermal brine at T_R, s_0 is the specific entropy of the geothermal brine at T_0, h_R is the specific enthalpy of geothermal brine at T_R, h_0 is the specific enthalpy of the geothermal brine at T_0.

The economics of geothermal energy development are highly dependent on the number of production wells necessary to achieve the required brine flow rates (Astolfi et al., 2014). The required brine flow rate $\dot{m}_{brine}$ is the amount of brine that must be extracted per unit time to produce the predicted gross power capacity P (Equation **4.5**). Equation **4.5** is derived from Williams et al. (2008, eq. 2) by dividing the mass of brine extracted from the well head by project lifetime. The brine flow rate per well $\dot{m}_W$ then determines the total number of production wells N_{Wells} required to produce gross power capacity P as follows:

$$\dot{m}_{brine} = \frac{Q_R r_g}{l(h_R - h_0)} \tag{4.5}$$

$$N_{Wells} = \frac{\dot{m}_{brine}}{\dot{m}_W} \tag{4.6}$$

4.3.5 Input Data to Estimating Power Generation Potential

Four areas are selected from the favourability map for power potential estimates. As described in Section 4.4.1, these areas are Horn River, Clarke Lake, Prophet River and Jedney. The Volume Method presented in Section 4.3.4 is applied using the data inputs described in Table 4-3. Values for the area, thickness and temperature of the reservoir are specific to each favourable area. Due to the uncertainty around temperatures, areas, thicknesses, recovery factors and reservoir porosities, Monte Carlo simulations with 100,000 iterations are performed for each favourable area. Stochastic input parameters are chosen from triangular probability distributions, consistent with work by Walsh (2013). The volumetric heat capacities ρC of brine and reservoir rock are obtained from density ρ and mass based heat capacity C. The C of rock is approximated from dolomite. The C of brine is approximated from an aqueous sodium chloride solution. Utilization efficiency, brine entropy and enthalpy are temperature dependant. For these parameters, an equation of best fit is derived from data listed in the ‘source’ column in Table 4-3.

Table 4-3. Summary of values applied to the Volume Method. A stochastic assessment of each favourable area is performed separately using 100,000 iteration Monte Carlo simulations. Parameters defined by minimum, mode and maximum value are selected from triangular probability distributions. Single-column values are deterministic.*

Parameter		Value Min.	Mode	Max.	Unit	Source
ϕ	**Reservoir Porosity**	0	3	20	%	Slave Point formation porosities (IHS Energy 2016; Lam & Jones 1985; Weides et al. 2013)
ρC	**Reservoir Heat Capacity**				kJ/m³K	Dolomite: (C) 0.928 kJ/kgK (Krupka et al., 1985) and density (ρ) 2870 kg/m³ (Gardner et al., 1974). Brine: (C) 3.6 kJ/kgK (Chen, 1982) and (ρ) 1166 kg/m³ (Garcia, 2001).
	Rock		2663			
	Geoth. Brine		4200			
A_R	**Reservoir Area**				km²	Lateral extent of geothermal reservoirs is unknown. Natural gas pool areas (BC Oil and Gas Commission 2016) serve as proxy. Details in *Reservoir Area* Section below.
	Horn River	8.0	10.0	12		
	Clarke Lake	101.6	127.0	152.4		
	Prophet River	36.6	45.7	54.8		
	Jedney	6.8	8.5	10.2		
D_R	**Reservoir Thickness**				m	Derived from stratigraphic cross sections (Ibrahimbas & Walsh 2005). Details in *Reservoir Thickness* Section below.
	Horn River	108	221	225		
	Clarke Lake	162	295	428		
	Prophet River	221	241	260		
	Jedney	221	316	410		
T_R	**Reservoir Temperature**				°C	Derived from BHTs and DSTs (IHS Energy, 2016) located within favourable area. Details in *Reservoir Temperature* Section below.
	Horn River	116.4	129.6	142.9		
	Clarke Lake	91.7	111.1	130.4		
	Prophet River	107	125.6	144.2		
	Jedney	122.8	142.8	162.7		
T_0	**Rejection Temperature**		0		°C	Annual average air temperature at Fort Nelson (Government of Canada, 2017)
r_g	**Reservoir Recovery Factor**	10	17.5	25	%	(Williams 2007)
l	**Project Lifetime**		30		Years	(Walsh 2013; Geoscience BC 2015)
η_u	**Utilization Efficiency**	Values are temperature dependant and calculated for each Monte Carlo iteration using an empirically derived equation that best fits data from 'Source' column.			%	Equation type: linear Data: subcritical plant efficiency (Augustine et al., 2009)
s	**Geothermal Brine Entropy**				kJ/kgK	Equation type: third order polynomial Data: H2O saturation temperature tables (Bhattacharjee, 2017)
h	**Geothermal Brine Enthalpy**				kJ/kg	Equation type: linear Data: H2O saturation temperature tables (Bhattacharjee, 2017)
$\dot{m}_W$	**Brine flow rate per well**		30 and 100		kg/s per well	Consistent with previous work (Majorowicz & Moore 2014; Majorowicz & Grasby 2014; Lam & Jones 1985; Geoscience BC 2015)

* Detailed descriptions of sources are available in (Palmer-Wilson et al., 2017).

Additional information on reservoir parameters is provided below.

Reservoir Area (A_R)

This study uses Slave Point formation natural gas pools as proxy geothermal reservoir areas. Table 4-4 lists gas pools, their associated fields and the total area (located within favourable areas). Area values are produced by geospatial analysis of gas pool contours provided by the BC Oil and Gas Commission (2016). The total area values are assigned to the mode of the probability distributions, with maximum and minimum values defined by a ±20% factor to account for uncertainty. No Slave Point gas pools are available at Horn River. Here, a mode geothermal reservoir area of 10 km² is chosen by the authors to allow comparison.

Table 4-4. The areas of gas pools of the Slave Point formation are used as proxy geothermal reservoir areas. Potential power generation in each favourable area is estimated using Total Gas Pool Area values. Geospatial analysis of data from the BC Oil and Gas Commission (2016) provides area values of individual gas pools.

Favourable Area	Slave Point Gas Pools	Gas Field	Total Gas Pool Area [km²]
Horn River	-	-	(10.0)[a]
Clarke Lake	A	Clarke Lake	127.0
Prophet River	A, B, C, H, I, J, L, M, N, O, P	Adsett	45.7
Jedney	A, B, C B, C	Bubbles Bubbles North	8.5

[a] Value chosen by authors

Reservoir Thickness (D_R)

This study uses stratigraphic cross-sections to infer reservoir thickness (Ibrahimbas & Walsh 2005). Carbonate and sandstone formations between Beaverhill Lake Group rocks and the Precambrian surface are assumed to contain a geothermal reservoir. Selected formations include the Slave Point, Sulphur Point, Keg River, Wokkpash, Stone, and Upper Chinchaga. The local thickness of these formations is the reservoir thickness value reported in Table 4-3. This data is available at several locations across the study area, so the three locations closest to each favourable area inform the respective maximum and minimum value of the probability distribution for that location. The mode of the probability distribution is assigned the average of the maximum and minimum thickness values.

<u>Reservoir Temperature</u> (T_R)

The reservoir temperature distributions are based on DST and BHT data filtered for 1) geographical location within favourable areas, 2) a favourability score above 0.43, and 3) minimum depth based on the top of the youngest formation considered for reservoir thickness. The mode of the temperature probability distribution is assigned the average value of filtered data. The minimum and maximum values are assigned ± 1 standard deviation from the average.

4.3.6 Power Generation Sensitivity

A 'Change in Output Mean Analysis' quantifies the sensitivity of Monte Carlo simulation results to stochastic input parameter changes (Palisade, 2017). Monte Carlo iteration datasets contain input and related output parameter values. Input parameters are temperature, recovery factor, reservoir area, reservoir thickness and porosity. Output parameters selected for analysis are gross power capacity per unit reservoir volume P/V_R and brine flow rate to produce 1 MW of power $\dot{m}_{brine}/P$. Iteration datasets are sorted by ascending value of an input parameter. Datasets are distributed equally across twenty bins. Each bin represents five percent of the input value distribution. The mean value of the selected output parameter is computed for the iteration datasets contained in each bin.

4.4 Results

4.4.1 Favourability Mapping Results

The results of the favourability mapping procedure are shown in Figure 4-6. To highlight areas of highest favourability, the top 10%, 20% and 30% are shown. The highest computed score is 0.61; hence each 10% interval represents a 0.06 score step. The top 10% to 30% areas occur in patches that range from tens to several hundred square kilometers. Larger patches cluster in the central west section and in the petroleum production areas in the northern section of the study area. Smaller patches occur along the Fort Nelson – Rainbow Lake transmission line and the southern-most section of the study area, 20 to 100 km north of Fort Saint John. Only three areas feature a score in the top 10% interval. These are located approximately 10 km south of the town of Trutch, in the Jedney region and adjacent to Fort Nelson.

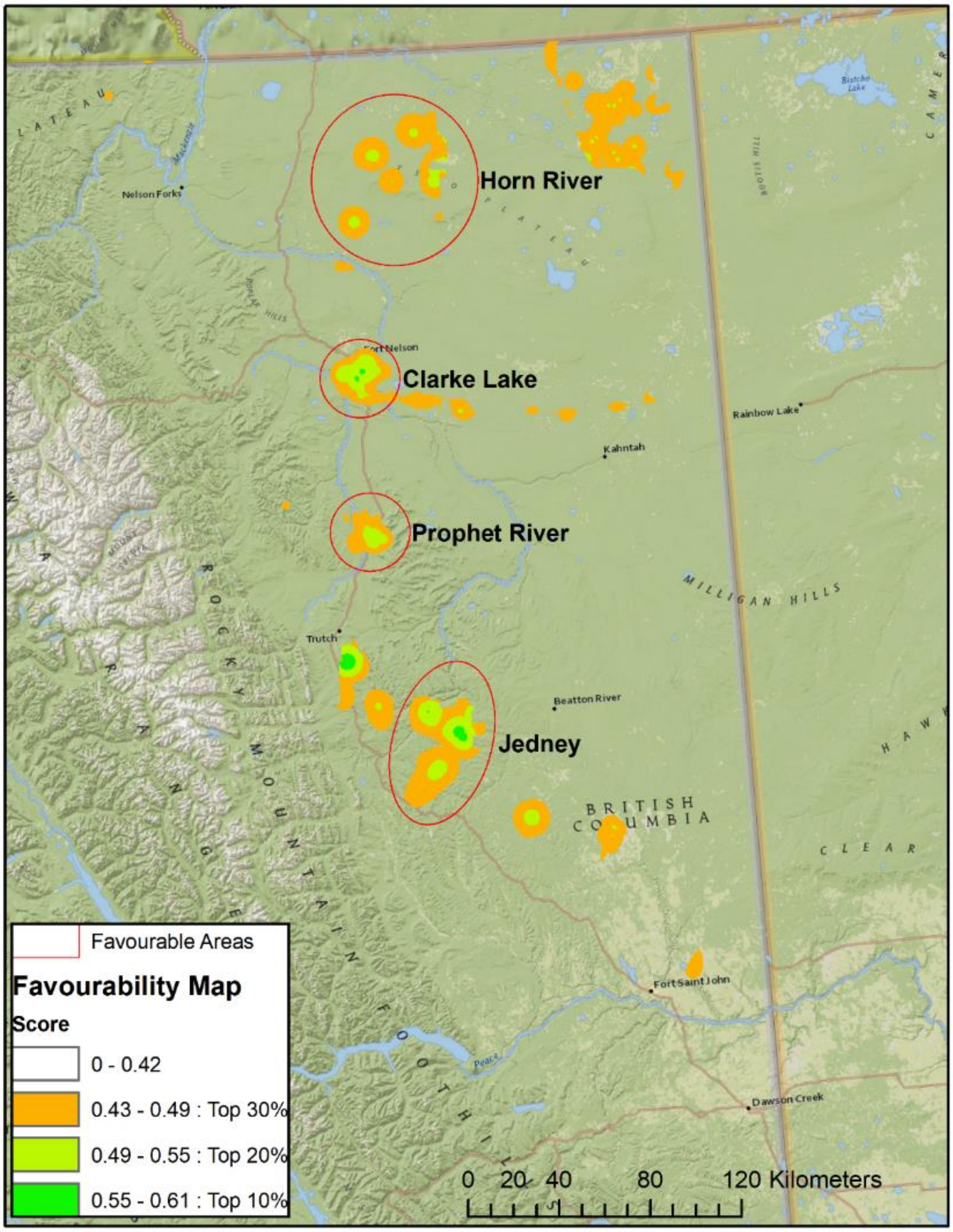

Figure 4-6. Geothermal Favourability Map of northeastern British Columbia. Scores range from the minimum 0 to the maximum 0.61. Colour gradients show 10% score range intervals, each representing a 0.06 score step. To highlight areas of highest geothermal favourability only the top three score intervals are shown. Coloured regions enclosed by red ellipses are selected for estimating power generation potential.

The four areas highlighted in red on Figure 4-6 are deemed 'Favourable Areas'. These areas include Horn River, Jedney, Clarke Lake and Prophet River. Selection is somewhat qualitative and based on each area's unique characteristics. Horn River and Jedney gas fields were chosen due to remote upstream natural gas electrification opportunities (Government of British Columbia, 2016). The Clarke Lake area features power export opportunities to Fort Nelson, and significant geological data is available from the adjacent Clarke Lake and Milo gas fields. Finally, Prophet River is a First Nation, where geothermal development may aid economic opportunities for the community.

Some areas with high favourability scores are excluded from further investigation in order to limit the scope to areas where geothermal development is most likely. Several excluded patches of high favourability in the northeastern study area feature economic opportunities similar to those at Horn River, but lower overall favourability. Exclusions along the Fort Nelson – Rainbow Lake transmission line are based on temperature being generally relatively low. Areas southeast of Jedney display high favourability, but indicated aquifers are scarce here. The excluded area ~10 km south of Trutch features economic opportunities similar to those at Jedney.

4.4.2 Estimates of Power Generation Potential

The Volume Method and data described in Section 4.3.4 – 4.3.6 is applied to assess the geothermal potential of the four favourable areas. Table 4-5 shows four metrics of evaluation. The gross power capacity P is the potential electric power generation for 30 years at continuous production. 'Gross' disregards self-consumed electricity needed to serve a power plant's internal load (e.g. pumps and cooling fans). The impact of reservoir volume uncertainty is mitigated by calculating the capacity per unit reservoir volume P/V_R. The $\dot{m}_{brine}/P$ metric states the required brine flow rate to produce 1 MW of electrical power. The number of production wells is based on conservative (30 kg/s) and optimistic (100 kg/s) assumed brine flow rates per well ($\dot{m}_W$). The feasibility of geothermal power increases with higher values for P and P/V_R and lower values for $\dot{m}_{brine}/P$ and N_{Wells}. All units of power (MW) refer to electrical power.

Table 4-5. Four evaluation metrics characterize the potential geothermal electric power generation at the four favourable areas of northeastern British Columbia. Stochastic Monte Carlo simulations of the Volume Method result in probability distributions. P90, P50 and P10 values are lower than 90, 50 and 10% of values in these distributions. The mode is the most likely value.

Evaluation Metric		Exceedance Probability or $\dot{m}_W$	Horn River	Clarke Lake	Prophet River	Jedney
P	Gross power capacity [MW]	**P90**	3.6	43.9	21.6	7.7
		P50	5.2	71.3	31.5	11.3
		Mode	4.8	63.2	28.9	10.4
$\frac{P}{V_R}$	Gross power capacity per unit reservoir volume [MW/km³]	**P90**	2.34	1.30	2.01	3.04
		P50	3.19	1.94	2.88	4.28
		Mode	3.00	1.80	2.54	4.10
$\frac{\dot{m}_{brine}}{P}$	Required brine flow rate per gross power capacity [kg/sMW]	**P90**	31.3	45.1	32.0	22.0
		P50	37.1	60.5	40.9	27.6
		P10	44.5	84.5	53.7	35.2
		Mode	37.0	60.4	40.8	27.5
N_{Wells}	Number of required production wells*	**at 30 kg/s per well**	5	90	31	8
		at 100 kg/s per well	2	27	10	3

*For P at P90 and $\dot{m}_{brine}/P$ at P50.

The P90 value is lower than 90% of Monte Carlo simulation results. The P50 and P10 values are lower than 50% and 10% of simulation results, respectively. The mode is the most likely value. The P90 values of P and P/V_R and the P10 values of $\dot{m}_{brine}/P$ represent conservative estimates.

The power capacity is greatest at Clarke Lake and lowest at Horn River, with respective P90 estimates of 43.9 and 3.6 MW. The difference is largely due to the different reservoir volumes. The volume normalized power infers greatest potential at Jedney and lowest at Clarke Lake, with P90 estimates of 3.04 and 1.30 MW/km^3, respectively. Similarly, $\dot{m}_{brine}/P$ is lowest at Jedney and highest at Clarke Lake, with respective P10 estimates of 35.2 and 84.5 kg/sMW.

Figure 4-7 shows P and $\dot{m}_{brine}/P$ histograms for Clarke Lake. The histograms plot the probability of Monte Carlo simulation results to fall into one of fifty bins of equal width.

Probability of P follow a gamma distribution. The $\dot{m}_{brine}/P$ distribution follows a skewed triangular shape, due to the required flow rate's exclusive dependence on reservoir temperature. The Clarke Lake histogram shapes are representative for all favourable areas.

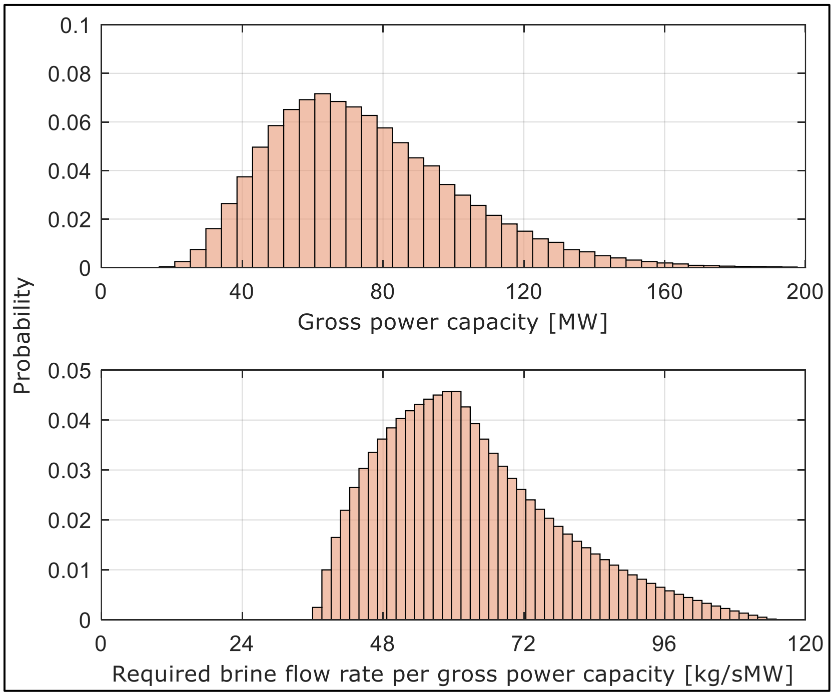

Figure 4-7. Histogram of Monte Carlo simulation results for P (top) and $\dot{m}_{brine}/P$ (bottom) at Clarke Lake. Respective probabilities follow a gamma and skewed triangular distribution shape. Results at other favourable areas follow similar distributions.

4.4.3 Power Generation Potential Sensitivity Analysis

Figure 4-8 shows the results of the sensitivity analysis for Clarke Lake, which is representative of the four favourable areas. The plot shows the input parameter percentiles on the horizontal axis and the mean output parameter values for the input percentiles on the vertical axis. For example, the 'Reservoir Temperature' curve in the left plot shows that the lowest 5% of temperature inputs to the Clarke Lake Monte Carlo simulation result in a mean P of 45.2 MW. The next 5% result in a mean P of 50.8 MW, and so on up the curve.

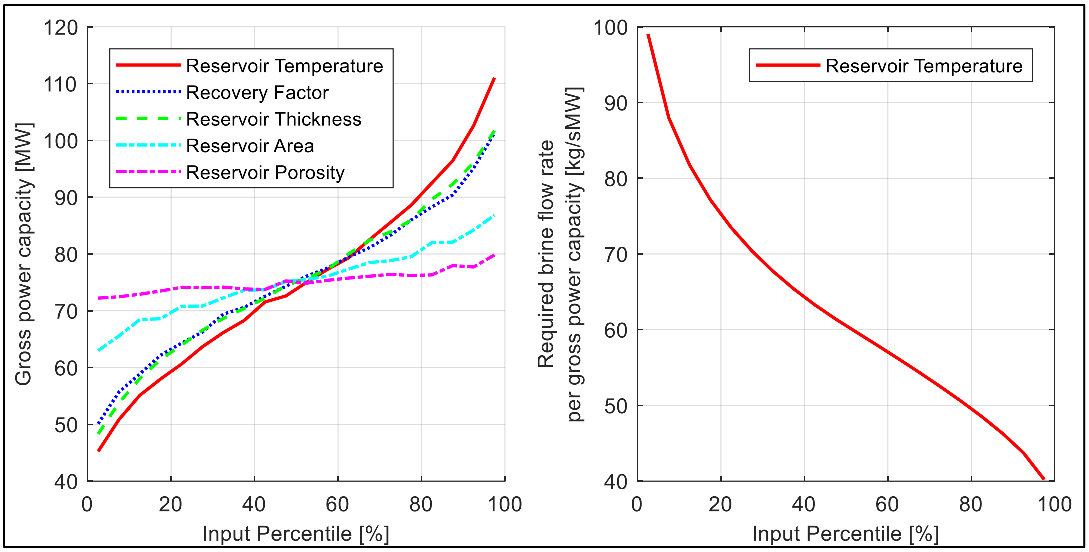

Figure 4-8 A Change in Output Mean Analysis shows the sensitivity of P (left plot) and $\dot{m}_{brine}/P$ to stochastic input parameters at Clarke Lake. Horizontal axes are percentiles of Monte Carlo input parameter value distributions. Vertical axes are mean output values of iteration datasets sorted into 20 bins. The P depends on reservoir temperature, recovery factor, reservoir thickness, reservoir area and porosity. The $\dot{m}_{brine}/P$ exclusively depends on reservoir temperature. Sensitivity at other favourable areas follows similar trends.

The sensitivity analysis shows that reservoir temperature, thickness and recovery factor significantly affect P. The respective impact factors (maximum over minimum mean value) are 2.45, 2.1 and 2.0. Reservoir area has a less pronounced effect on the output, with an impact factor of ~1.38. Reservoir porosity has a negligible effect on P, with an impact factor of 1.1. The effect of reservoir porosity on P is small because the total reservoir heat capacity increases only slightly when substituting a small porous fraction of the lower heat capacity rock with the higher heat capacity of geothermal brine. The $\dot{m}_{brine}/P$ exclusively depends on reservoir temperature. At Clarke Lake the mean values resulting from the bottom and top five percentile inputs are 99.1 and 40.2 kg/sMW. The impact factor is 2.5.

4.5 Discussion

This study describes a comprehensive approach for assessing geothermal resources in a sedimentary basin. The method identifies areas of high geothermal potential via favourability mapping and subsequently estimates power generation potential in these areas. Compared to the 12,635 MW of global installed geothermal capacity (Bertani, 2015) the total estimated mode value of 107.3 MW in the WCSB case study is small. Globally, however, many sedimentary basins are deep enough to host geothermal resources (Laske and Masters, 1997). The assessment method can be applied in any sedimentary basin where similar data is available. This study is therefore a significant step in reducing the time and cost involved with geothermal energy prospecting.

The case study of the British Columbian portion of the WCSB improves upon previous geothermal favourability maps and power generation estimates. Previous geospatial studies did not estimate power generation potential (Fairbank et al. 1992; Kimball 2010), or were not selected using a comprehensive favourability mapping approach (Walsh 2013; Geoscience BC 2015). The higher resolution analysis of geological and economic criteria identifies Clarke Lake, Jedney, Horn River and Prophet River as favourable areas for geothermal development, of which the latter two are new discoveries. Fairbank et al. (1992) identified Clarke Lake by deducing high geothermal potential from thermal gradients greater 45 °C/km, but did not consider economic criteria. This study shows that geothermal gradient alone is neither an indicator of high favourability nor increased power production potential. As shown, areas with high gradients (e.g. Clarke Lake) had both lower favourability and lower power potential per unit reservoir volume than areas with lower gradients (e.g. Jedney).

Two favourable areas identified in this study have been the subject of previous power generation estimates: Clarke Lake and Jedney (Walsh 2013; Geoscience BC 2015). At Clark Lake, this study estimated P90 and P50 gross power capacities of 43.9 and 71.3 MW respectively; larger than respective P90 and P50 values of 18.4 and 37.4 MW (Geoscience BC 2015), and the P50 value of 34 MW (Walsh 2013). Both previous works assumed smaller reservoir volumes. The Geoscience BC study uses proprietary information to justify reservoir volume, while Walsh (2013) uses the dolomitized section of the Slave Point formation. This study assumes a larger reservoir present in several carbonate and sandstone formations. At Jedney, this study's respective P90 and P50 gross power capacities are 7.8 and 11.3 MW; less than respective values of 12.2 and 24.7 MW (Geoscience BC 2015), based on that study's smaller reservoir volume.

The mode of the gross power capacity per unit reservoir volume P/V_R ranges from ~1.8 to ~4.10 MW/km^3 at Clarke Lake and Jedney, respectively. These results are significantly higher than ~0.23 to 1.6 MW/km^3 found in western Alberta (Banks & Harris, unpublished results). Several factors contribute to these differences. While this study focuses on the highest temperature reservoirs in the region, Banks & Harris (unpublished results) evaluated reservoirs with temperatures as low as 80 ˚C. Additionally, they applied a smaller recovery factor of 10%, while this study uses a range from 10 – 25%. As shown in Section 4.4.3, the selected temperature and recovery factor ranges can each affect gross power capacity by a factor of ~2.

This study estimates the brine flow rate required to produce 1 MW of electric power $\dot{m}_{brine}/P$ and deduces the number of production wells required to support the estimated gross power capacities. These are proxies for the technical and economic viability of a geothermal energy project (Majorowicz & Moore 2014; Ferguson & Ufondu 2017). The conservative P10 $\dot{m}_{brine}/P$ estimates in this study range from 35.2 to 84.5 kg/sMW at Clarke Lake and Jedney, respectively. A single production well might sustain between 0.41 to 1.0 MW under P10 conditions. Optimistic P90 $\dot{m}_{brine}/P$ values at Jedney are as low as 22 kg/sMW. Here, a single production well might sustain 1.6 MW. Brine flow rates as high as 35 kg/s are seen in co-produced fluid situations in narrow diameter gas well bores throughout the WCSB (Lam & Jones 1985; Ferguson & Ufondu 2017). If full-size geothermal wells were producing from the same conditions, flow rates as high as 100 kg/s may be achievable (Walsh 2013). Thus, hydrogeologic conditions in potential reservoirs throughout the WCSB appear favourable to geothermal energy production.

When estimating the power generation potential, assessing the reservoir size is a significant challenge. This study estimates reservoir thicknesses by spatially extrapolating stratigraphic cross-sections and assuming several carbonate and sandstone formations to be brine-saturated and hydraulically conductive. The lateral extent of geothermal reservoirs is derived from natural gas pools in the Slave Point formation, and by varying that extent by ±20% to account for uncertainty. Estimates of P and P/V_R assume brine extraction from all formations, in spite of potential hydraulic separation and brine temperature differences up to 20 °C due to varying formation depths. These assumptions introduce uncertainty to estimated power generation potential and may over-estimate the gross power potential of the area. In contrast, not all areas with high favourability scores are included in power potential estimates. These exclusions may lead to underestimating the total power potential in northeastern British Columbia.

In the Volume Method, a geothermal reservoir comprises a finite heat resource without thermal recharge. Some work suggests that heat flow in the WCSB is controlled primarily by conduction of heat from the Precambrian basement, rather than by convection via groundwater flow (Bachu and Burwash, 1994). In this case, thermal recharge can be neglected as conductive recharge is negligible on a human lifespan timescale (Barbier, 2002). Other studies suggest that groundwater flow influences the geothermal regime (Majorowicz et al., 1999). If thermal recharge occurs the Volume Method produces a conservative power generation estimate.

4.6 Conclusion

This study presents and demonstrates a comprehensive method to estimate geothermal power generation potential of a sedimentary basin. The two-step process of favourability mapping and volumetric power estimates significantly reduces the uncertainty surrounding the available geothermal resource on a regional basis.

As a case study, the method is applied to the British Columbian portion of the WCSB and identified previously undiscovered areas where geothermal power development is favourable (Horn River, Prophet River) and confirmed known locations (Clarke Lake, Jedney). Power generation potential estimates apply the Volume Method (Williams et al., 2008) and utilize a Monte Carlo simulation to identify the possible ranges in predictions. The mode of total power generation potential is 107.3 MW. The volume normalized mode of expected power potential for the four investigated favourable areas range from 1.8 – 4.1 MW/km^3. Mode brine flow rates of 27.5 – 60.4 kg/s are required to produce 1 MW of power, based on the temperatures present in these reservoirs.

The sensitivity study highlights the strong dependence of results on reservoir temperature, thickness, and recovery factor, each of which can affect the gross power capacity by a factor ~2 between the lowest 5% and highest 5% values selected from input distributions.

This two-step method can be applied to sedimentary basins with similar characteristics and data availability globally; thereby providing improved estimates of available low-carbon, dependable geothermal energy.

5 Renewable energy related land requirements of an electrified city: a case study of Metro Vancouver, Canada

5.1 Introduction

Urban energy consumption is a principal cause of climate change. Urban areas[4] consumed 64% of global primary energy and emitted 70% of global carbon emissions in 2013 (International Energy Agency, 2016). According to the World Energy Outlook, global final energy demand continues to increases by between 0.1% and 1.5% annually until 2040 (International Energy Agency, 2018). Urban areas will consume an increasing share as their populations grow from 4.2 to 6.7 billion people between 2018 and 2050 (United Nations, 2018). This urbanisation and related wealth creation causes the additional urban energy demand. This increasing demand conflicts with the need to reduce energy-related greenhouse gas emissions to near zero by mid-century (IPCC, 2014). Local municipal efforts to reducing emissions are therefore indispensable to mitigate the global climate change (United Nations Human Settlement Programme, 2011).

A number of municipalities across the globe have pledged to reduce emissions by transitioning to renewable energy sources. Stockholm, Sweden plans to expand renewable energy and be fossil fuel free by 2050 (Stockholm Stad, 2014); Adelaide, Australia plans to offset all carbon emissions by 2021 and work toward 100% renewable energy beyond that date (Adelaide City Council and Government of South Australia, 2016); Vancouver, Canada plans to fully transition its electricity, space heating and road transportation energy demand to 100% renewable energy by 2050 (City of Vancouver, 2015). To reach these goals, municipalities can deploy prospective urban renewable energy technologies including rooftop solar, small-scale wind, geothermal, biomass, and waste-to-energy (Kammen and Sunter, 2016). Implementation of these technologies can reduce greenhouse

[4] Attributing energy consumption and greenhouse gas emissions to urban areas is somewhat uncertain because previous studies have defined urban areas in a variety of ways. Gargiulo and Russo (2017) provide a comprehensive discussion on the physical, functional, geographical, and socio-economic features that have been applied in the pertinent literature. In this study, urban area is defined as the area within municipal jurisdiction.

gas emissions, avoid network upgrades, avoid transmission losses, enhance resiliency, and strengthen social acceptance of the energy transition through democratization of energy production (Adil and Ko, 2016).

However, the challenge of meeting urban energy demand entirely from renewable sources is immense. The historic transition from sparse land-based energy sources (e.g. forests, peats) to concentrated subterranean fossil fuel stocks (coal, petroleum) enabled enormous expansion of energy production in the industrial revolution (Huber and McCarthy, 2017). These dense fossil fuel stocks still provide the majority of the energy consumed in cities today (Kennedy et al., 2015). Harnessing the abundant but less concentrated renewable energy sources wind, solar and hydro reverses this historical trend because these energy flows provide relatively small amounts of energy per unit land area. Comparison of power densities (average annual power supply versus demand per unit area) reveals that densely populated cities cannot meet their present-day electricity demand from urban renewable sources alone (Smil, 2019). Reducing greenhouse gas emissions by electrifying the heating and transportation sectors adds to the future electricity demand (Williams et al., 2012). The average European city will not be energy self-sufficient even after efficiency measures significantly reduce energy demand (Oldenbroek et al., 2017). Cities will need to import renewable energy from rural sources to meet their renewable energy needs.

Public opposition to the development of renewable energy projects in rural areas is a potential barrier to implementing municipal renewable energy plans. Rural communities raise concerns about ecological, visual, cultural, and economic impacts of such projects on land and landscape (Botelho et al., 2016; Cohen et al., 2014; Devine-Wright, 2009; Jefferson, 2018; Jones and Pejchar, 2013; Pasqualetti, 2011; Rand and Hoen, 2017). Negative public perception of transmission lines adds to the challenge of connecting these decentralized energy technologies to urban centers of consumption (Soini et al., 2011). To achieve their renewable energy goals, municipalities will need to balance the need for renewable energy supplies with the impact of deploying its infrastructure in rural areas (Poggi et al., 2018).

A number of studies quantify the resource potential of urban renewable energy sources, subject to land area constraints. In three cities in Peru, the relatively low demand and high radiation would enable rooftop solar to supply the annual present-day electricity demands (Bazán et al., 2018). Rooftop solar could supply 61% of the annual electricity demand in Oeiras, Portugal (Amado and Poggi, 2014), and 38% of demand in Lethbridge, Canada (Mansouri Kouhestani et al., 2019). Biomass on all marginal lands in Boston, Massachusetts could supply 0.6% of the city's primary energy demand (Saha and Eckelman, 2015). In Kampala, Uganda municipal solid waste could provide 2.1% of the city's 2014 energy demand; ground-mounted solar covering 7.6 km^2 of land area could supply all electricity demanded that year (Munu and Banadda, 2016). In all of these studies, total annual energy demand is compared to the total annual supply of renewable energy. In the absence of significant energy storage capacity to balance supply and demand intra-annually, these estimates of urban resource potential are likely to be high.

There are studies that investigate urban energy production and land area requirements using temporally detailed energy system models with energy storage. Based on monthly averages, solar, wind, and biomass resources with battery storage occupying an area of 22 km^2 are found to be able to supply the electricity demand for the City of Vancouver, Canada (Bagheri et al., 2018). In Seville, Spain 10.8 km^2 of rooftop solar plus 11.2 km^2 of ground-mounted solar with single-day storage are found to be able to provide all building and electrified transportation energy demands at costs of 0.08 €/kWh if 78% surplus generation can be sold to the grid; alternatively, seasonal storage is found to reduce the rural land area to 3.5 km^2 and avoid surplus generation, but electricity costs would be a prohibitive 1 €/kWh (Arcos-Vargas et al., 2019). In Wroclaw, Poland rooftop solar is found to be able to supply up to 36.1% of annual electricity demand, but the prohibitive cost of storage reduces that potential to 29% (Jurasz et al., 2019). These studies provide estimates of urban energy potential, land area requirements and the feasibility of prescribed renewable energy system compositions. However, these studies do not assess a range of feasible systems that may require more or less land area than the prescribed composition. In addition, these studies do not include the land area required for energy storage.

To overcome these limitations, the work presented here investigates a broad range of electricity system compositions that use both urban and rural renewable sources to supply urban demand. The urban demand includes the present-day electricity, electrified space heat and electrified road transportation energy demands of Metro Vancouver, Canada. The electricity system compositions are determined by a one-year hourly capacity expansion and dispatch cost-optimization model for a broad range of *land impact costs*. The land impact costs internalize the rural land area impacts which are not normally borne by the electricity system. This approach provides the full range of lowest-cost electricity system compositions between the minimum feasible and maximum necessary rural land area requirements. The optimization minimizes net present system cost in determining: 1) the required electricity generation and storage capacities, 2) the rural land area impact, 3) the surplus electricity generation, 4) the share of urban energy production, and 5) the trade-off between reducing the rural land area impact and increasing the net present system cost. This study can inform municipal decarbonisation efforts, regional land-use planning, and policies to equitably mitigate impacts on rural communities.

5.2 Method

This study quantifies rural land area impacts associated with supplying the electrified urban energy demand of the Metro Vancouver Regional District in Canada with renewable electricity generation and storage technologies. The electrified demand includes space heat, transportation and electric energy demands observed in 2016. Space heat and transportation fossil fuel demands are converted to an equivalent electricity demand by assuming an "over-night" transformation to electric heaters and battery-electric vehicles. Combinations of four technology scenarios determine probable upper and lower bounds of additional annual and peak electricity demands. Two scenarios assume deployment of low efficiency electric resistance (LOW) or high efficiency electric heat pump technology (HIGH); two scenarios assume temporal demand profiles where battery-electric vehicle charging exacerbates the evening peak (PEAK) or remains constant throughout the day (UNIFORM). A one-year capacity expansion and hourly dispatch model chooses the cost-optimal mix of *rural* and *urban* technologies to satisfy the hourly electrified demand. The optimization applies 2050 forecasted technology costs to supply the 2016 electrified demand hind casted in the LOW and HIGH heat scenarios with evening peaking transportation demand.

In this study, the rural technologies - hydro, wind, ground solar and pumped storage - impact rural land area. The urban technologies - waste-to-energy, rooftop solar and battery storage - do not impact rural land area. Rural land area impact is an externality not normally borne by the electricity system. An exogenous *land impact cost* internalizes this externality. To identify the range where this externality might affect the choice of generation and storage technologies, the electricity system model determines the optimal technology mix for a wide range of land impact costs. As land impact costs increase, the optimal technology mix impacts a decreasing rural land area. Very high land impact costs minimize the rural land area impact and maximize expansion of urban technologies. This approach yields 1) the required rural land area impact that minimizes total costs to supplying electrified Metro Vancouver with renewable sources, 2) the minimum feasible rural land area impact, 3) the trade-off between impacting a smaller rural land area and bearing a higher total cost, and 4) the maximum electricity share urban technologies can contribute to Metro Vancouver's electrified demand.

5.2.1 Metro Vancouver case study

This study investigates the land area impacts of supplying the *Metro Vancouver Regional District* in British Columbia, Canada with renewable energy. The district includes 23 cities, municipalities, villages, and the Tsawwassen First Nation. Metro Vancouver's geographical boundaries are highlighted in red in Figure 5-1. The boundaries encompass a land area of 2,883 km² when excluding water bodies. The 2016 census counted 2,463,431 persons which is 53% of British Columbia's population (Statistics Canada, 2017). The mean population density is 854 persons/km².

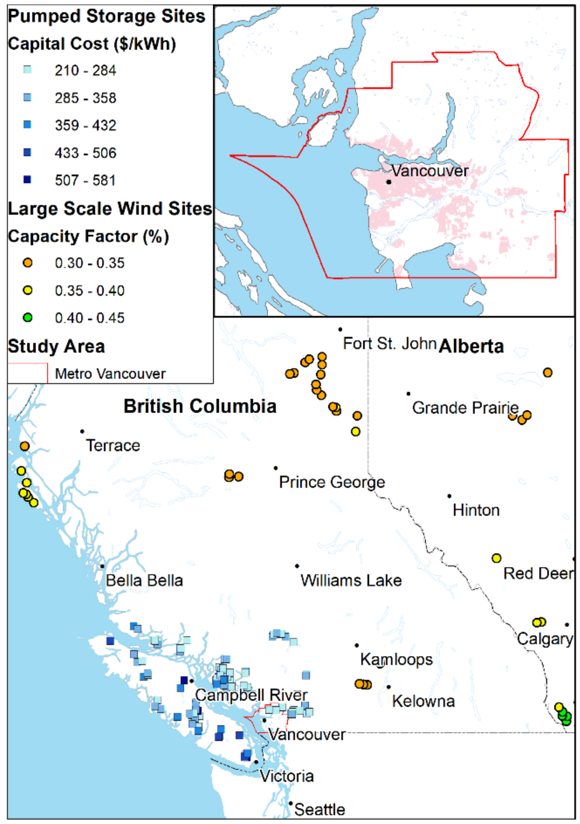

Figure 5-1. Land contained within the red outline of the Metro Vancouver Regional District is considered urban area for the purpose of this study. Actual built-up areas are solid red in the top map. Potential sites for pumped storage are located in southwestern British Columbia (Knight Piésold Ltd., 2010). Potential wind energy sites are clustered in four regions around south central, eastern, western and central British Columbia (GE Energy Consulting, 2016). Potential ground-mounted solar sites are not shown because solar potential is less site-specific than wind and pumped storage potential.

Metro Vancouver lends itself to investigating the land area impacts of urban renewable energy requirements, because the district is committed to reducing carbon emissions from all sectors by 80% between 2007 and 2050 (Metro Vancouver, 2018). This transition requires significant deployment of additional renewables. The largest city in the district, the City of Vancouver, aims to exclusively use renewable energy by 2050 (City of Vancouver, 2015). In 2014, renewable sources provided only 31% of total energy consumed, the majority of which was electricity produced from hydro (90%), forest biomass (6%) and small share of wind power (1%) (National Energy Board of Canada, 2019). The remaining 69% of energy consumed by space heat and transportation were derived from fossil fuels. The City of Vancouver plans to eliminate fossil fuel use by doubling the electricity consumption to a 75% share of total energy consumption and supplying the remaining 25% with biogas and biofuels (City of Vancouver, 2017). Increased building energy efficiency and deployment of district heating networks constitute additional transition plans. This study does not investigate reduced energy demand from energy efficiency measures or non-electric sources. Instead, electricity from renewable sources provides all space heat, road transportation and remaining electricity demand equivalent to the energy consumed in 2016.

5.2.2 Electricity System Model

The electricity system model (Figure 5-2) determines the required capacities of generation and storage technologies capable of supplying the exogenous electricity demand at the minimum total net present system cost. The model defines the installed capacities and dispatches each technology to supply the urban energy demand in every hour of the year. The installed capacities remain constant over the one-year modelling period. Installation is subject to technology specific constraints on available capacity. Dispatch is subject to technology specific generation profiles and annual energy production constraints. Section 5.2.4 details available capacity, profiles and production constraints.

The system cost includes capital costs, fixed and variable operating costs, and costs for impacting rural land area. Minimizing the net present system cost determines cost-optimal installation and dispatch of technologies. *Net present* means that discounted and depreciated salvage values of technology investments credit the total system cost at the end of the modelling period. Technology lifetimes exceed the modelling period. Crediting the salvage value attributes the amortized share of investment costs to the modelling period. The salvage value is discounted at 6%.

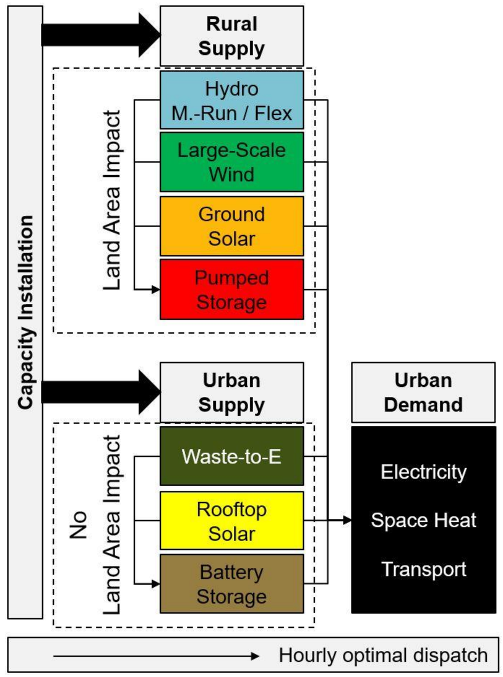

Figure 5-2. Representation of the electricity system model. The model defines and dispatches installed capacities of urban and rural electricity generation and storage technologies to meet the hourly urban energy demand. The total rural land area impact depends on the installed power capacity (km²/GW) of rural generation and the installed energy capacity (km²/GWh) of rural storage technologies. Urban technologies do not impact rural land area.

The electricity system model used in this study is based on the bottom-up, linear programming model OSeMOSYS (Howells et al., 2011). This model is well suited to investigate supply-side capacity expansion and dispatch in the context of land, demonstrated in studies that e.g. link sustainable energy constraints to available agricultural land and water resources in Uganda (Gardumi et al., 2018), investigate land use strategies in the context of bioenergy crops in post-conflict Columbia (Gonzalez-Salazar et al., 2017), and quantify the land area impacts of strict emission reductions in Alberta, Canada (Palmer-Wilson et al., 2019). To enable the investigation described in this study, the OSeMOSYS model is modified in three ways.

First, a new *land area impact* parameter defines the impacted area per installed capacity of generation and storage technologies. Generation technologies impact land area based on their installed power capacity in km²/GW (Palmer-Wilson et al., 2019). Storage technologies impact land area based on their installed energy capacity in km²/GWh (Knight Piésold Ltd., 2010). Section 5.2.6 describes technology specific land area impacts.

Second, the objective function is amended to include the cost of impacting land area in M$/km², subject to the installed capacities of generation and storage technologies. Within each optimization, this land impact cost per area is constant across all technologies, but the specific land area impact varies by technology. Land impact costs have no salvage value so that no value is credited towards the system cost at the end of a technology's operational lifetime.

Third, the storage module contained in the original OSeMOSYS is simplified to reduce computational complexity. This simplification removes additional *modes of operation* that normally distinguish between storage charging and discharging. Instead, storage may operate in reverse to alter the operating mode.

5.2.3 Electricity demand scenarios

This study assumes electrification of Metro Vancouver at the start of 2016. In this "over-night" transformation, electricity replaces all fossil fuels that served space heat and road transportation in that year. The *total electrified demand* is defined as the sum of the heat, transportation and remaining electricity demand. The heat demand includes residential, commercial and institutional space heat demand. The transportation demand includes passenger and freight transportation energy demand. Remaining electricity is the historically observed electricity demand but excludes the share of historically electric space heating to avoid double counting. Metro Vancouver's heat, transportation and electric energy demands are estimated from data available for British Columbia (BC Hydro, 2016; Natural Resources Canada, 2019) by scaling via their population ratio of 53.3% (Statistics Canada, 2017). Creation of this electrification demand data is detailed in supplementary information section 5.6.

The four electricity demand scenarios listed in Table 5-1 simulate possible heating system electrification options and battery-electric vehicle charging profiles. In the LOW scenarios, space heat is mostly provided by low-efficiency electric resistance heating with a mean efficiency of 1.08, equivalent to the building-stock weighted mean efficiency observed in 2016 (Natural Resources Canada, 2019). In the HIGH scenarios, space heat is exclusively provided by high-efficiency heat pumps with a seasonal coefficient of performance of 3.5 (Jadun et al., 2017). In the PEAK scenarios, electric vehicle charging peaks in the evening hours at 5 and 6 p.m. (Keller et al., 2019b). In the UNIFORM scenarios, electric vehicles charge at a constant rate. The heating efficiency affects the total annual and the peak electrified demand; the vehicle charging profile exclusively affects the peak electrified demand.

Table 5-1. Annual and peak electricity demand for Metro Vancouver in the year 2016 assuming electrified space heat and road transportation. The total electrified demand is the sum of space heat, road transportation and remaining electricity demand. The four rows contain the scenario name combinations that identify the assumed heating efficiency and vehicle charging profile such that e.g. the "HIGH-PEAK" scenario assumes high-efficiency heating with an evening-peaking vehicle charging profile.

	Annual Demand					Peak Demand
Scenario (efficiency-profile)	**Profile Figure 5-3**	**Space Heat (TWh)**	**Road Transport. (TWh)**	**Remaining Electricity (TWh)**	**Total Electrified (TWh)**	**Total Electrified (GW)**
LOW-PEAK	(A)	14	14.4	25.7	54.2	12.1
HIGH-PEAK	(B)	4.3			44.5	9.1
LOW-UNIFORM	(C)	14			54.2	10.3
HIGH-UNIFORM	(D)	4.3			44.5	6.8

The total electrified demand differs exclusively between the HIGH and LOW scenarios because space heat demand depends on the heating system efficiency. The annual road transportation and remaining electricity demand remain constant between scenarios. The peak demand in the right column of Table 5-1 is the maximum demand that occurs in any hour of the given scenario. The varying peak demand demonstrates the difference between PEAK and UNIFORM scenarios that occurs in spite of their equal annual demand.

Figure 5-3 shows the total hourly electricity demand over the course of the year in the left column. The center and right columns respectively show the stacked components of the total electricity demand during a high heat demand period (January) and a low heat demand period (July).

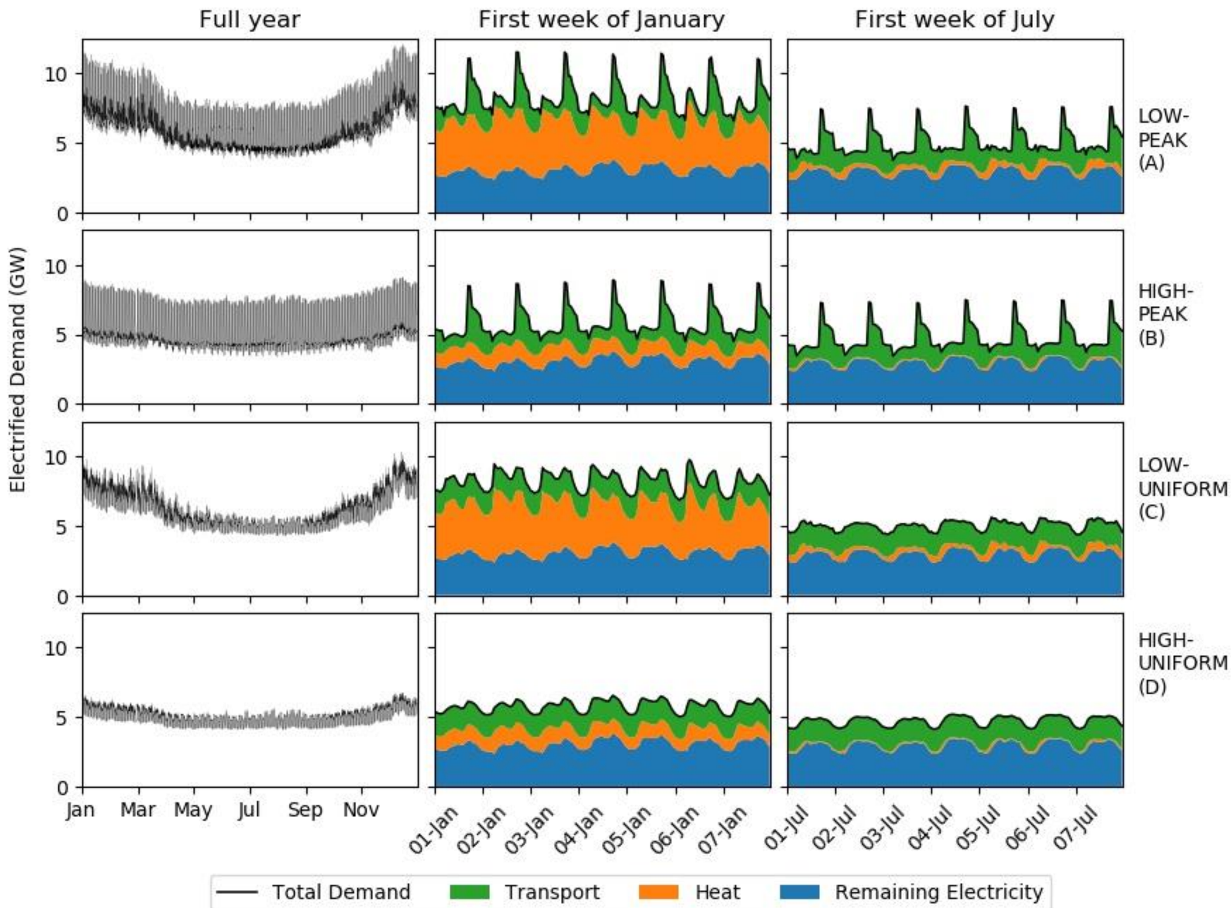

Figure 5-3. Assumed electricity demand profiles for Metro Vancouver with electrified space heat and road transportation. Rows show combinations of LOW- or HIGH-efficiency space heat demand, with PEAK- or UNIFORM road transportation demands that charge battery-electric vehicles. The left column shows the electrified total hourly demand for the year 2016. The middle column shows the first seven days of January with relatively high space heat energy demand. The right column shows seven days in July with relatively low space heat demand.

5.2.4 Electricity generation

Rural generation technologies include hydro, wind and ground solar. Urban generation technologies include rooftop solar and waste-to-energy. Generation technologies are limited by maximum installed capacity, maximum annual electricity production, or both. Hydro and rooftop solar are limited by capacity. Hydro and waste-to-energy are limited by maximum annual electricity production. Waste-to-energy is dispatchable. Wind and solar generate electricity via pre-determined hourly profiles.

Capital costs and operation and maintenance costs are the minimum costs forecast by the US National Renewable Energy Laboratory's (NREL) Annual Technology Baseline (National Renewable Energy Laboratory, 2018). This study applies the 2050 cost forecasts. Very small variable operation and maintenance costs define the order in which surplus electricity production is attributed to the non-dispatchable variable renewable generators wind, ground solar and rooftop solar. Wind produces surplus first, then ground solar, then rooftop solar.

Hydro is modelled via a partially flexible, partially exogenous dispatch profile to simplify the complex operating constraints observed by British Columbia's large hydro and run-of-river power stations. Real-world operating constraints include snowmelt-driven water inflows, minimum water discharge rates or flood control. In fiscal 2015, BC Hydro generated 60 TWh of electricity (BC Hydro, 2013b). This study estimates that ~ 41 TWh were dispatched to meet operating constraints rather than electricity demand; an estimated 19 TWh were freely dispatchable (BC Hydro, 2017). The model represents hydro as two separate hydro-flex and hydro-must run generation technologies. Hydro-flex represents the dispatchable share of hydro energy and capacity. Hydro-must run generates electricity according to an estimated exogenous monthly profile listed in Table 5-2. The model-exogenous capacities and maximum hourly capacity factors of hydro-flex and hydro-must run constrain total hydro generation in any hour to the 12,928 MW of total installed large hydro and run-of-river capacities observed in 2015 (BC Hydro, 2013b). All energy and power capacities listed in the paragraph are scaled Metro Vancouver's population share of 53%. The model must install and cannot exceed the exact exogenous hydro capacity. Hydro capital costs add to the net present system costs. Hydro's assumed lifetime is 80 years.

Table 5-2. Estimated monthly minimum capacity factors of hydro generation in British Columbia (BC Hydro, 2017). Generation peaks in June and July when snowmelt freshet inflows dominate.

Month	Capacity Factor [%]
January	31
February	29
March	29
April	31
May	43
June	47
July	47
August	43
September	37
October	35
November	31
December	31

Wind power capacity is unlimited. The exogenous hourly wind profile is the hourly mean capacity factor of four randomly author-selected wind sites located in southern, central, coastal, and eastern British Columbia. The wind profiles are taken from the Pan-Canadian wind integration study (GE Energy Consulting, 2016). The annual mean capacity factor is 35.6%.

Ground solar capacity is unlimited. The exogenous hourly ground solar profile is the hourly mean capacity factor of simulated 1-axis tracking systems located in Kamloops, Cranbrook and Victoria in British Columbia. All locations are weighted equally. The ground solar profiles are taken from NREL's PV Watts (National Renewable Energy Laboratory, 2013). The annual mean capacity factor is 24.3%.

Urban rooftop solar capacity in Metro Vancouver is limited to 8.8 GW-AC assuming a 1.1 DC/AC ratio and 63.4 km^2 of available rooftop area. This maximum capacity is based on available rooftop potential assessed by Google's Project Sunroof in King County, WA, USA (Google, 2018), and has been scaled by population. Project Sunroof applies digital elevation data and overhead imagery to optimally place 250 W panels on building rooftops that meet several technical potential criteria. Criteria include a minimum 2 kW capacity per rooftop, 75% minimum irradiance in comparison to optimum, and a maximum 60° roof pitch angle. Panel placements are set back from rooftop edges and exclude most shaded areas and obstacles. King County contains the City of Seattle and several smaller towns, with a total population of 2,188,649 persons (U.S. Census Bureau Population Division, 2018). King County is located ~180 km south of Vancouver. Geographic similarities including its seaside location, a dense city center, and sprawling suburbs make King County a viable proxy to Vancouver. The exogenous hourly rooftop solar profile is the capacity factor of a simulated fixed-tilt system located in Vancouver, British Columbia. The profile is taken from NREL's PV Watts (National Renewable Energy Laboratory, 2013). The annual mean capacity factor is 14.2%.

Urban waste-to-energy is limited by maximum annual electricity production. The available fuel is based on municipal, landfill, agricultural, pulp mill and waste water feedstocks. Hallbar Consulting (2017) estimates 11.9 PJ to be available at costs of up to 28 $\$/GJ_{th}$ in British Columbia. That available energy is scaled by population to Metro Vancouver and converted to 1.75 TWh of thermal energy or 0.33 TWh of electricity at 19% generator efficiency (Energy Information Administration, 2018). Waste heat recovery is not included in this study.

5.2.5 Electricity Storage

Electricity storage technologies provide flexibility to temporally balance electricity supply and demand. Storage technologies can store electric energy up to their installed *energy capacity*. Storage technologies can generate power to supply demand, or demand power to increase stored energy, up to the installed *power capacity*. The electricity system optimization determines energy and power capacity independently of each other.

This study includes rural pumped storage and urban battery storage. Both storage options are limited by energy capacity. Power capacity is unlimited. The rural land area impact of pumped storage is exclusively dependant on the installed energy capacity, because significant water reservoir area must be designated towards energy storage. Installed power capacity does not impact rural land area, because the power capacity determining turbines of pumped storage systems require insignificant amounts of land area in comparison to the reservoir.

Rural pumped storage is limited to 696 GWh, based on a geographic information analysis conducted by Knight Piésold Ltd. (2010). That study identified 121 potential fresh water sites (Figure 5-1) in the lower mainland of British Columbia with energy capacities of 3 or 6 GWh. The assumed operational lifetime is 80 years.

Urban battery storage does not impact land area. Battery storage is inspired by the *Tesla Power Wall 2*, a wall-mounted lithium-ion battery with an energy capacity of 13.5 kWh (Tesla, 2019). The 125 kg mass and 0.13 m^3 volume device is designed for commercial and residential use. This study exogenously limits battery storage energy capacity to 33.3 GWh, equivalent to one Tesla Power Wall 2 per person in Metro Vancouver. The assumed operational lifetime is 10 years, equivalent to the manufacturer's warranty period.

Capital costs apply to power and energy capacity separately. Capital costs for both storage technologies are based on Schmidt et al. (2019), who forecast capital costs of several storage technologies between 2015 and 2050 using experience curves. Power and energy capacity cost forecasts for 2050 and 2030 are listed in Table 5-3. This study applies 2050 costs; 2030 costs are listed for reference. This study does not apply storage operating costs. The state of charge of either storage technology must be the same at the beginning and at the end of the one-year modelling period. The initial state of charge is chosen by the model. Both storage technologies operate without efficiency losses to reduce computational complexity.

Table 5-3. Forecasted costs for installing power and energy capacity of storage technologies (Schmidt et al., 2019). The electricity system optimization determines energy and power capacity independently of each other. The total cost of storage is the sum of installed power and energy capacity costs.

	Power [M$/GW]		Energy [M$/GWh]	
Technology | Year	**2050**	**2030**	**2050**	**2030**
Pumped Storage	1152	1129	82	80
Battery Storage	95	156	112	184

5.2.6 Rural land area impacts of electricity generation and storage technologies

All rural technologies impact rural land area. This study defines rural land area impact (RLAI) as the physical footprint of the infrastructure and the spacing between devices typically located in rural areas. The spacing is the area between turbines of a wind farm, the arrays of a solar farm, and includes reservoir areas of hydro and pumped storage facilities.

Capacity dependant RLAIs are listed in Table 5-4. Generation technologies impact rural land area based on their installed power capacity. Storage technologies impact rural land area based on their installed energy capacity. RLAI of wind and ground solar is derived from (Trainor et al., 2016) and based on a comprehensive review of literature and discussion available in Palmer-Wilson et al. (2019). RLAI of hydro and pumped storage are based on data specific to British Columbia. Hydro RLAI is based on the 3093 km^2 total reservoir area on crown land licensed to BC Hydro (Government of British Columbia, 2019) divided by the 12,928 MW of total installed large hydro and run-of-river capacities observed in 2015 (BC Hydro, 2013b). RLAI of pumped storage is based on a geographic information analysis of 121 potential fresh water sites in the lower mainland of British Columbia (Knight Piésold Ltd., 2010). The data includes upper and lower reservoir areas for each site ranging from 0.06 to 37.2 km^2/GWh. In this study pumped storage RLAI is 6.67 km^2/GWh, the mean sum of upper and lower reservoir areas.

Table 5-4. Rural land area impact specific to electricity generation and storage technologies. Only rural technologies impact rural land area. Urban technologies do not impact additional land. Underlined values are applied in this study. Other values are provided for a sense of range.

Generator Technology	**Type**	**Power Capacity RLAI (km²/GW)**			**Rationale and Source**
Percentile		**25th**	**Median**	**75th**	
Hydro	Rural	-	239.2	-	(Government of British Columbia, 2019) (BC Hydro, 2013b)
Large-Scale Wind	Rural	202.3	368.3	465.4	(Trainor et al., 2016)
Ground Solar	Rural	28.2	34.4	38.9	(Trainor et al., 2016)
Rooftop Solar	Urban	0	0	0	No additional land needed
Waste-To-E	Urban	0	0	0	Use of urban waste stream
Storage Technology		**Energy Capacity RLAI (km²/GWh)**			
Range		**min**	**Median**	**max**	
Pumped Storage	Rural	0.06	6.67	37.2	(Knight Piésold Ltd., 2010)
Battery Storage	Urban	0	0	0	Urban residential & commercial wall mount

5.3 Results

This study investigates the *rural land area impact* (RLAI) associated with electricity generation and storage capacity required to supply electrified Metro Vancouver. This section compares cost-optimal electricity generation and storage systems for a broad range of exogenously defined *land impact costs* (LIC). The results describe electricity systems that supply the HIGH-PEAK or LOW-PEAK electrified demand using forecasted 2050 technology costs. The HIGH-UNIFORM and LOW-UNIFROM scenarios change system characteristics insignificantly and are not investigated further.

Figure 5-4 shows characteristics of systems optimized for a given LIC. LIC increases exponentially from left to right on the horizontal axes for all plots. The system characteristics plotted on the vertical axes include technology-specific power capacity and storage energy capacity (top row), annual electricity generation and share of demand supplied by urban energy production (center row), and rural land area impact and net present system costs (bottom row). Net present system costs do not include land impact costs. The left column represents the lower electricity demand (HIGH-efficiency space heat scenario). The right column represents the higher electricity demand (LOW-efficiency space heat scenario). PEAK means electric vehicle charging peaks in evening hours. Note that hydro is constant across all LICs and exogenously set to the values observed in 2016. The model cannot deviate from those historical values. These plots reveal six important findings.

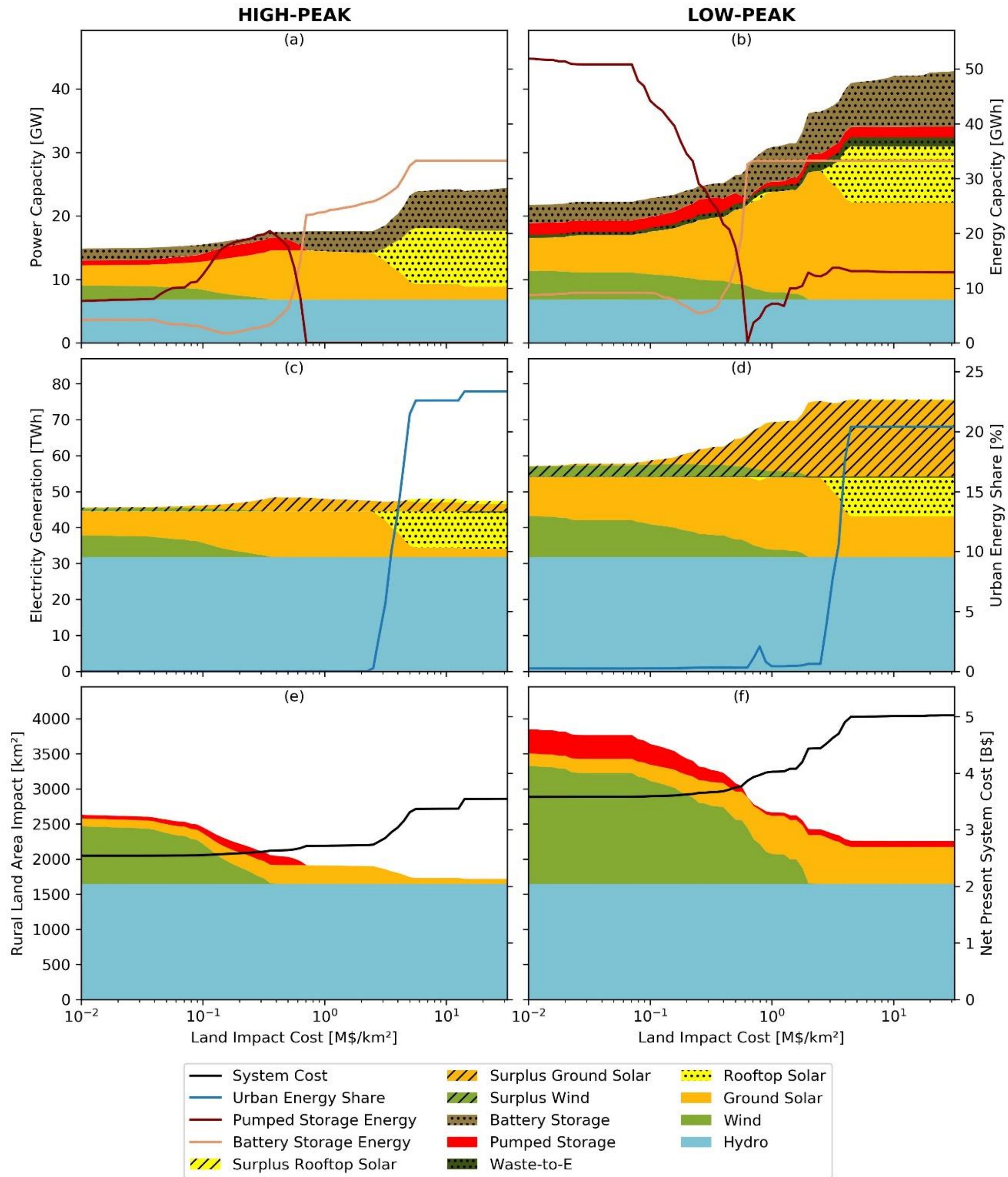

Figure 5-4. Electricity system compositions that can supply Metro Vancouver's electrified demand assuming evening-peaking transportation demand and HIGH-efficiency (left column) or LOW-efficiency space heating (right column). Rows show installed power capacity of generation and storage technologies (top row – left axis), energy capacity of storage technologies (top row – right axis), annual electricity generation by technology (center row – left axis), the share of annual demand supplied by urban energy production (center row – right axis), rural land area impact by generation and storage technologies (bottom row – left axis), and net present system costs (bottom row – right axis). Area plots are stacked and refer to left axes. Line plots are not stacked and refer to right axes. Urban

technologies appear dotted. Surplus electricity production appears diagonally hatched. Land impact costs on the horizontal axes increase logarithmically from 0.01 M$/km² on the left to 31.6 M$/km² on the right.

First, the composition of the optimal electricity supply system depends on LIC. A change in LIC changes the optimal system non-linearly. As LIC increases, technologies are gradually replaced. Abrupt replacements do not occur. In the HIGH-PEAK scenario, optimal systems include wind and pumped storage only at low LICs, and rooftop solar and waste-to-energy only at high LICs. All optimal systems include ground solar and battery storage in the HIGH-PEAK scenario. In the LOW-PEAK scenario, optimal systems include wind only at low LICs, and rooftop solar only at high LICs. All optimal system include ground solar, waste-to-energy, battery storage, and pumped storage in the LOW-PEAK scenario.

Second, increasing LIC increases the total installed power capacity. The increase is caused by substituting wind with ground solar and then rooftop solar; each substituting technology has a lower capacity factor than the previous technology. In the HIGH-PEAK scenario Figure 5-4(a), the initial installed power capacity increases by 64% from 14.9 to 24.4 GW. Ground solar fully replaces the initial 2.2 GW of wind at 0.4 M$/km² LIC. Rooftop solar starts replacing ground solar at 2.5 M$/km² LIC until rooftop solar reaches the exogenous maximum 8.8 GW at 5.6 M$/km² LIC. In the LOW-PEAK scenario Figure 5-4(b), the initial power capacity increases by 97% from 21.7 to 42.8 GW with similar technology replacement trends. The initial 4.6 GW of wind are extinguished at 2.5 M$/km² LIC. Rooftop solar expands from zero to 8.8 GW between 2.8 and 4.5 M$/km² LIC.

Third, the optimal choice of storage technologies and their installed energy and power capacities vary with LIC. Increasing LIC increases the total storage power capacity monotonically in both scenarios, but the total energy capacity trends differ significantly between scenarios. In the HIGH-PEAK scenario Figure 5-4(a), total energy capacity increases almost monotonically by a factor of 2.8 from 11.9 to 33.3 GWh between 0.01 and 5.6 M$/km² LIC, with varying contributions from individual technologies. First, pumped storage energy capacity increases by a factor of 2.6 from 7.7 GWh at 0.01 M$/km²

LIC to the maximum 20.4 GWh observed at 0.35 M$/km² LIC. This increase in energy capacity coincides with declining wind and its substitution with ground solar, because eliminating wind increases the system's overall variability of hourly power generation. Next, increasing LIC further extinguishes pumped storage and increases battery storage gradually. This gradual increase in battery storage capacity coincides with declining ground solar power capacity. Substitution of ground solar with rooftop solar then increases battery energy capacity more rapidly until battery energy capacity reaches the exogenous maximum of 33.3 GWh at 5.6 M$/km². In the LOW-PEAK scenario Figure 5-4(b), total energy capacity decreases from 60.6 to 30.5 GWh between 0.01 and 0.4 M$/km² LIC, then increases to 47.0 GWh at 3.5 M$/km² LIC, followed by a slight decline to 46.3 GWh at 5.6 M$/km² LIC. The initial decline of total energy capacity is caused almost exclusively by pumped storage capacities that decrease rapidly from 51.9 GWh at 0.01 M$/km² LIC until pumped storage energy capacity reaches the minimum value of 0.1 GWh to accommodate the rising cost of impacting land. Battery storage substitutes diminishing pumped storage until battery energy capacity reaches the exogenous maximum 33.3 GWh at 0.7 M$/km² LIC. Once battery storage reaches the maximum, pumped storage energy capacity increases until it remains constant at 12.9 GWh.

Fourth, all optimal systems produce surplus electricity that exceeds demand. In the HIGH-PEAK scenario Figure 5-4(c), increasing LIC increases surplus generation from 1 TWh at 0.01 M$/km² LIC to the maximum observed 3.9 TWh at 0.4 M$/km² LIC. This surplus is equivalent to 2.3% and 8.8% of the 44.5 TWh annual demand. In the LOW-PEAK scenario Figure 5-4(d), increasing LIC increases surplus generation from 2.9 TWh at 0.01 M$/km² LIC to the maximum observed 21.5 TWh at 4.5 M$/km² LIC. This surplus is equivalent to 5.3% and 39.5% of the 54.2 TWh annual demand. This higher surplus generation in the LOW-PEAK scenario is caused by the temporal mismatch between the space heating demand in winter and high solar generation in summer. It is LIC-effective to install more solar capacity and generate surplus than it is to add additional storage capacity.

Fifth, rooftop solar can generate a significant share of the urban energy demand while waste-to-energy generation is negligible. In Figure 5-4(c) and (d) rooftop solar generates

10.0 TWh in the HIGH-PEAK and 10.7 TWh in the LOW-PEAK scenario. Waste-to-energy generates an additional 0.3 TWh at most in both scenarios because feedstocks are limited to 6.3 PJ thermal energy and the assumed 19% thermal to electric efficiency is relatively low. The total generation of these two urban technologies leads to a maximum share of urban electricity generation of 23.3% in the HIGH-PEAK, and 20.4% in the LOW-PEAK scenario. Note that surplus generation is assigned first to wind, then ground solar, then rooftop solar. Achieving the aforementioned shares of urban electricity generation requires arbitrarily assigning surplus generation to ground solar before rooftop solar.

Sixth, increasing LICs reduces RLAIs and increases NPCs, but this trade-off is non-linear and increasing LIC to reduce RLAI has diminishing returns. In the HIGH-PEAK scenario Figure 5-4(e), RLAI decreases by 37.7% from 2635 km² to the minimum 1720 km² at 14.1 M$/km² LIC; simultaneously, NPCs increase by 39.6% from 2.53 to the maximum 3.55 B$ at the same LIC. The non-linearity of the RLAI/NPC trade-off is exemplified by the optimal system at a LIC of 1 M$/km² which impacts 1912 km² of rural land area at a 2.72 B$ NPC in the HIGH-PEAK scenario. This trade-off is equivalent to an RLAI reduction of 27.4% at a NPC increase of 7.5% in comparison the optimal system at 0.01 M$/km² LIC. In the LOW-PEAK scenario Figure 5-4(f), RLAI decreases by 41.2% from 3853 km² to the minimum 2264 km² at 4.5 M$/km² LIC; simultaneously, NPCs increase by 40.3% from 3.58 to 5.02 B$ at the same LIC. In both scenarios hydro RLAI is constant at 1650 km², equivalent to the BC Hydro's licensed reservoir area attributed Metro Vancouver's population.

5.4 Discussion

This study investigates the rural land area impact (RLAI) of supplying the electrified energy demand of the Metro Vancouver Regional District in Canada with electricity from renewable sources. The total electrified demand includes historical electricity demand, and the electricity-equivalent of fossil fuels consumed in the space heat and road transportation sectors in 2016. A one-year capacity expansion and dispatch model reveals a broad range of feasible electricity system compositions, net present costs, and their rural land area impacts. Two demand scenarios are presented and differ in their assumed efficiency of electrified space heat technology. The HIGH-PEAK scenario assumes deployment of high-efficiency heating resulting in a 44.5 TWh total electrified demand. LOW-PEAK scenario assumes deployment of low-efficiency heating resulting in a higher 54.2 TWh total electrified demand. Electrification therefore increases the 30 TWh electricity demand observed in 2016 by 48% to 81%. Both scenarios assume evening-peaking electrified transportation demand. Peak demands are 9.1 and 12.1 GW in the HIGH-PEAK and LOW-PEAK scenario, respectively.

Electrification of space heat and road transportation in Metro Vancouver requires designating between 70 and 2203 km² of additional rural land area to renewable electricity generation and storage, excluding transmission. Each of Metro Vancouver's 2.4 million residents would impact between 29 and 918 m² of additional rural land area. This area needs to be added to the existing 1650 km² hydro reservoir area attributed to Metro Vancouver's population, assuming that 53% of reservoir areas on crown land licensed to the utility BC Hydro supply Metro Vancouver. The *maximum necessary additional RLAI* of 2203 km² assumes transitioning space heat technology to low efficiency electric resistance heaters and designating 1681 km² to wind (4.6 GW), 176 km² to ground solar (5.1 GW), and 346 km² to pumped storage (1.8 GW / 51.9 GWh). Additionally, waste-to-energy (0.5 GW) and battery storage (2.8 GW / 8.7 GWh) need to be deployed in the urban area. The *minimum feasible additional RLAI* of 70 km² requires transitioning space heat technology to high efficiency heat pumps and designating all 70 km² to ground solar (15.3 GW). Additionally, 33.3 GWh of battery energy storage capacity (one Tesla Power Wall 2 with 13.5 kWh of capacity per Metro Vancouver resident) and 8.8 GW of rooftop solar on all viable rooftops in Metro Vancouver (63.4 km² - not included in RLAI) need to be deployed in the urban area. However, energy system planners can choose a range of technology options that impact additional rural land area anywhere in between the minimum feasible and maximum necessary RLAI.

Options to reduce RLAI include 1) increasing the efficiency of the electric space heating technology, and 2) selecting generation and storage technologies that impact a smaller rural land area, or deploying urban technologies, but at a higher total system cost.

The efficiency of the space heating technology significantly affects RLAI, generation and storage capacity requirements, and system costs. High efficiency heat pumps with a coefficient of performance (COP) of 3.5 reduce the annual electrified demand by ~18% or ~9.7 TWh. For perspective, the observed provincial average COP for residential electric heating was 1.08 in 2016 (Natural Resources Canada, 2019). The higher efficiency heating technology reduces additional RLAI by 55% or 1218 km² and the net present system costs by 29.3% (excluding the cost of deploying heat pumps). The higher efficiency has this significant impact on RLAI and costs because the space heat demand is negatively correlated with hydro and solar generation. Space heat demand occurs almost exclusively in the cold winter months November to February. Natural water inflows into the existing hydro system dominate in June and July and only ~1/3 of hydro's annual electricity generation can be dispatched flexibly. Solar generation also dominates in summer months. Supplying the higher winter demand therefore requires installing additional power and energy capacity. The additional power capacity increases surplus electricity generation from 4.1% to 10.9% of annual demand, but is more cost-effective than increasing storage energy capacity further. Space heating-related efficiency measures can therefore significantly reduce RLAI.

Additional RLAI reduction is possible at small additional costs, because the trade-off between RLAI and costs is non-linear. In the HIGH-PEAK scenario, eliminating wind and pumped storage while designating 262 km² to ground solar reduces the total additional RLAI by 73.4% while net present system costs increase by 6.5%. The RLAI reduction exceeds costs significantly because wind RLAI includes the space between turbines. This spacing requirement renders wind RLAI an order of magnitude larger than the RLAI of ground solar. Further reducing RLAI to the minimum feasible 70 km² substitutes lower-cost ground solar with higher-cost rooftop solar and waste-to-energy capacity. This substitution requires additional battery storage capacity. This system composition reduces additional RLAI by 92.9%, but increases net present system costs by 27.7%. This non-linear trade-off between RLAI and costs is significant because policy makers can choose the desired electricity system composition and determine the associated system costs and the required land area.

The minimum feasible RLAI is limited by urban renewable energy resources. The highest cost-optimal system generates 23.3% of annual demand from the urban sources rooftop solar and waste-to-energy, but rooftop solar provides the majority of that share. Waste-to-energy supplies a mere 0.7% of annual demand. These findings match previous work that found rooftop solar can supply at most 36% of the annual electricity demand in Wroclaw, Poland (Jurasz et al., 2019), 61% in Oeiras, Portugal (Amado and Poggi, 2014), or 38% in Lethbridge, Canada (Mansouri Kouhestani et al., 2019). Only select Peruvian cities feature sufficient rooftop area and solar radiation to supply the relatively low present-day electricity demand (Bazán et al., 2018). The low waste-to-energy potential also matches previous work. Waste-to-energy could provide at most 2.1% of the 2014 energy demand in Kampala, Uganda (Munu and Banadda, 2016). Additional urban sources are needed to further reduce the rural land area impact. These might include small-scale rooftop wind power or geothermal energy. However, these sources were not included in this study because these resources likely offer limited potential in Metro Vancouver. Small-scale wind is feasible only in the windiest cities (Mithraratne, 2009) and on the tallest buildings in the urban environment (Millward-Hopkins et al., 2013). Geothermal energy is limited to serving ground-source heat pumps in most cities (Kammen and Sunter, 2016), and this technology faces significant earthquake risks in urban areas (Kraft et al., 2009).

All scenarios and system compositions require significant storage energy capacity to balance intra-annual supply and demand. The largest observed energy storage capacities are 51.9 GWh for pumped storage and the exogenous maximum 33.3 GWh for battery storage. Installing this pumped storage capacity would require developing nine of the 121 potential sites investigated by Knight Piésold Ltd. (2010). The largest currently existing pumped storage facility in Bath County, Virginia provides 24 GWh and the cumulative global pumped storage energy capacity was 1389 GWh in 2013 (Schmidt et al., 2017). Deployment of the required pumped storage capacity is feasible with present-day technology. Installing the 33.3 GWh of battery energy storage is significantly more challenging. The cumulative global energy capacity of stationary lithium-ion batteries for residential and utility applications was only 3.43 GWh in 2017. Although market investments forecast a cumulative global capacity between 3239 and 4162 GWh for 2050

(Schmidt et al., 2017), installing 33.3 GWh of battery storage would represent between 1.0% and 0.8% of the global market share to provide low-carbon electricity to a much smaller share of the global population. This comparison exemplifies the high value of dispatchable electricity generation resources that can potentially lower the required energy storage capacity.

In this study, energy and power capacity of storage technologies are determined independently of each other. Across all determined electricity system compositions, storage durations (energy to power capacity ratios) range from 7.6 to 28.4 h for pumped storage and from 2 to 7.7 h for battery storage. These durations are in line with technology performance characteristics. Discharge duration collected by Schmidt et al. (2019) range from 1 to 24 h for pumped storage and from 0.25 to 5 h for lithium-ion batteries. However, the electricity system model applied in this work examines a snapshot for a single year due to limited demand data availability. Assessing a range of temporal demand and supply profiles may render more comprehensive insight into required storage capacity and duration. This area warrants further study.

The method of determining the full range of renewable energy related RLAIs of electrification using the most abundant renewable sources is an improvement upon previous approaches. Previous work assesses the RLAI of urban renewable energy requirements for prescribed system compositions and limits the technology options to rooftop and ground-mounted solar with battery storage (Arcos-Vargas et al., 2019), or compares annual energy supply and demands without considering the need for storage (Bazán et al., 2018; Munu and Banadda, 2016). Others may underestimate storage requirements by using monthly average wind and solar generation profiles (Bagheri et al., 2018). No previous study accounts for the land requirements of pumped storage reservoirs. These differences in methods make comparison of RLAI found in this and previous work challenging.

The work presented here has several limitations. First, Metro Vancouver's energy demand is scaled from values available for British Columbia, but hydro supply is scaled from values available by the utility BC Hydro. BC Hydro represents a large share but not all hydro resources available within the province.

Second, this study does not account for impacts of electricity trade. In 2016, BC Hydro net-exported 5.4 TWh (BC Hydro, 2019), which is equivalent to ~10% of the annual provincial demand. However, British Columbia has been a net electricity importer in 7 of the 11 years between 2005 and 2015 (Canada Energy Regulator, 2015). British Columbia's multi-year storage capacity provides arbitrage opportunities that generate significant revenues for the province. Investigating the impacts of electrification on electricity trade warrants further study.

Third, BC Hydro has surplus energy to potentially accommodate some electrification demand without requiring expansion of supply. The dammed hydropower project Site C will add 5 TWh and 1.1 GW of energy and power capacity in 2024. Demand side management measures could save ~ 5 TWh of annual demand. However, assessing the potential to accommodate electrification without expansion of supply is challenging, because publicly available information on present-day demand and supply varies by several TWh. Mismatched information sources include the Balancing Authority Load, BC Hydro's Revenue Rate Applications, Annual Service Plan Reports, and Resource Plans. Those sources draw different boundaries around the electricity system and insufficiently document those boundaries.

Fourth, the determined RLAI may be optimistic. The electricity system model operates with perfect foresight of variable demand and supply, and does not include efficiency losses between charging and discharging energy storage technologies. Supplementing operating and efficiency losses may require additional energy storage and power generation capacities that might impact additional rural land area. Furthermore, additional low-carbon energy sources are needed to reduce greenhouse gas emissions beyond the space heat and road transportation sectors. The industrial sector and the airline, marine and railway transportation sector energy demands are not included in the 100% renewable energy plans adopted by the City of Vancouver, and are not represented in this study. Therefore, significant additional emission reduction efforts are needed to meet net-zero emission targets by mid-century. Future work may opt to include all economic activity of urban areas to improve estimates of land area impacts associated with large-scale decarbonization via electrification with renewable energy sources.

5.5 Conclusion

Global energy consumption in cities will continue to increase in the coming decades as a growing number of people will move to and live in urban areas. With urban areas already consuming 64% of global primary energy and emitting 70% of global greenhouse gas emissions in 2013 (International Energy Agency, 2016), local municipal efforts to decarbonizing energy sources are indispensable to mitigate the global climate change (United Nations Human Settlement Programme, 2011). Investments into wind, solar, and hydro power deployment are expanding exponentially (International Energy Agency, 2018) and cities around the globe plan to decarbonize large sections of their economies with these renewable sources. Unfortunately, renewable energy sources require significantly more land area than fossil fuels to generate equivalent amounts of electricity (Palmer-Wilson et al., 2019). Decarbonizing the non-electric sectors by substituting their fossil fuels with low-carbon electricity adds to the electricity demand. Designating sufficient land area to meet the growing urban demand may pose a barrier to the rapid expansion of renewable generation capacity needed to reduce emissions to net-zero by mid-century.

This study quantifies the rural land area impacts of urban renewable energy demands. A broad range of electricity generation and storage systems source renewable energy from urban and rural areas to supply all electricity, and electrified space heat and road transportation energy demands in the Metro Vancouver Regional District in Canada. The systems differ in their assumed cost to impact rural land area. Higher land impact costs result in systems that impact a smaller area by deploying more compact or urban technologies. This approach renders the full range of lowest-cost electricity supply systems between the maximum necessary and minimum feasible rural land area impact.

Five main conclusions can be drawn from the results of this study. First, electrifying Metro Vancouver’s space heat and road transportation sectors with renewable sources will require designating additional rural land area to electricity generation. This additional area ranges from 70 to 2203 km², excluding land required for transmission. This area needs to be added to the 1650 km² of reservoir area licensed to BC Hydro and attributed to Metro Vancouver's population.

Second, the efficiency of the deployed space heating technology significantly affects the additional rural land area impact. Increasing the average coefficient of performance from 1.08 to 3.5 reduces the annual demand by 18% but reduces the additional rural land area impact by 55%, reduces the net present system cost of generation and storage technologies by 29%, and reduces energy capacities of battery and pumped storage by 52% and 85%. Space heating has this large effect because heating demand dominates in winter months and negatively correlates with hydro and solar resources dominating in summer months.

Third, rural land area impacts can be further reduced by deploying more compact but higher-cost rural or urban generation and storage technologies. The relationship between reducing the area and bearing a higher net present system cost is non-linear and land area can be reduced significantly for relatively small increases in cost. Substituting wind with ground solar, then rooftop solar reduces the land area but increases total installed capacity and energy storage requirements. Limiting additional generation to ground solar reduces the additional rural land area impact by 73% while increasing costs by 6.5%. Deploying urban rooftop solar, waste-to-energy and battery storage can reduce additional rural land area impacts by 93% to 70 km², which is the minimum feasible area, but the net present system costs increase by 28%.

Fourth, Metro Vancouver could avoid all rural land area impacts if the minimum feasible 70 km² of ground solar could be deployed within the 2,883 km² of land in its jurisdiction. However, this would also require installing a 13.5 kWh battery for each of the 2.4 million residents of Metro Vancouver. Other urban energy sources, rooftop solar and waste-to-energy, can provide only a fraction of the electrified demand. Rooftop solar can provide ~23% of Metro Vancouver's electrified demand by utilizing all feasible rooftop areas (63.4 km²) to install 8.8 GW. The waste-to-energy contribution is negligibly small.

Fifth, significant additional energy storage capacity is required to balance variable renewable sources with demand, in spite of British Columbia's flexible hydro capacity. Additional dispatchable resources could help reduce the required energy storage capacity.

This study contributes a method to assessing the rural land area requirements of urban renewable energy demands after full electrification of space heat and road transportation sectors. Results in this study are applicable to cities beyond Metro Vancouver, because the large share of hydro power is approximately equivalent to historic electricity demand. The additional electrification demand must be supplied by expansion of new electricity generation and storage technologies. The large range of assessed land area impacts demonstrates that energy policy can significantly shape the future impact of urban energy demand on the rural lands. This policy choice is relevant because the land and landscape impacts of renewable energy infrastructure may pose a barrier to rapid deployment. The demonstrated relationship between reducing the rural land area impacts and increasing the net present system cost shows that this trade-off is strongly non-linear and significant reductions can be achieved at little extra cost. This trade-off can help mitigate concerns of land and landscape change, and help municipal decision makers strike the balance between local land impacts and global climate change mitigation efforts by making an informed choice on feasible energy supply systems and their consequences.

5.6 Supplementary Information – Creating hourly electrified demand data

Electrified demand is the sum of all electricity demands after fully electrifying space heat and road transportation in the Metro Vancouver Regional District, British Columbia, Canada. Equation (5.1) defines the annual total electrified demand E_D as the sum of electricity-equivalent space heat E_H and road transportation energy E_T demands, and the remaining electricity demand E_E observed in the year 2016.

$$E_D = E_H + E_T + E_E \tag{5.1}$$

The following four sections describe the method of estimating the total electrified demand. The first section demonstrates a generalized form of converting annual energy demands between technologies or fuels, and their temporal representation by introducing a normalized demand profile. The second, third, and fourth section describe the application of the conversion and temporal representation for the space heating, road transportation and remaining electricity, respectively. Each of the latter sections first define the specific sector demands mathematically, then describe the annual demand estimate, and then describe the hourly profile estimate. The space heating section describes the LOW and HIGH scenarios. The road transportation section describes the PEAK and UNIFORM scenarios.

5.6.1 Representation of technology conversions and hourly energy demands

The conversion of energy demand from one technology, or fuel type, to another is represented by technology-specific efficiency ratios. The temporal distribution of annual demand is represented by a normalized demand profile. Electricity, heat and transportation energy demands are all represented in this form as described by equation (5.2). Before technology conversion, the observed annual energy demand $\hat{E}$ provides an energy service at an associated observed efficiency η_{obs}. After a technology conversion, the same energy service is provided using a technology efficiency η_{trans}, which results in the new (post-conversion) energy demand E. Thus, the ratio between the observed efficiency and the converted technology efficiency determines the converted annual energy demand E. Both $\hat{E}$ and E are scalar values.

$$E = \hat{E}\,\frac{\eta_{obs}}{\eta_{trans}} \tag{5.2}$$

Hourly energy demand data is often available as a vector where each element describes the demand in that hour. The sum of all vector elements over a year renders the annual energy demand. Dividing each vector element by the annual energy demand renders a *normalized hourly demand profile* $\vec{P}$. Any vector element P_i is the fraction of the annual demand observed in hour i. Thus, the converted energy demand in hour i is the product $P_i E$ or $P_i \hat{E}\,\frac{\eta_{obs}}{\eta_{trans}}$. The annual energy demand can be written as equation (5.3).

$$E = \sum_i \left(P_i \hat{E} \frac{\eta_{obs}}{\eta_{trans}} \right) \tag{5.3}$$

5.6.2 Space heat electrification

This dataset accounts for space heat energy demand in the residential and the commercial and institutional (C&I) building sectors. Both sectors consume fossil fuels and electricity. Equation (5.4) defines the total space heat demand E_H as the sum of residential (subscript R) and C&I (subscript C) heat demands. Each sector's energy demand includes a share of electricity (subscript e) and fossil fuels (subscript f) with specific observed efficiencies. The normalized demand profiles $\overrightarrow{P_R}$ and $\overrightarrow{P_C}$ are sector-specific but independent of fuel type. The converted technology efficiency $\eta_{H,trans}$ remains constant across sectors and fuel types, assuming that all space heating is converted to the same type of electric space heat technology.

$$\begin{aligned} E_H = \sum_i \Bigg(& P_{R,i} \left[\hat{E}_{R,e} \frac{\eta_{R,e,obs}}{\eta_{H,trans}} + \hat{E}_{R,f} \frac{\eta_{R,f,obs}}{\eta_{H,trans}} \right] \\ & + P_{C,i} \left[\hat{E}_{C,e} \frac{\eta_{C,e,obs}}{\eta_{H,trans}} + \hat{E}_{C,f} \frac{\eta_{C,f,obs}}{\eta_{H,trans}} \right] \Bigg) \end{aligned} \tag{5.4}$$

5.6.2.1 Annual space heat demand

The annual energy demands for space heating $\hat{E}_{R,e}$, $\hat{E}_{R,f}$, $\hat{E}_{C,e}$, and $\hat{E}_{C,f}$ in British Columbia are taken from the Comprehensive Energy Use Database (Natural Resources Canada, 2019) and scaled to Metro Vancouver by the population ratio of 53% (Statistics Canada, 2017). The residential sector's observed efficiencies $\eta_{R,e,obs}$ and $\eta_{R,f,obs}$ are weighted by number of systems per technology type installed in the 2016 residential building stock across British Columbia (Natural Resources Canada, 2019). Electric systems include resistance and heat pump technologies. Fossil fuel systems include natural gas, heating oil, coal and propane consuming technologies. The C&I sectors' observed efficiencies $\eta_{C,e,obs}$ and $\eta_{C,f,obs}$ are not available in the Comprehensive Energy Use Database and therefore taken to be equivalent to residential sector's observed efficiencies $\eta_{R,e,obs}$ and $\eta_{R,f,obs}$.

The scenarios LOW and HIGH define upper and lower bounds for the total annual electricity demand of electrified space heaters. LOW and HIGH scenarios differ exclusively in their assumed conversion efficiency $\eta_{H,trans}$. The LOW scenario models conversion of space heaters to mostly low-efficiency electric resistance technology with a mean efficiency of 1.08. This mean efficiency assumes the ratio of electric resistance to heat pump installations remains constant in Metro Vancouver. The HIGH scenario models exclusive conversion to high-efficiency heat pumps with a seasonal efficiency (coefficient of performance) of 3.5 (Jadun et al., 2017). All energy demands and efficiencies used in Equation (5.4) are listed in the Applied Value column of Table 5-5.

Table 5-5. Space heat annual energy demands, observed efficiencies and converted efficiencies for the residential and C&I sectors. The "Source Values" are those values that are listed in the "Source" documents. The "Applied Values" determine the electrified space heat demand using Equation (5.4). Applied values listed in the Annual Energy Demand section of the table have been scaled from British Columbia to Metro Vancouver via their population ratio of 53%. The values listed in the efficiencies sections are stock-weighted mean efficiencies of electric or fossil fuel type heating systems installed in the 2016 residential building stock of British Columbia.

	Sector	Parameter	Source Value	Source Unit	Applied Value	Applied Unit	Source
Annual Energy Demand	Residential, electricity	$\hat{E}_{R,e}$	23.6	PJ	3.50	TWh	(Natural Resources Canada, 2019)
	Residential, fossil fuel	$\hat{E}_{R,f}$	41.5	PJ	6.15	TWh	
	C&I, electricity	$\hat{E}_{C,e}$	6.8	PJ	1.01	TWh	
	C&I, fossil fuel	$\hat{E}_{C,f}$	41.2	PJ	6.10	TWh	
Efficiency, observed	Residential, electricity	$\eta_{R,e,obs}$	1.08	kWh/ kWh	1.08	kWh/ kWh	(Natural Resources Canada, 2019)
	Residential, fossil fuel	$\eta_{R,f,obs}$	0.84	kWh/ kWh	0.84	kWh/ kWh	
	C&I, electricity	$\eta_{C,e,obs}$	1.08	kWh/ kWh	1.08	kWh/ kWh	$\eta_{R,e,obs}$
	C&I, fossil fuel	$\eta_{C,f,obs}$	0.84	kWh/ kWh	0.84	kWh/ kWh	$\eta_{R,f,obs}$
Efficiency, converted	Residential and C&I	$\eta_{H,trans}$	1.08	kWh/ kWh	1.08	kWh/ kWh	(LOW) $\eta_{R,e,obs}$
	Residential and C&I	$\eta_{H,trans}$	3.5	kWh/ kWh	3.50	kWh/ kWh	(HIGH) (Jadun et al., 2017)

5.6.2.2 Hourly space heat demand profile

The hourly space heat demand profiles $\overrightarrow{P_R}$ and $\overrightarrow{P_C}$ differentiate between residential and C&I sectors because those building types are used at different times throughout the day and year. The top graph in Figure 5-5 shows the temporal distribution of both sectors' heat demands over the course of the year.

The residential heat demand profile is derived from proprietary residential electricity demand data provided by the utility BC Hydro. This hourly demand data spans two years from November 2015 to October 2017 and includes 2995 residential dwellings of which 890 dwellings use electric heating. The distribution of dwelling types is a representative sample of the dwelling population in Metro Vancouver. For each dwelling type the hourly space heat demand is the average difference between electrically and non-electrically heated dwelling demands in any hour where historical ambient temperatures are below a heating threshold. This threshold is statistically inferred by a piecewise linear regression that minimizes the variance between the predicted load and the observed difference between electrical and non-electrically heated dwellings at any given ambient temperature.

The C&I heat demand profile is created from commercial reference building models published by the U.S. Department of Energy (NREL, 2011). The reference building models include hourly space heat demand for fifteen commercial building types in location-dependant typified climate conditions. Reference buildings include, e.g. schools, office buildings, hotels or restaurants. This study uses reference buildings in climate conditions for Bellingham, Washington, U.S.A., which is located ~ 65 km south-southeast of Metro Vancouver. Reference building profiles are weighted to approximate the building stock surveyed in British Columbia (Table 2.1 in Natural Resources Canada, 2013).

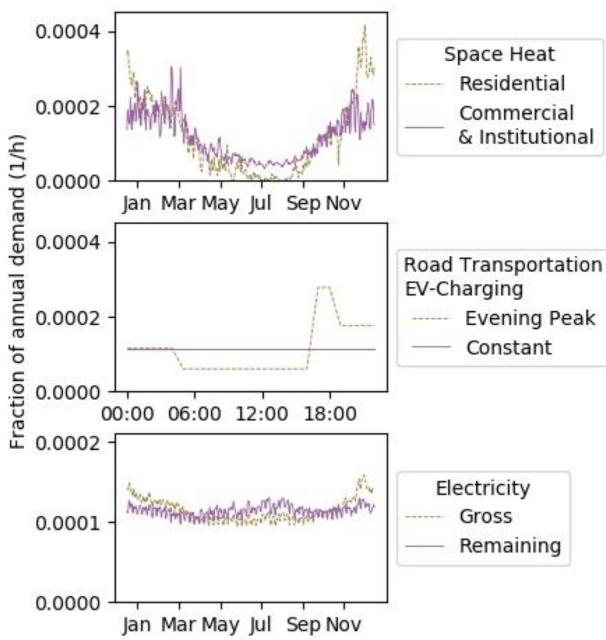

Figure 5-5. Components of the hourly space heat, road transportation and electricity demand profiles. The space heat profile consists of a residential and a C&I profile. The road

transportation profile is scenario dependant where the PEAK scenario assumes battery-electric vehicle charging peaks between 5 and 6 p.m. The UNIFORM scenario assumes that the battery-electric vehicle charging is temporally distributed to appear constant-rate. The gross electricity demand profile is the normalized observed 2016 electricity demand published by the British Columbia Balancing Authority (BC Hydro, n.d.). The remaining electricity demand profile excludes historically electric space heat energy consumed by the residential and the C&I sectors.

5.6.3 Road transportation electrification

This dataset accounts for road transportation energy demanded by passenger and freight vehicles. Equation (5.5) defines the total transportation energy demand E_T as the sum of the vehicle type-specific transportation energy demands and efficiencies. Vehicle specific demands include passenger cars $\hat{E}_{PC}$, passenger trucks $\hat{E}_{PT}$, light freight trucks $\hat{E}_{FL}$, medium freight trucks fueled by diesel $\hat{E}_{FMD}$, medium freight trucks fueled by gasoline $\hat{E}_{FMG}$, and heavy freight trucks $\hat{E}_{FH}$. Medium freight trucks are distinguished by fuel type because the efficiencies differ between fuels. All other vehicle types rely almost exclusively on either gasoline (passenger cars, passenger trucks, light freight trucks) or diesel (heavy freight trucks) making their distinction by fuel type negligible. Both the observed and the converted efficiencies distinguish between vehicle types because their metric (energy consumed per distance traveled) varies significantly between types. The normalized hourly demand profile $\overrightarrow{P_T}$ represents a single aggregate profile for the entire vehicle fleet.

$$\begin{aligned} E_T = \sum_i \Bigg(P_{T,i} \Bigg[& \hat{E}_{PC} \frac{\eta_{PC,obs}}{\eta_{PC,trans}} + \hat{E}_{PT} \frac{\eta_{PT,obs}}{\eta_{PT,trans}} + \hat{E}_{FL} \frac{\eta_{FL,obs}}{\eta_{FL,trans}} \\ & + \hat{E}_{FMD} \frac{\eta_{FMD,obs}}{\eta_{FMD,trans}} + \hat{E}_{FMG} \frac{\eta_{FMG,obs}}{\eta_{FMG,trans}} + \hat{E}_{FH} \frac{\eta_{FH,obs}}{\eta_{FH,trans}} \Bigg] \Bigg) \end{aligned} \tag{5.5}$$

5.6.3.1 Annual road transportation demand

The annual road transportation energy demands $\hat{E}_{PC}$, $\hat{E}_{PT}$, $\hat{E}_{FL}$, $\hat{E}_{FMD}$, $\hat{E}_{FMG}$, and $\hat{E}_{FH}$ in British Columbia are taken from the Comprehensive Energy Use Database (Natural Resources Canada, 2019) and scaled to Metro Vancouver by the population ratio of 53%

(Statistics Canada, 2017). Fossil fuel based road transportation efficiencies $\eta_{PC,obs}$, $\eta_{PT,obs}$, $\eta_{FL,obs}$, $\eta_{FMD,obs}$, $\eta_{FMG,obs}$, and $\eta_{FH,obs}$ are taken from the Comprehensive Energy Use Database (Natural Resources Canada, 2019) in L/100 km and multiplied with fuel type specific higher heating values (p. 132 in Statistics Canada, 2019) to calculate energy consumed per distance traveled. The battery-electric efficiencies $\eta_{PC,trans}$, $\eta_{PT,trans}$, $\eta_{FL,trans}$, $\eta_{FMD,trans}$, $\eta_{FMG,trans}$, and $\eta_{FH,trans}$ are taken from Keller et al. (2019b). All energy demands and efficiencies used in equation (5.5) are listed in the Applied Value column of Table 5-6.

Table 5-6. Road transportation annual energy demands, observed efficiencies and converted efficiencies per vehicle type. The "Source Values" are those values that are listed in the "Source" documents. The "Applied Values" determine the electrified road transportation demand using Equation (5.5). Applied values listed in the Annual Energy Demand section of the table have been scaled from British Columbia to Metro Vancouver via their population ratio of 53%. The applied values listed in the efficiencies sections have been converted to a common unit.

	Vehicle type	Parameter	Source Value	Source Unit	Applied Value	Applied Unit	Source
Annual Energy Demand	Passenger cars (gasoline)	$\hat{E}_{PC}$	57.6	PJ	8.53	TWh	(Natural Resources Canada, 2019)
	Passenger light trucks (mostly gasoline)	$\hat{E}_{PT}$	65.4	PJ	9.69	TWh	
	Light-freight trucks (mostly gasoline)	$\hat{E}_{FL}$	25.8	PJ	3.82	TWh	
	Medium-freight trucks (diesel)	$\hat{E}_{FMD}$	30.3	PJ	4.49	TWh	
	Medium-freight trucks (gasoline)	$\hat{E}_{FMG}$	27.6	PJ	4.09	TWh	
	Heavy-freight trucks (diesel)	$\hat{E}_{FH}$	30.7	PJ	4.55	TWh	
Efficiency, observed	Passenger cars (gasoline)	$\eta_{PC,obs}$	8.2	L/100km	1.25	km/kWh	(Natural Resources Canada, 2019)
	Passenger light trucks (mostly gasoline)	$\eta_{PT,obs}$	11.1	L/100km	0.93	km/kWh	
	Light-freight trucks (mostly gasoline)	$\eta_{FL,obs}$	11.3	L/100km	0.91	km/kWh	
	Medium-freight trucks (diesel)	$\eta_{FMD,obs}$	21.0	L/100km	0.45	km/kWh	
	Medium-freight trucks (gasoline)	$\eta_{FMG,obs}$	21.0	L/100km	0.49	km/kWh	
	Heavy-freight trucks (diesel)	$\eta_{FH,obs}$	37.6	L/100km	0.25	km/kWh	
Efficiency, converted	Passenger cars (gasoline)	$\eta_{PC,trans}$	0.23	kWh/km	4.35	km/kWh	(Keller et al., 2019b)
	Passenger light trucks (mostly gasoline)	$\eta_{PT,trans}$	0.30	kWh/km	3.33	km/kWh	
	Light-freight trucks (mostly gasoline)	$\eta_{FL,trans}$	0.30	kWh/km	3.33	km/kWh	
	Medium-freight trucks (diesel)	$\eta_{FMD,trans}$	1.22	kWh/km	0.82	km/kWh	
	Medium-freight trucks (gasoline)	$\eta_{FMG,trans}$	1.22	kWh/km	0.82	km/kWh	
	Heavy-freight trucks (diesel)	$\eta_{FH,trans}$	2.93	kWh/km	0.34	km/kWh	

5.6.3.2 Hourly road transportation demand profile

The hourly road transportation demand profile $\overrightarrow{P_T}$ is based on an assumed temporal distribution of battery-electric vehicle charging. Different profiles are chosen for scenarios

PEAK and UNIFORM to define upper and lower bounds for peak power capacity demand. PEAK and UNIFORM scenarios differ exclusively in their assumed demand profile $\overrightarrow{P_T}$.

The middle graph in Figure 5-5 shows the temporal distribution of both demand profiles over the course of a day. The UNIFORM scenario defines the lower bound of peak capacity demand by assuming charging events are sufficiently distributed in time to result in an aggregate profile that appears constant-rate. The PEAK scenario define the upper bound of peak capacity demand by assuming a large share of daily vehicle charging occurs in the evening hours at 5 and 6 p.m. This scenario simulates uncoordinated vehicle charging and the associated amplification of typical residential evening peaks (Muratori, 2018). The PEAK profile is an approximation made by Keller et al. (2019a).

5.6.4 Remaining electricity demand

The total electrified demand is the sum electrified space heat, road transportation and the *remaining electricity demand*. The *gross electricity demand* observed in 2016 includes some energy used in space heating because the residential and C&I sectors both used some electric heating systems in that year. The remaining electricity demand removes the electricity used for space heat from the gross electricity demand to avoid double counting.

Equation (5.6) defines the remaining electricity demand E_E as the difference between the gross demand E_G and residential $\hat{E}_{R,e}$ plus commercial $\hat{E}_{C,e}$ electric space heat demand. Note that electricity demands in this equation are not subject to a conversion efficiency ratio because this dataset excludes any electricity demand changes beyond space heat and road transport electrification.

$$E_E = \sum_i \left(P_{G,i}\, E_G - \left[P_{R,i} \hat{E}_{R,e} + P_{C,i} \hat{E}_{C,e} \right] \right) \tag{5.6}$$

5.6.4.1 Annual remaining electricity demand

The gross electricity demand E_G is 30.24 TWh and taken from the Fiscal 2017 - 2019 Revenue Requirements Application published by BC Hydro (BC Hydro, 2016), scaled to Metro Vancouver by the provincial population ratio of 53% (Statistics Canada, 2017). The gross electricity demand used from the source document is 56.7 TWh, which is the total electricity supplied to BC Hydro customers in the Fiscal year 2016, including losses and system use, after trade. The electric space heat demands $\hat{E}_{R,e}$ and $\hat{E}_{C,e}$ are taken from the Comprehensive Energy Use Database (Natural Resources Canada, 2019) as described in section 5.6.2.1.

5.6.4.2 Hourly remaining electricity demand profile

The normalized gross electricity demand profile $\overrightarrow{P_G}$ is determined by dividing each element of the observed 2016 hourly electricity demand by the annual demand. The observed 2016 hourly electricity demand is taken from the British Columbia Balancing Authority (BC Hydro, n.d.). The hourly space heat demand profiles $\overrightarrow{P_R}$ and $\overrightarrow{P_C}$ are described in section 5.6.2.2. The bottom graph in Figure 5-5 shows the temporal distribution of gross and remaining electricity demand profiles over the course of the year.

6 Contributions and Recommendations

6.1 Contributions

Global greenhouse gas emissions from fossil fuel combustion significantly contribute to climate change. Canada has committed limiting global warming to well below 2 °C in comparison to pre-industrial levels. This dissertation assesses technology options for Canada to meet that commitment by reducing combustion emissions in the western provinces, Alberta and British Columbia. The work investigates selected challenges on the strategy of decarbonizing the electricity supply and electrifying adjacent sectors. Three distinct but related studies assess 1) technology pathways and land area impacts to decarbonizing a fossil fuel dominated electricity system, 2) identify favourable sedimentary basin geothermal energy locations and quantify their electricity generation potential, and 3) quantify the electricity demand of space heat and road transport electrification and determine a broad range of feasible electricity system compositions and their land area required to supply the electrified demand with renewable energy sources. Overall, these studies aid the understanding of land requirements related to decarbonizing energy supplies.

The first study contributes a novel method to assessing and optimizing land area impacts of decarbonizing a fossil fuel-dominated electricity supply system. The work amends the Open Source Energy System Model (OSeMOSYS) to include technology-specific land area impacts and constraints. As a case study the method is applied to Alberta. This province has the highest electricity related greenhouse gas emissions in Canada because coal and natural gas fuels each generated 45% of the electricity in 2017 (Canada Energy Regulator, 2019). The amended model enables investigating land area impacts of technology transition pathways that reduce electricity related emissions by 90% between 2015 and 2060. Technology options include renewable, conventional, and fossil fuel power plants with carbon capture and sequestration (CCS). In the reference scenario, land area impacts of technology deployment can expand unconstrained. Land constrained scenarios limit land area impact expansion by between 0% and 5% annually to determine feasible technology pathways where competition for land exists. Subsequently, sensitivity scenarios show the significance of varying the spatial and temporal boundaries regarding 1) the elements included in technology-specific land area impacts and 2) the reclamation timeframes of fossil fuel extraction and carbon sequestration. This study contributes the following insights to literature:

1. Reducing emissions of a fossil fuel dominated electricity system by 90% over the next 45 years with a 70% share of wind, solar and hydropower may require expanding land area designated to electricity generation by 5% annually. This significant increase is predominantly attributed to wind power because the spacing between turbines of a wind farm requires a land area an order of magnitude larger than ground-mounted solar power, and two orders of magnitudes larger than fossil fueled power plants. The expansion is relevant to system planners and policy makers because public acceptance of the local land and landscape impacts are crucial to rapidly deploy low-carbon technologies needed to achieve decarbonisation targets.

2. System planners and policy makers can choose to limit the increasing land area designated to electricity generation at a higher system cost. The impacted land area remains constant in time by deploying higher cost but more compact fossil fuels with carbon sequestration (natural gas + CCS) and geothermal, rooftop solar and biomass renewable energy sources. Holding land area constant requires expedient reclamation of depleted natural gas and carbon sequestration infrastructure. Without reclamation, the land area impact increases fourfold over the 45-year modelling period. This study is the first to quantify this trade-off between designating additional land area to energy production and deploying higher-cost but more spatially compact technologies.

3. The study provides a comprehensive discussion and review of methods to quantifying the land area impacts of different technologies. Comparing the land area impact of e.g. a wind farm with a coal-fired power plant is challenging because their physical, visual and environmental impacts differ significantly. Based upon this discussion, the study applies three combinations of technology-

specific land area impact definitions and reclamation boundaries to show the sensitivity of results to changing these boundaries. Since the scholarly debate around energy technology-specific land area impacts is ongoing, policy makers should be aware of this significant sensitivity.

The second study assesses the geothermal energy resources of the British Columbian section of the Western Canada Sedimentary Basin. A geospatial analysis identifies four favourable locations for geothermal power plants by overlaying economic and geologic favourability criteria. Economic criteria include proximity to energy consumers and electrical transmission infrastructure; geologic criteria include temperatures at-depth and indicators of geothermal fluid availability. The subsequent estimation of geothermal reservoir characteristics and application of the Volume Method quantifies location-specific and volume-normalized electric power generation potentials and their probabilities. The sensitivity analysis varies reservoir temperature, spatial dimensions, recovery factor, and porosity to determine upper and lower bounds of potential power generation capacity and required geothermal fluid flow rates. This study contributes the following insights to literature:

4. The potential for sedimentary basin geothermal energy to contribute to low-carbon electricity generation in British Columbia is small in comparison to the provincial demand. The total estimated mode value of potential power generation in the four most favourable areas is 107 MW. The electricity demand in British Columbia ranged from ~ 5 to 10 GW in 2018, so sedimentary basin geothermal would contribute only 1% to 2% of demand at any given time. However, communities in the study area in northeastern British Columbia are not directly connected to the main electric grid. Geothermal energy may offer additional local benefits including increased energy security for those communities or use of waste heat. These potential benefits justify further investigating this resource.

5. The uncertainty of potential sedimentary basin geothermal electricity generation was reduced significantly in comparison to the ~ 5 GW found in previous work that did not account for geothermal fluid availability (CanGEA, 2014).

Nevertheless, some uncertainty remains because power potential is sensitive to temperature, achievable geothermal brine flow rate, and hydrothermal reservoir volume. Each parameter effects power potential by a factor of two.

6. The study develops and demonstrates a new method of assessing geothermal resources regionally using the two-step method of geospatial favourability analysis and estimating electricity generation potential from publicly available petroleum production data. An adaptation of this method was used in a study of geothermal potential in neighbouring Alberta (Banks and Harris, 2018). That study applied similar petroleum production data and found 1.2 GW of potential electricity generation. The author of that study co-authored the work in this dissertation and developed the study of Alberta simultaneously.

The third study assesses electrification demand impacts and a broad range of renewable energy supply options for the Metro Vancouver Regional District, British Columbia. First, the district's observed 2016 space heat and road transportation energy demands are converted to equivalent electricity demands at hourly temporal resolution. These demands are added to the historically observed electricity demand to estimate the total electrified demand. Upper and lower bounds of the electrified annual and peak demands are determined by four scenario combinations. Two space heat technology conversions assume deployment of high-efficiency heat pumps or low-efficiency electric resistance technology. Two road transportation scenarios assume electric vehicle charging to be constant-rate or evening-peaking. Next, electricity system compositions that use renewable energy sources to supply the electrified demand are determined. The electricity system model installs and dispatches the lowest-cost combination of rural and urban electricity generation and storage technologies. Rural technologies impact rural land area and include wind, ground-mounted solar, hydro, and pumped storage. Urban technologies do not impact rural land area and include rooftop solar, waste-to-energy, and battery storage. Land impact costs internalize the impacts of energy technologies on rural land and landscapes. The cost optimization is repeated for a broad range of land impact costs. This method reveals the full range of feasible electricity system compositions and their 1) maximum necessary and minimum feasible rural land area impact, 2) generation and storage capacities, 3) surplus electricity generation from variable renewables, 4) the maximum share of electricity generation from urban sources, and 5) the trade-off between impacting a smaller rural land area and bearing a higher electricity system cost. This study contributes the following insights to literature:

7. The study estimates annual and hourly electricity demands after full electrification of space heat and road transportation sectors in a major metropolis. Electrification of those sectors increases the annual electricity demand of 30 TWh in Metro Vancouver by between 48% (44.5 TWh) and 81% (54.2 TWh), depending on the efficiency of the space heating technology. Electrified peak demands range from 6.8 to 12.1 GW, depending on the efficiency of space heating technology and the battery electric vehicle charging profile.

8. The minimum feasible and maximum necessary additional rural land area impact to supply Metro Vancouver with renewable energy ranges from 70 to 2203 km². These impacts are additional to the existing 1650 km² hydro reservoir area attributed the Metro Vancouver population. The maximum necessary area results from deployment of wind, ground-mounted solar generation, and pumped and battery storage technologies. These technologies supply the higher electricity demand of the low-efficiency space heat scenario. The minimum feasible 70 km² assume deployment of ground-mounted solar, rooftop solar, waste-to-energy generation and battery storage technologies to supply the lower electricity demand of the high-efficiency space heat scenario. System costs increase by ~40% between minimum and maximum land area impacts in both scenarios. This cost trade-off is non-linear.

9. The efficiency of the electric space heat technology significantly impacts rural land area impacts, system costs, installed capacities and surplus electricity generation. Although the annual electrified demand differs by only 9.7 TWh or 18% between space heat scenarios, the higher efficiency halves rural land area

impacts and reduces system costs by 29%, excluding the cost of deploying the space heat technology.

10. The study demonstrates that the Metro Vancouver Regional District cannot meet the additional demand from electrifying space heat and road transportation with urban renewable energy sources alone. The maximum share of urban electricity generation is 23% and almost entirely generated by the 8.8 GW of rooftop solar maximally available on the 63 km^2 of potentially feasible rooftop area. The limited feedstock make the available 0.3 TWh of waste-to-energy generation negligible in comparison to the annual demand.

11. During model development an error in the formulation of the Open Source Energy System Model (OSeMOSYS) objective function was found, and a fix was contributed to and adopted by the open source project. The faulty objective function significantly overestimated the capital cost of installing storage technologies. The error may have falsified results in any third-party studies that have investigated storage technology expansion with the MathProg Short version of OSeMOSYS prior to the fix adopted on GitHub on 10 July 2019.

6.2 Recommendations

This dissertation demonstrates that electrification and decarbonization of electricity supplies can require designating significant additional land area to electricity generation. However, the magnitude of this land requirement depends on 1) the chosen spatial boundary of technology-specific land area impacts and 2) the chosen temporal boundary of the assumed time required to reclaim land impacted by fuel extraction and carbon sequestration.

The chosen boundary of technology-specific land area impacts can vary their value by several orders of magnitude. Wind turbine footprints directly impact a small fraction of the land area designated to a wind farm when defining that wind farm area to include the space between turbines. The acoustic and visual land area impact is larger again. Natural gas producing infrastructure impacts a relatively small footprint per unit energy produced, but the diffuse characteristic of this infrastructure can fragment wildlife habitat. Related edge effects impact a much larger land area than the footprint itself. Equitably reconciling these different impacts of fossil fuels and renewable energy sources warrants further study. Furthermore, the ecological and social impact of both renewable and fossil fuel technologies likely vary by location. The literature has sampled land area impacts of energy technologies only regionally. Locational differences are not yet well understood.

The assumed time to full reclamation affects land area impact because fossil fuels require continuous development as sources deplete. Reclaiming depleted area is sometimes neglected and restoring original ecosystems can take multiple decades or more. In some open pit coal mines reclamation may not achieve full ecosystem restoration within human lifetimes. Similarly, the feasibility of reclaiming land used for carbon sequestration warrants further research.

Land related to electricity transmission was not included in this work, but warrants further study. Availability of some renewable energy sources like wind, hydro and geothermal power are location dependant and may not be available in close proximity to energy consumers. Further geospatial analysis could 1) quantify the transmission related land requirements of electricity supply options presented in this work and 2) quantify the trade-off between transmission related land area requirements and costs of deploying less distant or spatially concentrated low-carbon energy sources. Such studies would allow regional planners, policy makers and the general public to anticipate transmission related land and landscape impacts and potentially develop mitigation strategies. Further insight could be drawn from investigating the non-land related benefits of using less distant energy sources. Such benefits might include avoided transmission upgrades, avoided transmission losses, and improved energy security resulting from a more resilient decentralized electricity system.

Electrification of demand and decarbonization of electricity supply require significant storage capacities or dispatchable low-carbon resources. Pumped storage is presently the lowest-cost option to store electricity long-term, but this technology comes with significant land area impact. Battery technology cannot yet be deployed at sufficient scale to substitute pumped storage capacity. Further investigating 3) dispatchable resource options like gas from low-carbon and renewable sources or 4) amending the energy system models to include demand side options (e.g. energy efficiency measures) may mitigate some of the challenges related to deploying sufficient storage. Such studies may identify alternative system planning and policy options and their land area impacts.

This dissertation indicates that significant additional energy infrastructure is needed to substitute fossil fuel combustion and eliminate related greenhouse gas emissions in the electricity, space heat, and road transportation sectors. Further investigating the elimination of fossil fuels in the 5) industrial, and 6) the non-road transportation sectors marine, airline and railway is warranted to provide more insights on the full impact of decarbonizing the economy.

7 References

Adelaide City Council, Government of South Australia, 2016. Carbon Neutral Adelaide - Action Plan 2016-2021.

Adil, A.M., Ko, Y., 2016. Socio-technical evolution of Decentralized Energy Systems: A critical review and implications for urban planning and policy. Renew. Sustain. Energy Rev. 57, 1025–1037. https://doi.org/10.1016/j.rser.2015.12.079

Alberta Electric System Operator, 2018. AESO 2017 Annual Market Statistics.

Alberta Electric System Operator, 2017. AESO 2017 Long-term Outlook.

Alberta Electric System Operator, 2007. Wind integration in Alberta: market & operational framework implementation. AESO stakeholder information session [WWW Document]. URL https://slideplayer.com/slide/6598/ (accessed 9.12.17).

Alberta Government, 2018. Climate Leadership Plan - Implementation Plan 2018-19.

Allen, L., O’Connell, A., Kiermer, V., 2019. How can we ensure visibility and diversity in research contributions? How the Contributor Role Taxonomy (CRediT) is helping the shift from authorship to contributorship. Learn. Publ. 32, 71–74. https://doi.org/10.1002/leap.1210

Amado, M., Poggi, F., 2014. Solar urban planning: a parametric approach. Energy Procedia 48, 1539–1548. https://doi.org/10.1016/j.egypro.2014.02.174

Arcos-Vargas, A., Gomez-Exposito, A., Gutierrez-Garcia, F., 2019. Self-sufficient renewable energy supply in urban areas: Application to the city of Seville. Sustain. Cities Soc. 46. https://doi.org/10.1016/j.scs.2019.101450

Arent, D., Pless, J., Mai, T., Wiser, R., Hand, M., Baldwin, S., Heath, G., Macknick, J., Bazilian, M., Schlosser, A., Denholm, P., 2014. Implications of high renewable electricity penetration in the U.S. for water use, greenhouse gas emissions, land-use, and materials supply. Appl. Energy 123, 368–377. https://doi.org/10.1016/j.apenergy.2013.12.022

Arianpoo, N., 2009. The Geothermal Potential of Clarke Lake and Milo Gas Fields in northeast British Columbia. Master Thesis. Department of Mining Engineering. University of British Columbia (Vancouver).

Astolfi, M., Romano, M.C., Bombarda, P., Macchi, E., 2014. Binary ORC (Organic Rankine Cycles) power plants for the exploitation of medium-low temperature geothermal sources - Part B: Techno-economic optimization. Energy 66, 435–446. https://doi.org/10.1016/j.energy.2013.11.057

ATCO Power, 2015. ATCO Ministerial Exemption Request.

Augustine, C., Field, R., DiPippo, R., Gigliucci, G., Fastelli, I., Jefftester, J., 2009. Modeling and analysis of sub- and supercritical binary rankine cycles for low- to mid-temperature geothermal resources. Trans. - Geotherm. Resour. Counc. 33, 604–608.

Bachu, S., Burwash, R.A., 1994. Geothermal Regime in the Western Canada Sedimentary Basin, Geological Atlas of the Western Canada Sedimentary Basin.

Bagheri, M., Shirzadi, N., Bazdar, E., Kennedy, C.A., 2018. Optimal planning of hybrid renewable energy infrastructure for urban sustainability : Green Vancouver. Renew. Sustain. Energy Rev. 95, 254–264. https://doi.org/10.1016/j.rser.2018.07.037

Banks, J., Harris, N., 2018. Geothermal Potential of Foreland Basins: A case study from the Western Canadian Sedimentary Basin. Geothermics 76, 74–92. https://doi.org/10.1016/j.geothermics.2018.06.004

Barbier, E., 2002. Geothermal energy technology and current status: An overview. Renew. Sustain. Energy Rev. 6, 3–65. https://doi.org/10.1016/S1364-0321(02)00002-3

Bazán, J., Rieradevall, J., Gabarrell, X., Vázquez-rowe, I., 2018. Low-carbon electricity production through the implementation of photovoltaic panels in rooftops in urban environments: A case study for three cities in Peru. Sci. Total Environ. 622–623, 1448–1462. https://doi.org/10.1016/j.scitotenv.2017.12.003

BC Hydro, 2019. Historical Data - Net Actual Flow [WWW Document]. URL https://www.bchydro.com/energy-in-bc/operations/transmission/transmission-system/actual-flow-data/historical-data.html (accessed 11.25.19).

BC Hydro, 2017. Transmission Service Freshet Rate. Preliminary Evaluation Report for Year 1. Appendix D. BC Hydro System Conditions during Freshet and Associated Management Strategies.

BC Hydro, 2016. Fiscal 2017 to Fiscal 2019 Revenue Requirements Application.

BC Hydro, 2013a. 2013 Resource Options Report Update.

BC Hydro, 2013b. Integrated Resource Plan. Appendix 9A. Base Resource Plans and Contingency Resource Plans.

BC Hydro, 2012a. Transmission System Map.

BC Hydro, 2012b. 2013 Resource Options Report Update - Appendix 5 B - Roads & Power Lines Cost Estimation using GIS.

BC Hydro, 2002. Green Energy Study for British Columbia Phase 2: Mainland, Report No. E44 36.

BC Hydro, n.d. Historical Transmission Data - Gross Telemetred Load: British Columbia

[WWW Document]. URL https://www.bchydro.com/energy-in-bc/operations/transmission/transmission-system/balancing-authority-load-data/historical-transmission-data.html (accessed 4.21.19).

BC Oil and Gas Commission, 2016. Pool Contours [WWW Document]. BCOGC Open Data Portal. URL http://data-bcogc.opendata.arcgis.com/datasets/c9c7ebb8c12041ddab4c93685269ddec_0?geometry=-123.09%2C57.286%2C-120.584%2C57.508 (accessed 4.7.17).

Berrill, P., Arvesen, A., Scholz, Y., Gils, H.C., Hertwich, E.G., 2016. Environmental impacts of high penetration renewable energy scenarios for Europe. Environ. Res. Lett. 11. https://doi.org/10.1088/1748-9326/11/1/014012

Bertani, R., 2015. Geothermal Power Generation in the World 2010-2014 Update Report, in: World Geothermal Congress 2015. Melbourne, Australia.

Bhattacharjee, S., 2017. Saturation Temperature table (PC Model) of H2O [WWW Document]. URL http://www.thermofluids.net/ (accessed 4.5.17).

Botelho, A., Pinto, L.M.C., Lourenco-Gomes, L., Valente, M., Sousa, S., 2016. Social sustainability of renewable energy sources in electricity production: An application of the contingent valuation method. Sustain. Cities Soc. 26, 429–437. https://doi.org/10.1016/j.scs.2016.05.011

Breukers, S., Wolsink, M., 2007. Wind power implementation in changing institutional landscapes: An international comparison. Energy Policy 35, 2737–2750. https://doi.org/10.1016/j.enpol.2006.12.004

Canada Energy Regulator, 2019. Provincial and Territorial Energy Profiles – Alberta [WWW Document]. URL https://www.cer-rec.gc.ca/nrg/ntgrtd/mrkt/nrgsstmprfls/ab-eng.html (accessed 11.6.19).

Canada Energy Regulator, 2015. Market Snapshot: British Columbia Uses its Hydro System to Maximize Gains from Electricity Trade [WWW Document]. URL https://www.cer-rec.gc.ca/nrg/ntgrtd/mrkt/snpsht/2015/12-03-1bchdrsstm-eng.html (accessed 11.9.19).

CanGEA, 2014. The Renewable and Cost Effective Alternative to Site C. An Assessment of the True Value of Geothermal Energy.

Chen, C.A., 1982. Specific Heat Capacities of Aqueous Sodium Chloride Solutions at High Pressures. J. Chem. Eng. Data 27, 356–358. https://doi.org/10.1021/je00029a038

Cheng, V.K.M., Hammond, G.P., 2017. Life-cycle energy densities and land-take requirements of various power generators: A UK perspective. J. Energy Inst. 90, 201–213. https://doi.org/10.1016/j.joei.2016.02.003

City of Vancouver, 2017. Renewable City Action Plan - November 2017. Vancouver.

City of Vancouver, 2015. Renewable City Strategy 2015 - 2050. Vancouver.

Cohen, J.J., Reichl, J., Schmidthaler, M., 2014. Re-focussing research efforts on the public acceptance of energy infrastructure: A critical review. Energy 76, 4–9. https://doi.org/10.1016/j.energy.2013.12.056

Danfoss, 2014. The heating book: Instructions for designing district heating system, Instruction for designing district heating systems.

Denholm, P., Hand, M., Jackson, M., Ong, S., 2009. Land-Use Requirements of Modern Wind Power Plants in the United States. National Renewable Energy Laboratory. Technical Report NREL/TP-6A2-45834.

Devine-Wright, P., 2009. Rethinking NIMBYism: The Role of Place Attachment and Place Identity in Explaining Place-protective Action. J. Community Appl. Soc. Psychol. 19, 426–441. https://doi.org/10.1002/casp.1004

EIA, 2013. Updated Capital Cost Estimates for Utility Scale Electricity Generating Plants.

Energy Information Administration, 2018. Cost and Performance Characteristics of New Generating Technologies, Annual Energy Outlook 2018.

Energy Information Administration, 2017a. Cost and Performance Characteristics of New Generating Technologies, Annual Energy Outlook 2017.

Energy Information Administration, 2017b. Annual Energy Outlook 2017 - Table: Energy Prices by Sector and Source [WWW Document]. URL https://www.eia.gov/outlooks/aeo/data/browser/#/?id=3-AEO2017&region=1-8&cases=ref2017~highrt&start=2015&end=2050&f=A&linechart=~~ref2017-d120816a.38-3-AEO2017.1-8~highrt-d120816a.38-3-AEO2017.1-8&map=highrt-d120816a.3-3-AEO2017.1-8&sourcekey=0 (accessed 7.16.18).

English, J., Niet, T., Rowe, A., Lyseng, B., Keller, V., Moazzen, I., Pitt, L., Wild, P., 2017. Impact of electrical intertie capacity on carbon policy effectiveness. Energy Policy 101, 571–581. https://doi.org/10.1016/j.enpol.2016.10.026

Environment and Climate Change Canada, 2019a. National inventory report 1990 – 2017: Greenhouse gas sources and sinks in Canada - Part 1. Ottawa.

Environment and Climate Change Canada, 2019b. National inventory report 1990 – 2017: Greenhouse gas sources and sinks in Canada - Part 3. Ottawa.

European Commission, n.d. Paris Agreement [WWW Document]. URL https://ec.europa.eu/clima/policies/international/negotiations/paris_en (accessed 5.30.18).

Fairbank, B.P., Faulkner, R.L., Hickson, C.J., Roots, C., Souther, J.G., Woodsworth, G.J., Jessop, A.M., Bentkowski, W.H., Lewis, T.J., Macrae, J.M., Rowling, J., Church, B.N., Finvers, M., 1992. Geothermal resources of British Columbia - Open File 2526. https://doi.org/10.4095/133397

Fargione, J., Kiesecker, J., Slaats, M.J., Olimb, S., 2012. Wind and Wildlife in the Northern Great Plains: Identifying Low-Impact Areas for Wind Development. PLoS One 7. https://doi.org/10.1371/journal.pone.0041468

Ferguson, G., Ufondu, L., 2017. Geothermal energy potential of the Western Canada Sedimentary Basin: Clues from coproduced and injected water. Environ. Geosci. 24, 113–121.

Fthenakis, V., Kim, H.C., 2009. Land use and electricity generation: A life-cycle analysis. Renew. Sustain. Energy Rev. 13, 1465–1474. https://doi.org/10.1016/j.rser.2008.09.017

Gagnon, L., Belanger, C., Uchiyama, Y., 2002. Life-cycle assessment of electricity generation options: The status of research in year 2001. Energy Policy 30, 1267–1278.

Garcia, J.E., 2001. Density of Aqueous Solutions of CO 2. Lawrence Berkeley Natl. Lab.

Gardner, G.H.F., Gardner, L.W., Gregory, A.R., 1974. FORMATION VELOCITY AND DENSITY—THE DIAGNOSTIC BASICS FOR STRATIGRAPHIC TRAPS. GEOPHYSICS 39, 770–780. https://doi.org/10.1190/1.1440465

Gardumi, F., Shivakumar, A., Morrison, R., Taliotis, C., Broad, O., Beltramo, A., Sridharan, V., Howells, M., Jonas, H., Niet, T., Almulla, Y., Ramos, E., Burandt, T., Pena Balderrama, G., Pinto De Moura, G.N., Zepeda, E., Alfstad, T., 2018. From the development of an open-source energy modelling tool to its application and the creation of communities of practice: The example of OSeMOSYS. Energy Strateg. Rev. 20, 209–228. https://doi.org/10.1016/j.esr.2018.03.005

Gargiulo, C., Russo, L., 2017. Cities and Energy Consumption: a Critical Review. J. L. Use, Mobil. Environ. 10, 259–278. https://doi.org/10.6092/1970-9870/5182

Garland, G.D., Lennox, D.H., 1962. Heat Flow in Western Canada. Geophys. J. Int. 6, 245–262. https://doi.org/https://doi.org/10.1111/j.1365-246X.1962.tb02979.x

GE Energy Consulting, 2016. Pan-Canadian Wind Integration Study.

Geoscience BC, 2015. An Assessment of the Economic Viability of Selected Geothermal Resources in British Columbia. Geoscience BC Report 2015-11.

Geothermal Resources Act, 1996. (RSBC 1996) Chapter 171, Part 1 - Interpretation.

Gonzalez-Salazar, M.A., Venturini, M., Poganietz, W.-R., Finkenrath, M., Regis L.V.

Leal, M., 2017. Combining an accelerated deployment of bioenergy and land use strategies: Review and insights for a post-conflict scenario in Colombia. Renew. Sustain. Energy Rev. 73, 159–177. https://doi.org/10.1016/j.rser.2017.01.082

Google, 2018. Project Sunroof data explorer [WWW Document]. URL https://www.google.com/get/sunroof/data-explorer/place/ChIJN3gtg4xckFQRPuBki2urgOI/ (accessed 3.29.19).

Government of British Columbia, 2019. Data Catalogue - Reservoir Permits Over Crown Land [WWW Document]. Minist. For. Lands, Nat. Resour. Oper. Rural Dev. - Water Manag. URL https://catalogue.data.gov.bc.ca/dataset/af082452-aaa6-49eb-a71d-0a42219bb764 (accessed 11.17.19).

Government of British Columbia, 2016. Climate Leadership Plan - British Columbia, 2016.

Government of Canada, 2017. Canadian Climate Normals 1981-2010 Station Data - Fort Nelson A, British Columbia [WWW Document]. URL http://climate.weather.gc.ca/climate_normals/results_1981_2010_e.html?searchType=stnProv&lstProvince=BC&txtCentralLatMin=0&txtCentralLatSec=0&txtCentralLongMin=0&txtCentralLongSec=0&stnID=1455&dispBack=0 (accessed 4.5.17).

Grasby, S.E., Allen, D.M., Bell, S., Chen, Z., Ferguson, G., Jessop, A., Kelman, M., Ko, M., Majorowicz, J., Moore, M., Raymond, J., Therrien, R., 2012. Geothermal Energy Resource Potential of Canada, Geological Survey of Canada - Open File 6914. Geological Survey of Canada - Open File 6914. https://doi.org/10.4095/291488

Greene, R., Devillers, R., Luther, J.E., Eddy, B.G., 2011. GIS-Based Multiple-Criteria Decision Analysis. Geogr. Compass 5, 412–432. https://doi.org/10.1111/j.1749-8198.2011.00431.x

Hallbar Consulting, 2017. Resource Supply Potential for Renewable Natural Gas in B.C.

Harrison, W.E., Luza, K. V., Prater, M.L., Cheung, P.K., 1983. Geothermal resource assessment in Oklahoma. Oklahoma Geol. Surv. Spec. Publ.

Hermann, S., Welsch, M., Segerstrom, R.E., Howells, M.I., Young, C., Alfstad, T., Rogner, H.H., Steduto, P., 2012. Climate, land, energy and water (CLEW) interlinkages in Burkina Faso: An analysis of agricultural intensification and bioenergy production. Nat. Resour. Forum 36, 245–262. https://doi.org/10.1111/j.1477-8947.2012.01463.x

Hertwich, E.G., Gibon, T., Bouman, E.A., Arvesen, A., Suh, S., Heath, G.A., Bergesen, J.D., Ramirez, A., Vega, M.I., Shi, L., 2014. Integrated life-cycle assessment of electricity-supply scenarios confirms global environmental benefit of low-carbon technologies. Proc. Natl. Acad. Sci. U. S. A. 112, 6277–6282. https://doi.org/10.1073/pnas.1312753111

Howells, M., Rogner, H., Strachan, N., Heaps, C., Huntington, H., Kypreos, S., Hughes, A., Silveira, S., DeCarolis, J., Bazillian, M., Roehrl, A., 2011. OSeMOSYS: The Open Source Energy Modeling System. An introduction to its ethos, structure and development. Energy Policy 39, 5850–5870. https://doi.org/10.1016/j.enpol.2011.06.033

Huber, M.T., McCarthy, J., 2017. Beyond the subterranean energy regime? Fuel, land use and the production of space. Trans. Inst. Br. Geogr. n/a-n/a. https://doi.org/10.1111/tran.12182

Ibrahimbas, A., Walsh, W., 2005. Stratigraphy and Reservoir Assessment of Pre-Givetian Strata in Northeastern British Columbia. Br. Columbia Minist. Energy Mines 1–14.

Idaho National Laboratory, 2006. The Future of Geothermal Energy, INL/EXT-06-11746. Idaho Falls, Idaho.

IHS Energy, 2016. AccuMap. IHS Energy, V.23.05. Englewood, Colorado.

International District Heating Association, 1983. District heating Handbook.

International Energy Agency, 2018. World Energy Outlook 2018. https://doi.org/https://doi.org/10.1787/weo-2018-en

International Energy Agency, 2016. Energy Technology Perspectives 2016 - Towards sustainable urban energy systems. https://doi.org/https://doi.org/10.1787/energy_tech-2016-en

International Renewable Energy Agency, 2017. Global Land Outlook Working Paper. Energy and Land Use.

IPCC, 2019. Global Warming of 1.5°C. An IPCC Special Report on the impacts of global warming of 1.5°C above pre-industrial levels and related global greenhouse gas emission pathways, in the context of strengthening the global response to the threat of climate change,. Geneva.

IPCC, 2014. Climate Change 2014: Mitigation of Climate Change. Working Group III Contribution to the Fifth Assessment Report of the Intergovernmental Panel on Climate Change. Cambridge University Press, Cambridge, United Kingdom and New York, NY, USA. https://doi.org/10.1017/CBO9781107415416

Jaccard, M., Melton, N., Nyboer, J., 2011. Institutions and processes for scaling up renewables : Run-of-river hydropower in British Columbia. Energy Policy 39, 4042–4050. https://doi.org/10.1016/j.enpol.2011.02.035

Jacobson, M.Z., 2009. Review of solutions to global warming, air pollution, and energy security. Energy Environ. Sci. 2, 148–173. https://doi.org/10.1039/B809990C

Jacobson, M.Z., Delucchi, M.A., 2011. Providing all global energy with wind, water, and solar power, Part I: Technologies, energy resources, quantities and areas of infrastructure, and materials. Energy Policy 39, 1154–1169. https://doi.org/10.1016/j.enpol.2010.11.040

Jadun, P., Mcmillan, C., Steinberg, D., Muratori, M., Vimmerstedt, L., Mai, T., 2017. Electrification Futures Study: End-Use Electric Technology Cost and Performance Projections through 2050.

Jefferson, M., 2018. Safeguarding rural landscapes in the new era of energy transition to a low carbon future. Energy Res. Soc. Sci. 37, 191–197. https://doi.org/10.1016/j.erss.2017.10.005

Jenkins, J.D., Luke, M., Thernstrom, S., 2018. Getting to Zero Carbon Emissions in the Electric Power Sector. Joule 2, 2498–2510. https://doi.org/10.1016/j.joule.2018.11.013

Jones, F.W., Lam, H.L., Majorowicz, J.A., 1985. Temperature distributions at the Paleozoic and Precambrian surfaces and their implications for geothermal energy recovery in Alberta. Can. J. Earth Sci 22, 1774–1780.

Jones, N.F., Pejchar, L., 2013. Comparing the Ecological Impacts of Wind and Oil & Gas Development: A Landscape Scale Assessment. PLoS One 8. https://doi.org/10.1371/journal.pone.0081391

Jordaan, S.M., Heath, G.A., Macknick, J., Bush, B.W., Mohammadi, E., Ben-horin, D., Urrea, V., Marceau, D., 2017. Understanding the life cycle surface land requirements of natural gas-fired electricity. Nat. Energy 2, 804–812. https://doi.org/10.1038/s41560-017-0004-0

Jordaan, S.M., Keith, D.W., Stelfox, B., 2009. Quantifying land use of oil sands production: a life cycle perspective. Environ. Res. Lett. 4, 24004. https://doi.org/10.1088/1748-9326/4/2/024004

Jurasz, J.K., Dąbek, P.B., Campana, P.E., 2019. Can a city reach energy self-sufficiency by means of rooftop photovoltaics? Case study from Poland. J. Clean. Prod. https://doi.org/10.1016/j.jclepro.2019.118813

Kammen, D.M., Sunter, D.A., 2016. City-integrated renewable energy for urban sustainability. Science (80-.). 352, 922–927. https://doi.org/10.1126/science.aad9302

Keller, V., English, J., Fernandez, J., Wade, C., Fowler, M., Scholtysik, S., Palmer-Wilson, K., Donald, J., Robertson, B., Wild, P., Crawford, C., Rowe, A., 2019a. Electrification of road transportation with utility controlled charging: A case study for British Columbia with a 93% renewable electricity target. Appl. Energy 253. https://doi.org/10.1016/j.apenergy.2019.113536

Keller, V., Lyseng, B., Wade, C., Scholtysik, S., Fowler, M., Donald, J., Palmer-wilson, K., Robertson, B., Wild, P., Rowe, A., 2019b. Electricity system and emission impact of direct and indirect electrification of heavy-duty transportation. Energy 172, 740–751. https://doi.org/10.1016/j.energy.2019.01.160

Kennedy, C.A., Stewart, I., Facchini, A., Cersosimo, I., Mele, R., Chen, B., Uda, M., Kansal, A., Chiu, A., Kim, K., Dubeux, C., Lebre, E., Rovere, L., Cunha, B., 2015. Energy and material flows of megacities. Proc. Natl. Acad. Sci. U. S. A. https://doi.org/10.1073/pnas.1504315112

Kimball, S., 2010. Favourability Map of British Columbia Geothermal Resources. Univ. Br. Columbia. Master Thesis. Department of Mining Engineering. University of British Columbia (Vancouver).

Knight Piésold Ltd., 2010. BC Hydro - Evaluation of pumped storage hydroelectric potential - Screening assessment report. Vancouver.

Konadu, D.D., Sobral, Z., Allwood, J.M., Richards, K.S., Kopec, G., Mcmahon, R., Fenner, R., 2015. Land use implications of future energy system trajectories — The case of the UK 2050 Carbon Plan. Energy Policy 86, 328–337. https://doi.org/10.1016/j.enpol.2015.07.008

Kondziella, H., Bruckner, T., 2016. Flexibility requirements of renewable energy based electricity systems - A review of research results and methodologies. Renew. Sustain. Energy Rev. 53, 10–22. https://doi.org/10.1016/j.rser.2015.07.199

Kraft, T., Mai, P.M., Wiemer, S., Deichmann, N., Ripperger, J., Kästli, P., Bachmann, C., Fäh, D., Wössner, J., Giardini, D., 2009. Enhanced Geothermal Systems: Mitigating Risk in Urban Areas. EOS Trans. AGU 90, 273–274. https://doi.org/10.1029/2009EO320001

Kristmannsdottir, H., Armannsson, H., 2003. Environmental aspects of geothermal energy utilization. Geothermics 32, 451–461. https://doi.org/10.1016/S0375-6505(03)00052-X

Krupka, K.M., Hemingway, B.S., Borie, R.A., Kerrick, D.M., 1985. High-temperature heat capacities and derived thermodynamic properties of anthophyllite, diopside, dolomite, enstatite, bronzite, talc, tremolite and wollastonite. Am. Mineral. 70, 261–271.

Lam, H.L., Jones, F.W., 1985. Geothermal energy potential in the Hinton–Edson area of west-central Alberta. Can. J. Earth Sci. 22, 369–383. https://doi.org/10.1139/e85-036

Lam, H.L., Jones, F.W., Majorowicz, J.A., 1985. A statistical analysis of bottom-hole temperature data in southern Alberta. GEOPHYSICS 50, 677–684.

Laske, G., Masters, G., 1997. A Global Digital map of Sediment Thickness. EOS Trans. AGU 78, F483.

Lloyd, S.P., 1982. Least Squares Quantization in PCM. IEEE Trans. Inf. Theory 28, 129–137. https://doi.org/10.1109/TIT.1982.1056489

Lund, J.W., Boyd, T.L., 2015. Direct Utilization of Geothermal Energy 2015 Worldwide Review, in: Proceedings World Geothermal Congress. pp. 19–25.

Lyseng, B., Rowe, A., Wild, P., English, J., Niet, T., Pitt, L., 2016. Decarbonising the Alberta power system with carbon pricing. Energy Strateg. Rev. 10, 40–52. https://doi.org/10.1016/j.esr.2016.05.001

Majorowicz, J.A., Garven, G., Jessop, A.M., Jessop, C., 1999. Present Heat Flow Along a Profile Across the Western Canada Sedimentary Basin: The Extent of Hydrodynamic Influence, in: Geothermics in Basin Analysis. Springer, Heidelberg, Germany, pp. 61–79.

Majorowicz, J.A., Jessop, A.M., 1981. Regional heat flow patterns in the Western Canadian Sedimentary Basin. Tectonophysics 74, 209–238.

Majorowicz, J., Gosnold, W.D., Gray, A.D., Safanda, J., Klenner, R., Unsworth, M.J., 2012. Implications of post-glacial warming for northern Alberta heat flow-correcting for the underestimate of the geothermal potential. Geotherm. Resour. Counc. Trans. 36, 693–698.

Majorowicz, J., Grasby, S.E., 2014. Geothermal Energy for Northern Canada: Is it Economical? Nat. Resour. Res. 23, 159–173. https://doi.org/10.1007/s11053-013-9199-3

Majorowicz, J., Moore, M., 2014. The feasibility and potential of geothermal heat in the deep Alberta foreland basin-Canada for CO2 savings. Renew. Energy 66, 541–549. https://doi.org/10.1016/j.renene.2013.12.044

Malczewski, J., 2000. On the Use of Weighted Linear Combination Method in GIS: Common and Best Practice Approaches. Trans. GIS 4, 5–22. https://doi.org/10.1111/1467-9671.00035

Malczewski, J., Rinner, C., 2015. Multicriteria Decision Analysis in Geographic Information Science, Advances in Geographic Information Science. https://doi.org/10.1007/978-3-540-74757-4

Mansouri Kouhestani, F., Byrne, J., Johnson, D., Spencer, L., Hazendonk, P., Brown, B., 2019. Evaluating solar energy technical and economic potential on rooftops in an urban setting: the city of Lethbridge, Canada. Int. J. Energy Environ. Eng. 10, 13–32. https://doi.org/10.1007/s40095-018-0289-1

Massam, H., 1988. Multi-criteria (MCDM) Decision Making Techniques in Planning. Prog. Plann. 1–84.

McDonald, R.I., Fargione, J., Kiesecker, J., Miller, W.M., Powell, J., 2009. Energy sprawl or energy efficiency: Climate policy impacts on natural habitat for the United States of America. PLoS One 4. https://doi.org/10.1371/journal.pone.0006802

Metro Vancouver, 2018. Climate 2050 Strategic Framework.

Millward-Hopkins, J.T., Tomlin, A.S., Ma, L., Ingham, D.B., Pourkashanian, M., 2013. Assessing the potential of urban wind energy in a major UK city using an analytical model. Renew. Energy 60, 701–710. https://doi.org/10.1016/j.renene.2013.06.020

Ministry of Natural Gas Development, 2016. Summary of Shale Gas Activity in Northeast British Columbia - Oil and Gas Report 2016-1. Victoria.

Mithraratne, N., 2009. Roof-top wind turbines for microgeneration in urban houses in New Zealand. Energy Build. 41, 1013–1018. https://doi.org/10.1016/j.enbuild.2009.05.003

Moeck, I.S., 2014. Catalog of geothermal play types based on geologic controls. Renew. Sustain. Energy Rev. 37, 867–882. https://doi.org/10.1016/j.rser.2014.05.032

Mossop, G.D., Shetsen, I., 1994. Geological atlas of the Western Canada Sedimentary Basin.

Munu, N., Banadda, N., 2016. Can cities become self-reliant in energy? A technological scenario analysis for Kampala, Uganda. Environ. Eng. Res. 21, 219–225. https://doi.org/10.4491/eer.2016.023

Muratori, M., 2018. Impact of uncoordinated plug-in electric vehicle charging on residential power demand. Nat. Energy 3, 193–201. https://doi.org/10.1038/s41560-017-0074-z

National Energy Board of Canada, 2019. Provincial and Territorial Energy Profiles – British Columbia [WWW Document]. URL https://www.cer-rec.gc.ca/nrg/ntgrtd/mrkt/nrgsstmprfls/bc-eng.html (accessed 4.20.19).

National Renewable Energy Laboratory, 2018. Annual Technology Baseline.

National Renewable Energy Laboratory, 2013. PVWatts [WWW Document]. URL https://pvwatts.nrel.gov/pvwatts.php (accessed 10.4.19).

Natural Resources Canada, 2019. Comprehensive Energy Use Database [WWW Document]. URL http://oee.nrcan.gc.ca/corporate/statistics/neud/dpa/menus/trends/comprehensive_tables/list.cfm (accessed 6.20.19).

Natural Resources Canada, 2013. Survey of commercial and institutional energy use: establishments 2009.

Niet, T., Lyseng, B., English, J., Keller, V., Palmer-Wilson, K., Moazzen, I., 2017. Hedging the risk of increased emissions in long term energy planning. Energy Strateg. Rev. 16, 1–12. https://doi.org/10.1016/j.esr.2017.02.001

NREL, 2011. U.S. Department of Energy Commercial Reference Building Models of the National Building Stock, National Renewable Energy Laboratory. Golden, CO.

Nyerges, T.L., Jankowski, P., 2010. Regional and Urban GIS: A Decision Support Approach. The Guilford Press, New York.

Ong, S., Campbell, C., Denholm, P., Margolis, R., Heath, G.A., Ong, S., Campbell, C., Denholm, P., Margolis, R., Heath, G., 2013. Land-Use Requirements for Solar Power Plants in the United States.

Ong, S., Campbell, C., Heath, G.A., 2012. Land Use for Wind, Solar, and Geothermal Electricity Generation Facilities in the United States.

Palisade, 2017. 7.8. Interpreting Change in Output Statistic in Tornado Graph [WWW Document]. URL http://kb.palisade.com/index.php?pg=kb.page&id=248 (accessed 8.28.17).

Palmer-Wilson, K., Donald, J., Robertson, B., Lyseng, B., Keller, V., Fowler, M., Wade, C., Scholtysik, S., Wild, P., Rowe, A., 2019. Impact of land requirements on electricity system decarbonisation pathways. Energy Policy 129, 193–205. https://doi.org/10.1016/j.enpol.2019.01.071

Palmer-Wilson, K., Walsh, W., Banks, J., 2017. Techno-Economic assessment of Geothermal Energy Resources in the Sedimentary Basin in Northeastern British Columbia, Canada. Geoscience BC. Vancouver.

Pasqualetti, M.J., 2011. Opposing Wind Energy Landscapes: A Search for Common Cause. Ann. Assoc. Am. Geogr. 101, 907–917. https://doi.org/10.1080/00045608.2011.568879

Pimentel, D., Rodrigues, G., Wang, T., Abrams, R., Goldberg, K., Staecker, H., Brueckner, L., Trovato, L., Chow, C., Govindarajulu, U., Boerke, S., Brueckner, L., Trovato, L., Chow, C., Govindarajulu, U., Boerke, S., 1994. Renewable Energy: Economic and Environmental Issues. Bioscience 44, 536–547. https://doi.org/10.2307/1312281

Pinto de Moura, G.N., Legey, L.F.L., Balderrama, G.P., Howells, M., 2017. South America power integration , Bolivian electricity export potential and bargaining power : An OSeMOSYS SAMBA approach. Energy Strateg. Rev. 17, 27–36. https://doi.org/10.1016/j.esr.2017.06.002

Pletka, R., Finn, J., 2009. Western Renewable Energy Zones, Phase 1: QRA Identification Technical Report.

Poggi, F., Firmino, A., Amado, M., 2018. Planning renewable energy in rural areas: Impacts on occupation and land use. Energy 155, 630–640. https://doi.org/10.1016/j.energy.2018.05.009

Rand, J., Hoen, B., 2017. Thirty years of North American wind energy acceptance research: What have we learned? Energy Res. Soc. Sci. 29, 135–148. https://doi.org/10.1016/j.erss.2017.05.019

Robeck, K.E., Ballou, S.W., South, D.W., Davis, M., Chiu, S.Y., Baker, J.E., Dauzvardis, P.A., Carvey, D.B., Torpy, M.F., 1980. Land Use and Energy.

Rochelle, G.T., 2009. Amine Scrubbing for CO2 Capture. Science (80-.). 325, 1652–1654.

Saha, M., Eckelman, M.J., 2015. Geospatial assessment of potential bioenergy crop production on urban marginal land. Appl. Energy 159, 540–547. https://doi.org/10.1016/j.apenergy.2015.09.021

Salmon, J.P., Meurice, J., Wobus, N., Stern, F., Duaime, M., Salmon, J.P., Meurice, J., Wobus, N., Stern, F., Duaime, M., 2011. Guidebook to Geothermal Power Finance. NREL/SR-6A20-49391. National Renewable Energy Laboratory. Boulder, CO.

Schmidt, O., Hawkes, A., Gambhir, A., Staffell, I., 2017. The future cost of electrical energy storage based on experience rates. Nat. Energy 2. https://doi.org/10.1038/nenergy.2017.110

Schmidt, O., Melchior, S., Hawkes, A., Staffell, I., 2019. Projecting the Future Levelized Cost of Electricity Storage Technologies. Joule 3, 81–100. https://doi.org/10.1016/j.joule.2018.12.008

Sims, S., Dent, P., 2005. High-voltage Overhead Power Lines and Property Values: A Residential Study in the UK. Urban Stud. 42, 665–694. https://doi.org/10.1080/00420980500060541

Smil, V., 2019. Distributed Generation and Megacities: Are Renewables the Answer? IEEE Power Energy Mag. 17, 37–41. https://doi.org/10.1109/MPE.2018.2884112

Smil, V., 2010. Energy Transitions: History, Requirements, Prospects. ABC-CLIO, Santa Barbara.

Soini, K., Pouta, E., Salmiovirta, M., Uusitalo, M., Kivinen, T., 2011. Land Use Policy Local residents' perceptions of energy landscape: the case of transmission lines. Land use policy 28, 294–305. https://doi.org/10.1016/j.landusepol.2010.06.009

Sovacool, B.K., 2008. The Dirty Energy Dilemma: What's Blocking Clean Power in the United States. ABC-CLIO, Westport, Connecticut.

Statistics Canada, 2019. Report on Energy Supply and Demand in Canada - 2016 Revised.

Statistics Canada, 2017. Focus on Geography Series, 2016 Census. Statistics Canada Catalogue no. 98-404-X2016001. Ottawa, Ontario. Data products, 2016 Census. [WWW Document]. URL https://www12.statcan.gc.ca/census-recensement/2016/as-sa/fogs-spg/Facts-cma-eng.cfm?LANG=Eng&GK=CMA&GC=933&TOPIC=1 (accessed 3.29.19).

Stockholm Stad, 2014. Roadmap for a fossil fuel-free Stockholm 2050.

Taliotis, C., Shivakumar, A., Ramos, E., Howells, M., Mentis, D., Sridharan, V., Broad, O., Mofor, L., 2016. Energy for Sustainable Development An indicative analysis of investment opportunities in the African electricity supply sector — Using TEMBA (The Electricity Model Base for Africa). Energy Sustain. Dev. 31, 50–66. https://doi.org/10.1016/j.esd.2015.12.001

Tesla, 2019. Tesla Powerwall [WWW Document]. URL https://www.tesla.com/en_CA/powerwall (accessed 3.29.19).

Trainor, A.M., Mcdonald, R.I., Fargione, J., 2016. Energy Sprawl Is the Largest Driver of Land Use Change in United States. PLoS One 11, 1–16. https://doi.org/10.1371/journal.pone.0162269

Trottier Energy Futures Project, 2016. Canada's Challenge & Opportunity - Transformations for major reductions in GHG emissions - Full technical report and modelling results.

Trumpy, E., Botteghi, S., Caiozzi, F., Donato, A., Gola, G., Montanari, D., Pluymaekers, M.P.D., Santilano, A., van Wees, J.D., Manzella, A., 2016. Geothermal potential assessment for a low carbon strategy: A new systematic approach applied in southern Italy. Energy 103, 167–181. https://doi.org/10.1016/j.energy.2016.02.144

Trumpy, E., Donato, A., Gianelli, G., Gola, G., Minissale, A., Montanari, D., Santilano, A., Manzella, A., 2015. Geothermics Data integration and favourability maps for exploring geothermal systems in Sicily , southern Italy. Geothermics 56, 1–16. https://doi.org/10.1016/j.geothermics.2015.03.004

U.S. Census Bureau Population Division, 2018. Annual Estimates of the Resident Population: April 1, 2010 to July 1, 2017 [WWW Document]. URL https://factfinder.census.gov/faces/nav/jsf/pages/index.xhtml (accessed 3.29.19).

Ulloa, P., 2007. Potential for Combined Heat and Power and District Heating and Cooling from Wasteto-Energy Facilities in the U.S. – Learning from the Danish Experience. Master Thesis. Department of Earth and Environmental Engineering. Columbia University.

United Nations, 2018. World Urbanization Prospects: The 2018 Revision.

United Nations Human Settlement Programme, 2011. Cities and Climate Change: Global

Report on Human Settlements 2011. UN-HABITAT.

United States Geological Survey, 2014. National Hydrography Dataset [WWW Document]. URL https://www.usgs.gov/core-science-systems/ngp/national-hydrography/nhdplus-high-resolution (accessed 4.14.14).

Vaillancourt, K., Bahn, O., Frenette, E., Sigvaldason, O., 2017. Exploring deep decarbonization pathways to 2050 for Canada using an optimization energy model framework. Appl. Energy 195, 774–785. https://doi.org/10.1016/j.apenergy.2017.03.104

Voogd, H., 1983. Multicriteria evaluation for urban and regional planning.

Voorspools, K.R., D'haeseleer, W.D., 2006. An analytical formula for the capacity credit of wind power. Renew. Energy 31, 45–54. https://doi.org/10.1016/j.renene.2005.03.017

Waite, J.L., 2017. Land Use Policy Land reuse in support of renewable energy development. Land use policy 66, 105–110. https://doi.org/10.1016/j.landusepol.2017.04.030

Walsh, W., 2013. Geothermal resource assessment of the Clarke Lake Gas Field, Fort Nelson, British Columbia. Bull. Can. Pet. Geol. 61, 241–251. https://doi.org/10.2113/gscpgbull.61.3.241

Wei, M., Nelson, J.H., Greenblatt, J.B., Mileva, A., Johnston, J., Ting, M., Yang, C., Jones, C., 2013. Deep carbon reductions in California require electrification and integration across economic sectors. Environ. Res. Lett. 8. https://doi.org/10.1088/1748-9326/8/1/014038

Weides, S.N., Majorowicz, J., 2014. Implications of spatial variability in heat flow for geothermal resource evaluation in large foreland basins: The case of the Western Canada sedimentary basin. Energies 7, 2573–2594. https://doi.org/10.3390/en7042573

Weides, S.N., Moeck, I.S., Majorowicz, J.A., Grobe, M., 2014a. The Cambrian Basal Sandstone Unit in central Alberta – an investigation of temperature distribution, petrography and hydraulic and geomechanical properties of a deep saline aquifer. Can. J. Earth Sci. 51, 783–796. https://doi.org/10.1139/cjes-2014-0011

Weides, S.N., Moeck, I.S., Majorowicz, J.A., Palombi, D., Grobe, M., 2013a. Geothermal exploration of Paleozoic formations in Central Alberta. Can. J. Earth Sci. 50, 519–534. https://doi.org/10.1139/cjes-2012-0137

Weides, S.N., Moeck, I.S., Schmitt, D.R., Majorowicz, J.A., 2014b. An integrative geothermal resource assessment study for the siliciclastic Granite Wash Unit, northwestern Alberta (Canada). Environ. Earth Sci. 72, 4141–4154.

https://doi.org/10.1007/s12665-014-3309-3

Weides, S.N., Moeck, I.S., Schmitt, D.R., Majorowicz, J.A., Ardakani, E.P., 2013b. Characterization of Geothermal Reservoir Units in Northwestern Alberta By 3D Structural Geological Modelling and Rock Property Mapping Based on 2D Seismic and Well Data. Proceedings, 38 Work. Geotherm. Reserv. Eng 1–8.

Welsch, M., Hermann, S., Howells, M., Rogner, H.H., Young, C., Ramma, I., Bazilian, M., Fischer, G., Alfstad, T., Gielen, D., Le Blanc, D., Röhrl, A., Steduto, P., Müller, A., 2014. Adding value with CLEWS - Modelling the energy system and its interdependencies for Mauritius. Appl. Energy 113, 1434–1445. https://doi.org/10.1016/j.apenergy.2013.08.083

Williams, C.F., 2007. Updated methods for estimating Recovery Factors for geothermal resources. Thirty-Second Work. Geotherm. Reserv. Eng. 7.

Williams, C.F., Reed, M., Mariner, R., 2008. A Review of Methods Applied by the U.S. Geological Survey in the Assessment of Identified Geothermal Resources, Open-File Report 2008–1296. U.S. Geological Survey. Open-File Report 2008–1296.

Williams, J.H., DeBenedictis, A., Ghanadan, R., Mahone, A., Moore, J., Morrow, W.R.I., Price, S., Torn, M.S., 2012. The Technology Path to Deep Greenhouse Gas Emissions Cuts by 2050: The Pivotal Role of Electricity. Science (80-.). 335, 53–59. https://doi.org/10.1126/science.1208365

Wu, G.C., Torn, M.S., Williams, J.H., 2015. Incorporating Land-Use Requirements and Environmental Constraints in Low-Carbon Electricity Planning for California. Environ. Sci. Technol. 49, 2013–2021. https://doi.org/10.1021/es502979v